Dissertation zur Erlangung des Doktorgrades

der Fakultät für Chemie und Pharmazie

der Ludwig-Maximilians-Universität München

Investigations into Carbon Nitrides and Carbon Nitride Derivatives

Hongji Wang

aus

Yantai, China

2013

Erklärung

Diese Dissertation wurde im Sinne von § 7 der Promotionsordnung vom 28. November 2011von Frau Professor Dr. Bettina Lotsch betreut.

EIDESSTATTLICHE VERSICHERUNG

Diese Dissertation wurde selbständig, ohne unerlaubte Hilfe erarbeitet.

München, 26.02.2013

_____

Hongji Wang

Dissertation eingereicht am 26.02.2013

1. Gutachter: Prof. Dr. Bettina Lotsch

2. Gutachter: Prof. Dr. Thomas Bein

Mündliche Prüfung am 25. März 2013

Acknowledgement

are group numbers of Prof. Wolfgan Schnick, shared lots of experience about carbon nitrides with me. Christian Minke did lots of SEM and NMR of my samples and Kulpreet Virdi (group of Prof. Christina Scheu) did many TEM measurements for me. Maria Mesch and Kilian Bärwinkel (group of Prof. Jürgen Senker) did many NMR experiments and simulations on my samples.

My great appreciation also goes to secretaries and technical assistants of Prof. Bettina Lotsch and the MPI-FKF. With their help I could easily handle all kinds of paperworks and also I got used to the new environment in Stuttgart easily.

My great and deep thanks go to my parents and my girlfriend for their boundless love and unconditional support over all these past years.

Last but not least, I'd like to thank the Siemens Company, Deutsche Akademische Austauschdienst (DAAD) and Deutsche Forschungsgemeinschaft (DFG) for financially supporting me to conduct the Ph.D. study at the University of Munich and Max Planck Institute for Solid State Research in Stuttgart and to live a life in Germany.

Abstract

Carbon nitrides and carbon nitride derivatives are promising photocatalysts. The main focus of this thesis is the synthesis and characterization of various carbon nitrides (incompletely condensed melon, carbon nitride doped cesium titanate, ultra-long calcined melon, and OH-melem). Those carbon nitrides were then tested with regard to their photocatalytic properties.

In the first part of chapter 3 of this thesis, we focus on a material called ''melem oligomer''. Two different synthesis routes were applied (open system and half open system) and the composition and structure of this material was studied. Melem with two different crystalline structures and some amorphous residues were found in the product. We also tested the photocatalytic activity of melem oligomer and confirmed hydrogen production from water with a relatively low rate of $2\ \mu mol\ g^{-1}\ h^{-1}$. In the second part of chapter 3, we synthesized ultra-long calcined melamine which may have a morphology similar to the ''g-C$_3$N$_4$ nanosheets''. We analyzed both the composition and structure and investigated the efficiency of the presumed g-C$_3$N$_4$ nanosheets for hydrogen production from water. Ultra-long calcined melamine showed the best photoactivity which is twice that of melon at 490 °C. This is most likely due to the interesting morphology and high surface area.

In chapter 4, melem oligomer was doped with cesium titanate *in situ*. Different calcination times were applied and various characterization techniques were used to investigate the composition, structure and morphology of the obtained materials. The efficiency of this hybrid photocatalyst for hydrogen production did not show higher photoactivity than the pure carbon nitrides except in the case of 16 h calcination which was the optimum calcination time overall.

In chapter 5, OH-melem with a composition close to 2-oxo-6,10-diamino-*s*-heptazine, which could be a precursor of oxygen-doped g-C$_3$N$_4$, was synthesized and characterized by various techniques. Crystallinity is rather low in this oxygen containing species. NMR spectra differ from melem or cyameluric acid and XPS results confirm the presence of C=O groups.

Overall, different carbon nitrides and carbon nitride derivatives were synthesized and chemically investigated to gain further knowledge on their synthesis, chemical properties and their resulting application as photocatalysts.

Contents

Curriculum Vitae

Chapter 1

Introduction

Carbon nitrides are, put simply, compounds of carbon and nitrogen as the backbone forming elements. Carbon nitride in the strict sense, however, refers to the binary carbon nitride with formula C_3N_4, which still is an elusive compound.[1,2] Five different crystalline modifications of the binary carbon nitride, which were put forward in an early paper by Teter and Hemely, are shown in Fig. 1.1.[3] Carbon nitride materials are in the focus of this thesis. Graphitic carbon nitrides, derived from the parent binary compound g-C_3N_4, are a family of largely planar structures with a composition close to "C_3N_4", yet with varying amounts of hydrogen, and are based on either triazine or heptazine units (Fig. 1.2). These exhibit, depending on the reaction conditions, different degrees of condensation, physical and chemical properties and reactivities.
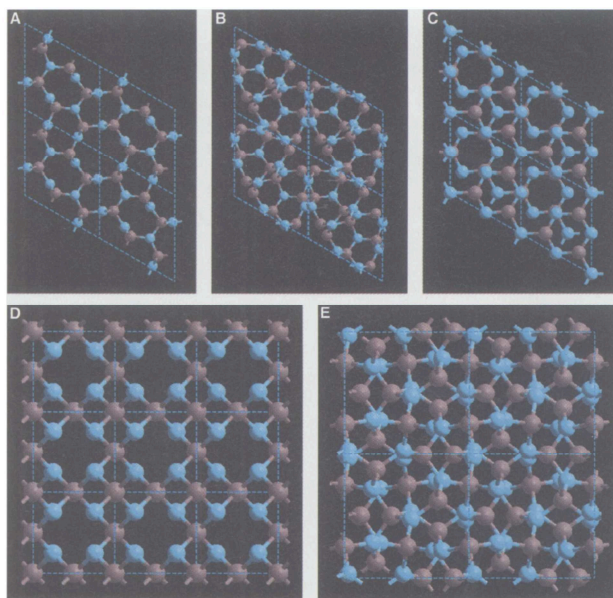
Fig. 1.1 Representation of (A), β-C_3N_4 (B), α-C_3N_4 (C), graphitic-C_3N_4 (D), pseudocubic-C_3N_4 and (E), cubic-C_3N_4 modifications, viewed down the [001] axis. The carbon and nitrogen atoms are depicted as gray and blue spheres, respectively.[3]
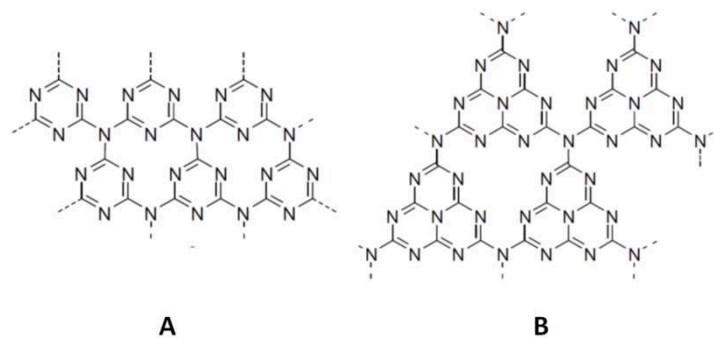
Fig. 1.2 Structural models of two prototypic fully condensed forms of g-C_3N_4 based on (A) triazine and (B) heptazine building blocks.

History of Carbon Nitrides

The first work of carbon nitride originates from the early 19th century. Jöns Jakob Berzelius, considered the father of modern chemistry who famously coined the word "polymer", first synthesized a carbon nitride material through heating of Hg(SCN)₂.[4] This product was found to have a formula corresponding to $C_6N_9H_3$, which is the same formula as that of a material discovered by Justus von Liebig in 1834.[5] He identified several triazine and heptazine-based molecular compounds such as melamine, melam, melem, ammeline, ammelide, and melon. His synthesis was based on the pyrolysis of ammonium chloride with potassium thiocyanate, yielding a yellow, amorphous, and insoluble product which was named melon. As his products were of high purity, the first reliable characterizations of several carbon nitride compounds by elemental analysis were recorded.[6–9] However, not all of his products could be well synthesized and characterized, and by elemental analysis of melon, he could not ascertain a clearly reproducible formula. In 1835, another important discovery was potassium hydromelonate, $K_3C_6N_7(NCN)$, by Leopold Gmelin.[10] The initial synthesis was conducted using potassium ferricyanide, and sulfur, which were heated in a crucible. When the potassium hydromelonate was acidified, hydromelonic acid was formed. In 1855, Hennenberg discovered cyameluric acid ($H_3C_6N_7O_3$) by hydrolyzing hydromelonate salts.[11]

The structure of these above mentioned compounds remained unclear due to the lack of appropriate analytical methods at that time. In the early 20th century names like melon, melem or cyameluric acid were merely footnotes, if they were mentioned at all. In 1922, Edward C. Franklin published a review of the carbon-nitrogen family of compounds which also included the

well-known guanidine, biguanidine, melamine, cyanamide, and dicyanodiamide.[12] He found that the empirical composition of melon derivatives derived from mercuric thiocyanate varied with the method of preparation, and the hydrogen content varied from 1.1 to 2.0 wt%. This brought these compounds into consideration once more. In this review, carbonic nitride with the formula $(C_3N_4)_x$ was mentioned, which could also possibly be the final polymerization product of heating Liebig's melon, though actual evidence was far from unambiguous. Franklin also proposed some possible structures for these so-called ammono carbonic acids, but these proposals were only conjectures, without X-ray analytical evidence. In 1933, Franklin gave Linus Pauling some crystals with the formula $C_6N_7O_3Na_3 \cdot 3H_2O$ to perform an X-ray study. After studying this material and some related materials, the assertion was that the most likely structure would be a coplanar arrangement of three fused rings. Therefore, Pauling introduced the cyameluric nucleus, C_6N_7, which is shown in Fig. 1.3.
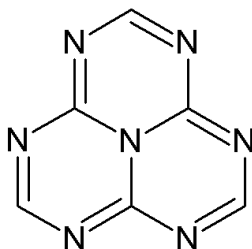
Fig. 1.3 Pauling's proposed structure for the cyameluric nucleus.

In the second half of the 20th century, the Russian chemist Finkel'shtein explored the spectroscopic properties of these known cyameluric molecules by IR and UV-Vis spectroscopy.[13] In 1961, the compound 2-oxo-6,10-diamino-*s*-heptazine, which was synthesized by a careful partial alkaline hydrolysis of melon, was reported by Finkel'shtein. [14–18] Until now, there have been no further reports about this compound. In 1982, Leonard and coworkers reported the first crystal structure of a cyameluric derivative, after successfully synthesizing the unsubstituted cyameluric nucleus, $C_6N_7H_3$, by a bottom-up assembly starting from 2,4-diamino-1,3,5-triazine and methyl *N*-cyanomethanimidate.[19] The crystal structure showed a coplanar arrangement of three fused triazine units, which proved the structure proposition predicted by Pauling forty-five years earlier.
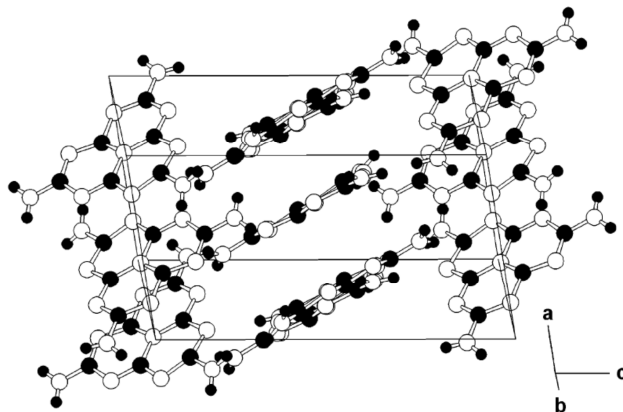
Fig. 1.4 Crystal structure of melem.[20]

Current State of Research

More recently, Tamikuni Komatsu's group reported on a relatively ordered carbon nitride polymer, $C_{91}H_{14}N_{124}$.[21] Meanwhile, a moderately crystalline species was reported by the same authors, which they called ''high molecular weight'' melon.[22] Komatsu's work was one of the first to discuss the idea of a heptazine-based g-C3N4, thus linking Berzelius' and Liebig's earlier work with the predictions of fully condensed carbon nitride C_3N_4. In 2003, the Schnick group reported an important intermediate during the condensation of melamine rings to graphitic carbon nitride, melem (2,5,8-triamino-tri-s-triazine, $C_6N_7(NH_2)_3$), which can be considered the elementary building block of all heptazine-based polymeric carbon nitrides (Fig. 1.4).[20] X-ray powder diffractometry and solid-state NMR were used to determine the structure. After that, the crystal structures of melam with two triazine units condensed *via* a bridging NH group and semicrystalline melon were characterized.[23,24] In addition, several structure models for melon (Fig. 1.5) and fully condensed graphitic carbon nitride were put forward (Fig. 1.6). These works contributed to a much better understanding of the structure of graphitic carbon nitrides.
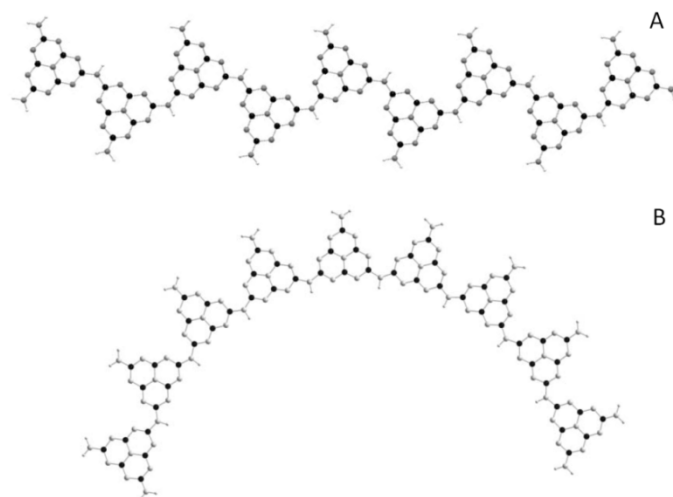
Fig. 1.5 (A) Zig-zag chain of melon, and (B) "classical" model of an initially linear melon chain after geometry optimization based on the semiempirical PM3 method. Gray: nitrogen; black: carbon; gray: hydrogen; the positions of the latter are empirically fitted.[25] [26]
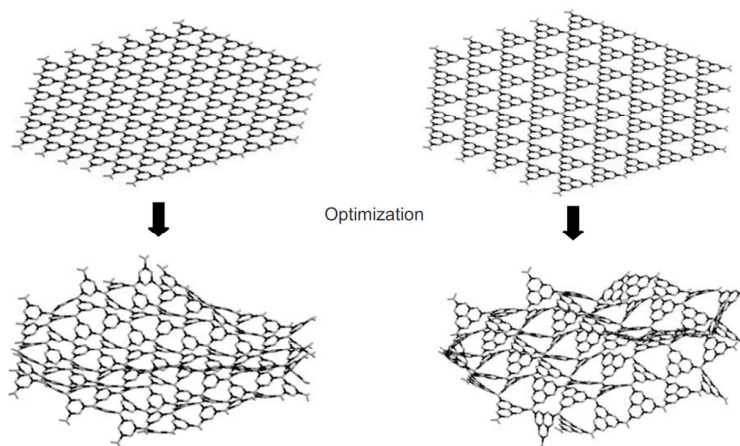
Fig. 1.6 Starting geometries (top) and optimized structures (bottom) of fully condensed triazine- (left) and heptazine-based (right) networks, using the PM3 method. [25][26]

The investigations of carbon nitrides aim to understand the properties of these materials, especially their photocatalytical properties. Photocatalysis enables one to use light to drive catalytic reactions. The energy brought in by photons can be employed to accelerate a reaction. Photocatalytic water splitting is currently one of the most interesting ways to achieve a clean and renewable energy system based on hydrogen as a solar fuel. It relies on a conversion of solar energy to hydrogen and oxygen, which is assisted by photocatalysts suspended directly in water (Fig. 1.7). The choice of suitable, i.e. stable, non-toxic and effective photocatalysts is very

8

important. Recently, carbon nitrides, which are cheap and green materials, have turned out to be a promising choice as photocatalysts.
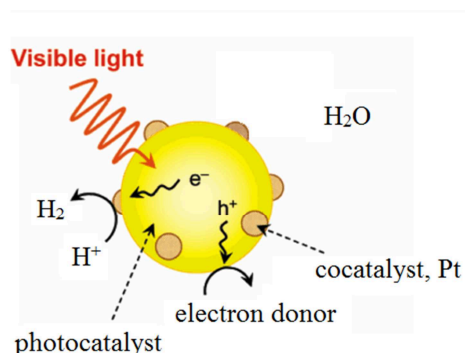
In 2008, Kisch and coworkers published a form of nitrogen-modified titanium dioxide.[27–30] This modified titanium dioxide shows high photocatalytic activity in the visible region of the electromagnetic spectrum. In that paper, carbon nitride modified powders were prepared by calcining TiO_2 with urea or cyanuric acid in air at 400 °C for 1 h in an open rotating flask. The authors claim that through condensation of the amino groups of the heptazine rings with the hydroxyl groups of the titania surface Ti-N bonds are generated. The proposed structure of the photocatalyst ''TiO_2-N,C/melem'' is shown in Fig. 1.8. The heptazine component was regarded as a visible light absorber and, hence, as a photosensitizer for TiO_2. In the same year, Antonietti's group reported a metal-free polymeric photocatalyst for hydrogen production from water under visible light.[31] The metal free polymeric photocatalyst was called g-C_3N_4. This was the first time that graphitic carbon nitride itself was considered as a photocatalyst to generate hydrogen from water, even in the absence of noble metals used as co-catalysts. Although the estimated quantum efficiency of the g-C_3N_4 catalyst is still rather low, this result opens new areas for research into energy production. After that, the graphitic carbon nitride material, which is cheap and easily available, was brought to general interest. [32–35]

9
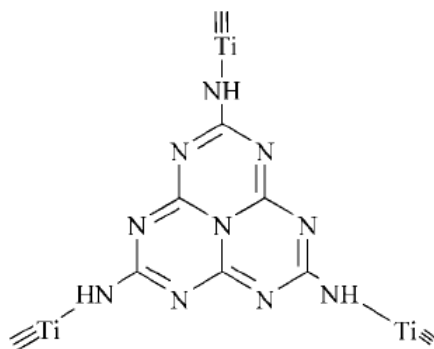
Fig. 1.8 The proposed structure of a TiO$_2$-N,C/melem hybrid photocatalyst.[27]

A lot of work was done to increase the efficiency of the g-C$_3$N$_4$ photocatalyst for hydrogen production from water and photodegradation of pollutants. The synthesis of carbon nitrides is strongly dependent on the synthesis conditions, such as calcination temperature[36], calcination time, synthesis atmosphere, and whether the synthesis is carried out in an open or closed system[37]. With different conditions, a variety of carbon nitride species with different hydrogen content and degrees of crystallinity can be gained. Antonietti has demonstrated that highly condensed and crystalline carbon nitrides tend to be less active photocatalysts than "defect-containing" carbon nitrides.[37] The carbon nitrides typically have a number of defects which was mentioned by Lotsch et al. while reporting melon.[24] In addition, the possible existence of a "melem oligomer" was conjectured, which can be regarded as an incompletely condensed carbon nitride.[26] This melem oligomer could be an interesting material possessing sufficient defects for photocatalysis.

The calculated energy diagram for the synthesis of carbon nitrides is outlined in Fig. 1.9.[37] The material intermediate in condensation degree between melem and melon is called dimelem, which also belongs to the incompletely condensed melon group of materials. Because of the expected larger bandgap, these kinds of carbon nitride materials have not been considered as photocatalysts as yet. However, recently, Zou and coworkers reported on effectively narrowing the bandgap of carbon nitride photocatalysts by coupling with a narrow gap molecule.[38] In that paper, experimental and theoretical methods were combined to investigate why PMDA (Pyromellitic Dianhydride) can extend light absorption of wide bandgap carbon nitride polymers (incompletely condensed melon), and insights for modifying wide bandgap photocatalysts to

enable visible light absorption was provided. However, until now not many papers about the composition, morphology and structure of incompletely condensed melon species have been published.
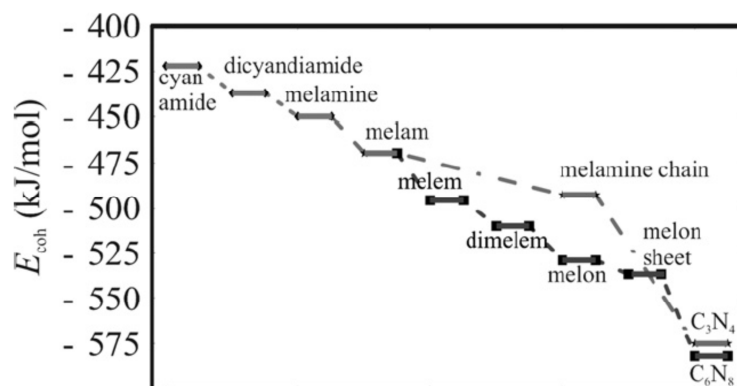
Fig. 1.9 Calculated energy diagram for the synthesis of carbon nitride. The starting precursor cyanamide condenses into melamine. Further condensation can then proceed *via* the triazine route (dash-dot line) to C_3N_4, or melamine can form melem and then follow the tri-*s*-triazine route (dashed line) to form C_6N_8. The energies are presented per atom.[37]

The morphology of carbon nitrides can also influence the photocatalytic activity. From this, Antonietti reported ordered mesoporous SBA-15-type graphitic carbon nitride as a photocatalyst for hydrogen evolution with visible light.[39] Because of the large external surface area and the ordered mesostructure which permits structural orientation of guest molecules in the periodic nanopores, the selectivity and activity of these photocatalysts were enhanced. Building mesoporous structures is an excellent way to control the morphology, however it requires elaborate procedures and therefore is rather costly. As the *in situ* formation of mesoporous structures from carbon nitrides by soft templating is difficult, hard templating procedures (such as those based on SiO_2–based SBA-15) must be used, where the hard template is removed in the last step. Liu developed a simple method to prepare g-C_3N_4 nanosheets by a direct thermal oxidation ''etching'' process of bulk g-C_3N_4 in air, which can improve the surface area and control the morphology.[40] The assumed basis of this method is that the parallel hydrogen bonded strands of polymeric melon units in the layers, which are not stable against oxidation in air, will be gradually oxidized away from the bulk material at the exposed surfaces such that the thickness of bulk g-C_3N_4 will be decreased down to a few nanosheets (Fig. 1.10). However, for the inferred thinning process to hold, a 2D polymer with stable covalent links in two dimensions

is required. As it is known that melon is a 1D polymer (Fig. 1.5), it is still unclear whether the thermal treatment of melon will actually lead to 2D g-C_3N_4 nanosheets. Nevertheless, the superior photocatalytic activity of this kind of high surface area carbon nitride is very attractive.
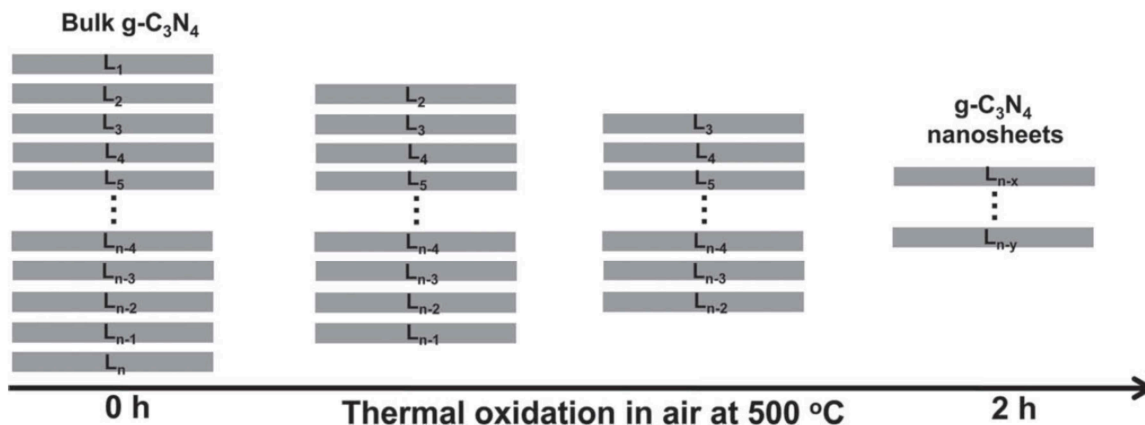
Fig. 1.10 Schematic of the formation process of g-C_3N_4 nanosheets by thermal oxidation etching of bulk g-C_3N_4 at 500 °C in air.[40]

Many reports which included doped carbon nitrides, such as B-[41], F-[42], S-[43] and P-doping,[44] have been published by several groups. In addition, a carbon-rich carbon nitride photocatalyst was synthesized to enhance photocatalytic properties by a copolymerization strategy.[45] A graphene/g-C_3N_4 composite with improved conductivity and electrocatalytic performance was published by Shi and coworkers.[46] Besides this, metal carbon nitride heterojunctions (Fig. 1.11) also show an improved photocatalytic performance. A zinc-doped carbon nitride catalyst was synthesized by Kako and coworkers to improve optical, electronic, magnetic and catalytic properties.[47] Au/g-C_3N_4 heterojunctions were reported that can effectively promote the transfer of charge from light-excited g-C_3N_4, enabling photocatalytic hydrogen production with visible light.[48] Doping of TiO_2 with g-C_3N_4 was also investigated by many researchers. Apart from these dopants, there are a few papers outlining cesium titanate doping with g-C_3N_4.
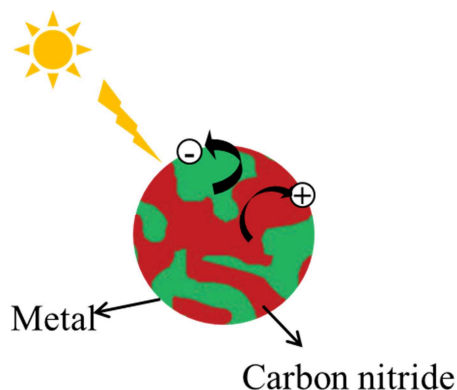
Fig. 1.11 Schematic of the metal carbon nitride heterojunctions.

The compound 2-oxo-6,10-diamino-*s*-heptazine, which was reported by the Russian chemist Finkel'shtein in 1962, can be regarded as an oxygen-doped carbon nitride. However, there are few reports on oxygen doping in carbon nitrides, which may be an efficient way of enhancing the photocatalytic activity of carbon nitrides. Besides, the controlled introduction of oxygen in structurally well-defined positions may be a first step towards the more rational design of photocatalytically active doped carbon nitrides. Only recently Chen published a facile approach to synthesize oxygen-doped *g*-C_3N_4, which shows superior visible light photocatalytic abilities.[49] However, the structure and composition of the doped material is still elusive. Nevertheless, this offers a reference route for developing high performance metal-free photocatalysts, which is a major objective of this thesis

Summary and Objectives

In the first part of chapter 3 of this thesis, we focus on a material christened ''melem oligomer''. Two different synthesis routes were applied (open system and half open system) and the composition and structure of this material was studied. We also tested the photocatalytic activity of melem oligomer for hydrogen production from water. In the second part of chapter 3, we synthesized ultra-long calcined melamine which may have a morphology similar to the ''*g*-C_3N_4 nanosheets'' outlined above.[40] We analyzed both the composition and structure and investigated the efficiency of the presumed *g*-C_3N_4 nanosheets for hydrogen production from water.

In chapter 4, melem oligomer was doped with cesium titanate *in situ*. Different calcination times were applied and various characterization techniques were used to investigate the composition,

structure and morphology of the obtained materials. The efficiency of this photocatalyst for hydrogen production from water was also tested.

In chapter 5, a material with a composition close to 2-oxo-6,10-diamino-*s*-heptazine, which could be a precursor of oxygen-doped *g*-C$_3$N$_4$, was synthesized and characterized by various techniques.

The main goals of this study are as follows:

- Structural investigations of heptazine-based compounds have already been conducted, but many heptazine based carbon nitrides were not yet fully characterized with respect to their composition and structure owing to their largely amorphous nature. We therefore aim at characterizing heptazine-based carbon nitrides with relevance to the broader field of carbon nitride-based photocatalysis, both with respect to their composition, structure, morphology and photocatalytic activity.

- Although there were many investigations, the thermal condensation of carbon nitrides is not fully understood. Further investigations into incompletely condensed melon will be helpful to understand the condensation process from melem to melon, as well as the implications of low degrees of condensation and the presence of defects for the photocatalytic activity.

Chapter References

[1]   C. Niu, Y. Z. Lu, C. M. Lieber, *Science (New York, N.Y.)* **1993**, *261*, 334–337.

[2]   A. Y. Liu, M. L. Cohen, *Science (New York, N.Y.)* **1989**, *245*, 841–842.

[3]   D. M. Teter, R. J. Hemley, *Science* **1996**, *271*, 53–55.

[4]   L. Gmelin, *Handbook of Chemistry* **1855**, *9*, 378–394.

[5]   J. Liebig, *Annalen der Pharmacie* **1834**, *10*, 1–48.

[6]   J. Liebig, *Annalen der Chemie und Pharmacie* **1844**, *50*, 337.

[7]   J. Liebig, *Annalen der Chemie und Pharmacie* **1845**, *53*, 330.

[8]   J. Liebig, *Annalen der Chemie und Pharmacie* **1847**, *61*, 262.

[9]   J. Liebig, *Annalen der Chemie und Pharmacie* **1855**, *95*, 257.

[10]   L. Gmelin, *Annalen der Pharmacie* **1835**, *15*, 252.

[11]   W. Henneberg, *Annalen der Chemie und Pharmacie* **1850**, *73*, 228.

[12]   E. C. Franklin, *Journal of the American Chemical Society* **1922**, *44*, 486–509.

[13]   A. I. Boitsov, E. N.; Finkel'shtein, *Zhurnal Obshchei Khimii* **1962**, *32*, 321–322.

[14]   N. V. Finkel'shtein, A. I.; Spiridonova, *Uspekhi Khimii* **1964**, *33*, 900–911.

[15]   A. I. Spiridonova, N. V.; Finkel'shtein, *Trudy po Khimii i Khimicheskoi Tekhnologii* **1967**, 38–40.

[16]   V. A. Simkina, L. A.; Finkel'shtein, A. I.; Gal'perin, *Zavodskaya Laboratoriya* **1973**, *39*, 287.

[17]   A. I. Karlik, V. M.; Gal'perin, V. A.; Zagranichnyi, V. I.; Finkel'shtein, *application:US* **1974**.

[18]   V. A. Spasskaya, R. I.; Finkel'shtein, A. I.; Zil'berman, E. N.; Gal'perin, *Plast. Massy* **1977**, 10–11.

[19]   N. J. Hosmane, R. S.; Rossman, M. A.; Leonard, *Journal of the American Chemical Society* **1982**, *104*, 5497–5499.

[20]   B. Jürgens, E. Irran, J. Senker, P. Kroll, H. Müller, W. Schnick, *Journal of the American Chemical Society* **2003**, *125*, 10288–300.

[21]   T. Komatsu, *Journal of Materials Chemistry* **2001**, *11*, 802–803.

[22]   T. Komatsu, *Macromolecular Chemistry and Physics* **2001**, *202*, 19–25.

[23]   B. V Lotsch, W. Schnick, *Chemistry (Weinheim an der Bergstrasse, Germany)* **2007**, *13*, 4956–68.

[24]   B. V Lotsch, M. Döblinger, J. Sehnert, L. Seyfarth, J. Senker, O. Oeckler, W. Schnick, *Chemistry (Weinheim an der Bergstrasse, Germany)* **2007**, *13*, 4969–4980.

[25]   J. Sehnert, *Universität Bayreuth Ph.D thesis* **2007**.

[26]   B. V. Lotsch, *LMU München Ph.D thesis* **2006**.

[27]   D. Mitoraj, H. Kisch, *Angewandte Chemie (International ed.)* **2008**, *47*, 9975–8.

[28]   R. Beranek, H. Kisch, *Photochemical & photobiological sciences* **2008**, *7*, 40–48.

[29]   R. Beranek, H. Kisch, *Electrochemistry Communications* **2007**, *9*, 761–766.

[30]   D. Mitoraj, H. Kisch, *Chemistry A European Journal* **2010**, *16*, 261–269.

[31]   X. Wang, K. Maeda, A. Thomas, K. Takanabe, G. Xin, J. M. Carlsson, K. Domen, M. Antonietti, **2009**, *8*, 6–11.

[32] X. Wang, K. Maeda, A. Thomas, K. Takanabe, G. Xin, J. M. Carlsson, K. Domen, M. Antonietti, *Nature materials* **2009**, *8*, 76–80.

[33] X.-H. Li, J. Zhang, X. Chen, A. Fischer, A. Thomas, M. Antonietti, X. Wang, *Chemistry of Materials* **2011**, *23*, 4344–4348.

[34] F. Vilela, K. Zhang, M. Antonietti, *Energy & Environmental Science* **2012**, *5*, 7819.

[35] X. Wang, S. Blechert, M. Antonietti, *ACS Catalysis* **2012**, *2*, 1596–1606.

[36] Y. Cui, J. Zhang, G. Zhang, J. Huang, P. Liu, M. Antonietti, X. Wang, *Journal of Materials Chemistry* **2011**, *21*, 13032–13039.

[37] A. Thomas, A. Fischer, F. Goettmann, M. Antonietti, J.-O. Müller, R. Schlögl, J. M. Carlsson, *Journal of Materials Chemistry* **2008**, *18*, 4893–4905.

[38] Y. Guo, J. Yang, S. Chu, F. Kong, L. Luo, Y. Wang, Z. Zou, *Chemical Physics Letters* **2012**, *550*, 175–180.

[39] X. Chen, Y.-S. Jun, K. Takanabe, K. Maeda, K. Domen, X. Fu, M. Antonietti, X. Wang, *Chemistry of Materials* **2009**, *21*, 4093–4095.

[40] P. Niu, L. Zhang, G. Liu, H.-M. Cheng, *Advanced Functional Materials* **2012**, *22*, 4763–4700.

[41] Y. Wang, J. Zhang, X. Wang, M. Antonietti, H. Li, *Angewandte Chemie (International ed. in English)* **2010**, *49*, 3356–3359.

[42] Y. Wang, Y. Di, M. Antonietti, H. Li, X. Chen, X. Wang, *Chemistry of Materials* **2010**, *22*, 5119–5121.

[43] G. Liu, P. Niu, C. Sun, S. C. Smith, Z. Chen, G. Q. M. Lu, H.-M. Cheng, *Journal of the American Chemical Society* **2010**, *132*, 11642–11648.

[44]   Y. Zhang, T. Mori, J. Ye, M. Antonietti, *Journal of the American Chemical Society* **2010**, *132*, 6294–6295.

[45]   J. Zhang, X. Chen, K. Takanabe, K. Maeda, K. Domen, J. D. Epping, X. Fu, M. Antonietti, X. Wang, *Angewandte Chemie (International ed.)* **2010**, *49*, 441–444.

[46]   Y. Sun, C. Li, Y. Xu, H. Bai, Z. Yao, G. Shi, *Chemical communications (Cambridge, England)* **2010**, *46*, 4740–4742.

[47]   B. Yue, Q. Li, H. Iwai, T. Kako, J. Ye, *Science and Technology of Advanced Materials* **2011**, *12*, 034401.

[48]   Y. Di, X. Wang, A. Thomas, M. Antonietti, *ChemCatChem* **2010**, *2*, 834–838.

[49]   J. Li, B. Shen, Z. Hong, B. Lin, B. Gao, Y. Chen, *Chemical communications (Cambridge, England)* **2012**, *48*, 12017–12019.

Chapter 2

Experimental Methods

2.1 Preparative Methods

2.1.1 Furnaces

Reactions at elevated temperatures were carried out using muffle furnaces with a maximum continuous operation temperature of 1200 °C and programmed temperature control, allowing for heating rates > 0.01 °C min^{-1}. Typically, crucibles made of porcelain were chosen as reaction vessels, together with a porcelain lid.

Ampoules were heated in a tube furnace with electric resistance heating. The programmable controller allowed for a maximum continuous operation temperature of 1200 °C and heating rates of > 0.01 °C min^{-1}. The temperature was measured in the reaction zone with a thermocouple, the reliability being ±20 °C. A slightly tilted rather than flat set-up was chosen, thus leading to a separation of the reaction products within the reaction tube.

2.1.2 Vacuum and Inert Gas line

Thermolyses and manipulations of air-sensitive compounds were carried out using inert atmosphere of dry argon (purity grade 4.8 Messer) to exclude humidity and oxygen out of the reactions. The reaction vessels (normally ampules) were connected to the vacuum line via ground necks and dried using a heat gun. Evacuation of the vessels was accomplished using a rotary vane pump (RZ8, suction capacity 8.6 m^{3}h^{-1}, Vacuubrand) to pressures of 0.1 Pa. Argon was distributed via an inert gas line combined with the vacuum line. Purification and drying of inert gas was successively conducted by passing the inert gas through columns filled with blue silica gel (Merk), potassium hydroxide pellets (purum, Merck), molecular sieve (porewidth 0.3 nm, Merk), and phosphorous pentoxide.

2.2 Operating Techniques

2.2.1 Neutralization

Neutralization reactions were carried out using basic solutions (such as NaOH, KOH) with various concentrations which were added into acid (H_2SO_4) solutions slowly. Since neutralization reactions are exothermic, solutions were stirred with magnetic stirrer during the dropping procedure. Using pH paper, the pH value of the solutions was adjusted to 7.

2.2.2 Filtration

Filtration was used for the separation of solids from liquids and carried out by interposing a filter paper with a pore size of around 30μm into a porcelain Büchner funnel through which only the liquids can pass quickly by vacuum suction.

2.3 Analytical Methods

Various methods were employed to characterize the properties of carbon nitride materials. The main methods are diffraction techniques, spectroscopic methods, elemental analysis, mass spectrometry and thermal analysis.

2.3.1 X-ray Diffraction (XRD)

X-ray diffraction studies the materials phase composition and crystal structure by utilization of monochromatic electromagnetic radiation with a wavelength of only a few angstroms. It is one of the most important techniques for structure determination and has developed into a powerful and versatile tool for scientists.

The X-ray spectrum emitted by the X-ray source is composed of two parts, one part is „Bremsstrahlung" and the other part is characteristic X-rays. The latter part results from the atomic relaxation by filling the lost inner shell electrons with upper shell electrons, which contains characteristic information of atomic species. The process of „Bremsstrahlung" does not involve losing inner shell electrons, thus is no longer characteristic of a particular atom. Through the application of blocking filters, the characteristic X-rays with single wavelength can be obtained and then used for the experiments.
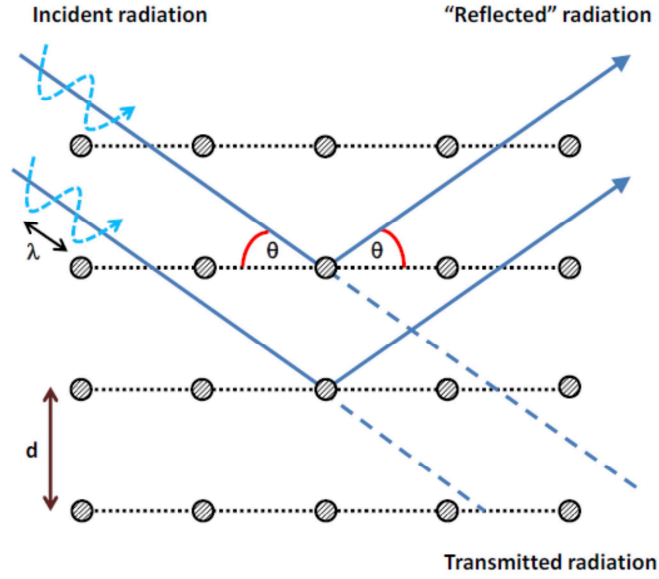
Fig. 2.1 Schematic illustration of an X-ray scattering.[2]

X-ray diffraction is a non-destructive method of characterization of solid materials. When X-rays are directed onto the solid sample, they will scatter in predictable patterns based upon the internal structure of the solid.[1] The detector will receive the diffracted beam. When the X-rays hit a sample, it can interact with the electron cloud of the sample and undergo elastic scattering.[2] To visualize the X-ray scattering process, Figure 2.1 displays an X-ray directed with an angle θ onto a system with a lattice-plane distance d. As the X-ray (with a wavelength λ) enters the system, the waves reflected from different planes will have different optical paths towards the detector plane. The difference in path length of two reflected waves is calculated as '$2d \sin \theta$'. In case of constructive interference, this difference equals the integer multiples of the wavelength λ, which is known as Bragg's law (Fig. 2.1).

$2d \sin \theta = n \lambda$

where d: lattice plane distance,

θ: angle of incidence,

n: order of interference, and

λ: X-ray wavelength.

21

If θ is known, the distance d between the lattice planes can be easily deduced.

Bragg's equation shows the relationship between diffraction and plane-to-plane distance d. It means that, only in solids which consist of a periodic arrangement of atoms, diffraction occurs. Meanwhile, the diffraction position corresponds to the characteristic information of the related crystal structure. Furthermore, the relative intensity of diffraction peaks depends on the type and arrangement of the atoms in the crystals. Therefore, if the diffraction pattern is compared with the JCPDS cards in the database, one can obtain insights into the phase composition and crystal structure of the studied materials.[3]
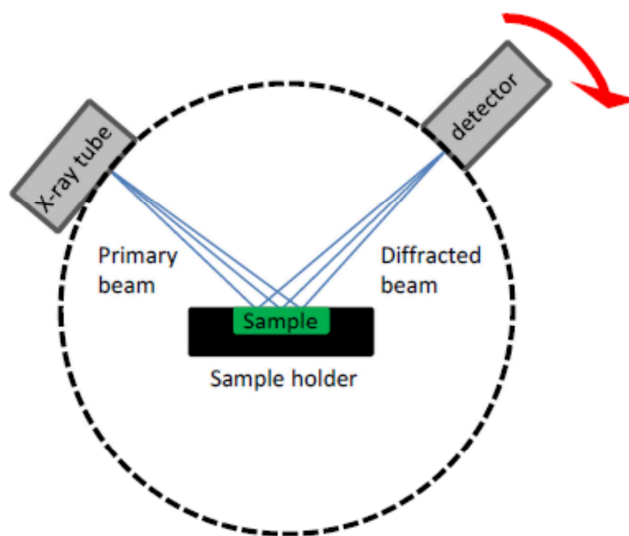
Fig. 2.2 Schematic illustration of Bragg-brentano geometry.[4]

X-ray powder diffraction patterns were recorded on a Bruker D8 Discover with Ni-filtered Cu-Kα radiation (1.5406 Å). Measurements were performed in Bragg-Brentano geometry (Fig. 2.2). The radiation diffracted by the sample was registered by a position-sensitive detector (Vantec).[4]

2.3.2 Electron Microscopy

Electron microscopy is most frequently used in solid state physics and chemistry to study the crystal structure of solids and the samples' surface topography, and composition. Normally electron microscopes use a beam of electrons focused by magnetic lenses to illuminate a sample and produce a magnified image. According to E. K. Abbe, in microscopy, distances d are

resolvable if $d \geq \lambda \,/\, n \; \sin\alpha$ where $n \; \sin\alpha$ is defined as numerical aperture and α is half the angle of aperture of the objective. Increase of α leads to a maximum resolution of $d_{min} = \lambda/2$. The use of visible light in optical microscopy therefore limits the resolution to d_{min} = ca. 200 nm. As the electrons have wavelengths that are much shorter than those of visible light photons, electron microscopes are able to achieve very high resolution. Commonly two different microscopic techniques are used, namely Scanning Electron Microscopy (SEM) and Transmission Electron Microscopy (TEM).

2.3.3 Scanning Electron Microscopy (SEM)

The SEM instrument is made up of two main components, the electronic console and the electron column. Control knobs and switches that allow for instrument adjustments such as filament current, accelerating voltage, focus, magnification, brightness and contrast are provided by the electronic console. The electron column is where the electron beam is generated under vacuum, focused to a small diameter, and scanned across the surface of a sample by electromagnetic deflection coils. The secondary electron detector is located above the sample holder (Fig. 2.3).
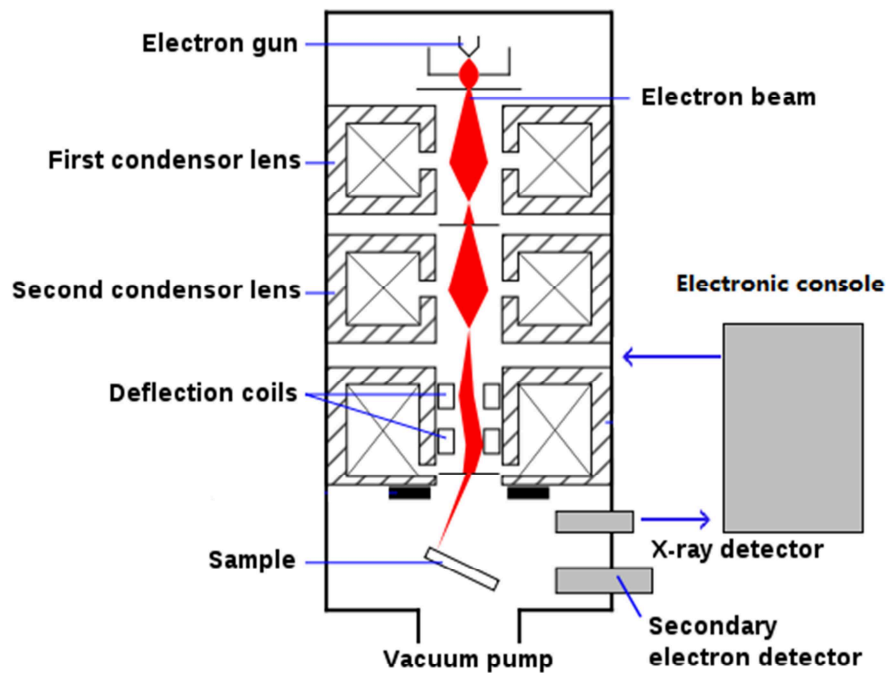
Fig. 2.3 Schematic illustration of scanning electron microscopy.[5]

When the electron beam hits the sample, there are several possible interactions of the impinging elecrons with the sample (Fig. 2.4). The so-called secondary electrons are dislodged by primary electrons from the sample, meanwhile transferring their energy to the sample by inelastic scattering. The signal generated by the detection of secondary electrons is amplified, and pixel intensity proportional to the number of emitted electrons is obtained.[5]
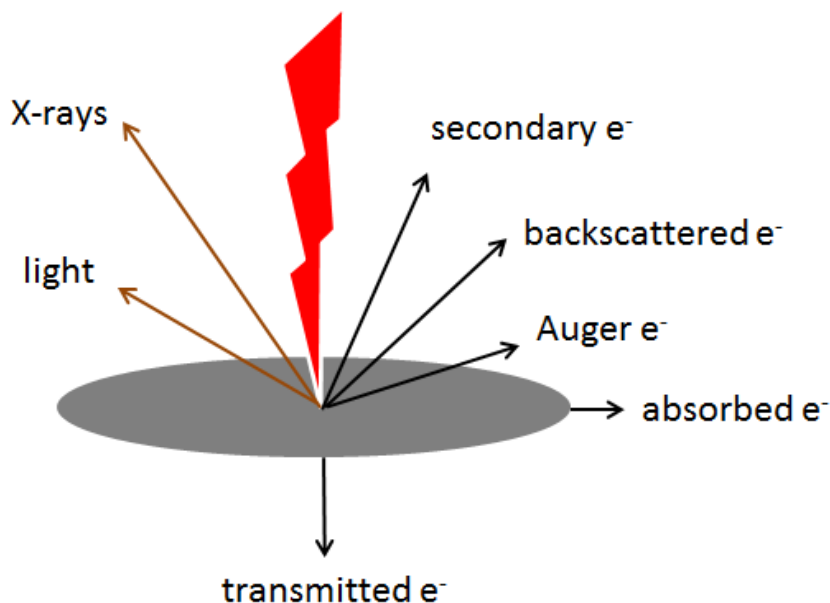
Fig. 2.4 Possible interactions between electron beam and samples.[4]

The backscattered electrons, which result from elastic scattering interactions with the atomic nucleus, can provide information about the composition of the scanned material, as electrons are backscattered more efficiently from heavier elements. X-ray photons excited by an outer shell electron that re-occupy the vacancy can provide the characteristic wavelength distributions for different elements. The amounts of secondary and backscattered electrons are dependent on the acceleration voltage of the primary electron beam and of course on the sample morphology.[6] Therefore, with the help of SEM we can obtain information about the morphology and the elemental composition of the particular sample.

Scanning electron microscopy was conducted on a JSM-6500F instrument (Jeol). Nonconductive samples were sputtered with carbon by low-vacuum sputter coating.

2.3.4 Transmission Electron Microscopy (TEM)

TEM, which can facilitate the analysis of features at the atomic scale by high energy electron beam, provide a much higher resolution than SEM, as the acceleration voltage is significantly higher (80 – 300 kV). TEM records images by collecting electrons that are transmitted through the sample, unlike SEM which produces images by collecting electrons ejected from or near the surface of the sample. Therefore TEM specimens are required to be at most hundreds of nanometers thick. The transmitted electrons are firstly focused by the objective lens to form a magnified 'image' which is further magnified by the projective lenses to create the final image that can be detected by a fluorescent screen or by a CCD camera (Fig. 2.5).
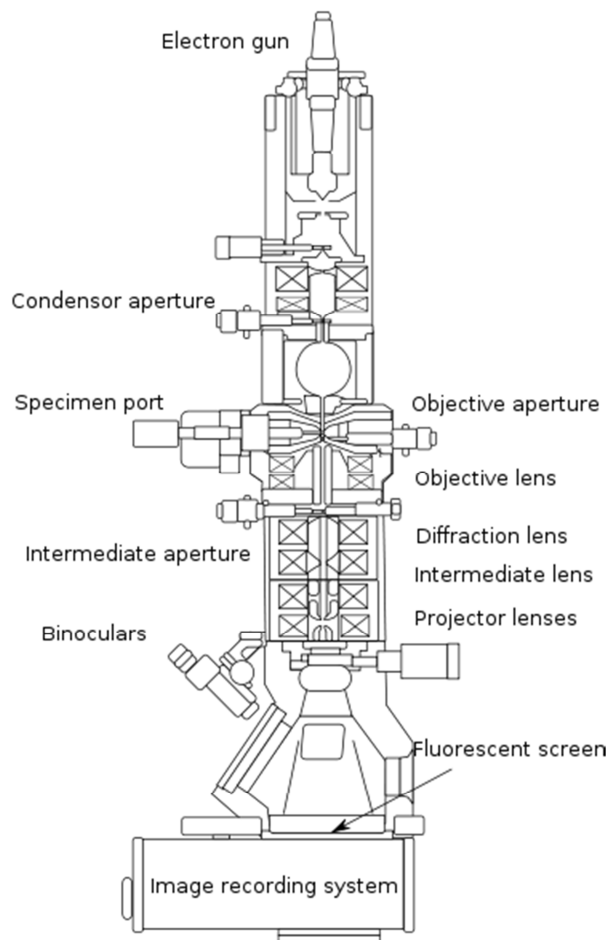
Fig. 2.5 Schematic illustration of transmission electron microscopy, containing four main parts - electron source, electromagnetic lens system, specimen holder and imaging system.[7]

TEM measurements were carried out on a JEOL 2001 instrument equipped with a tungsten cathode operating at 200 kV. The images were recorded by a TVIPS CCD camera.

2.3.5 X-ray Photoelectron Spectroscopy (XPS)

X-ray photoelectron spectroscopy is a quantitative spectroscopic technique that measures the elemental composition, empirical formula, chemical state and electronic state of the elements that exist within a material. By irradiating a material with an X-ray beam while simultaneously measuring the kinetic energy and number of electrons that escape from the surface (1-10 nm) of the material being analyzed, XPS spectra are obtained. Meanwhile XPS requires ultra-high vacuum (UHV) conditions to provide an unobstructed path for emission and detection of photoelectrons. Typically XPS uses either monochromatic Aluminum Kα or non-monochromatic Magnesium Kα X-rays[8] to eject a photoelectron from an atom at the sample's surface. An electron from a higher energy level can then refill the hole left behind and its emitted radiation energy is used to eject an Auger electron. Thus, XPS emits both photoelectrons and Auger electrons which can be seen in the spectrum. The electrons ejected are analyzed in the XPS detector by measuring the electron's kinetic energy which provides the information to determine the kind of elements present in the sample. Fig. 2.6 illustrates the schematic representation of the X-ray photoelectron process.
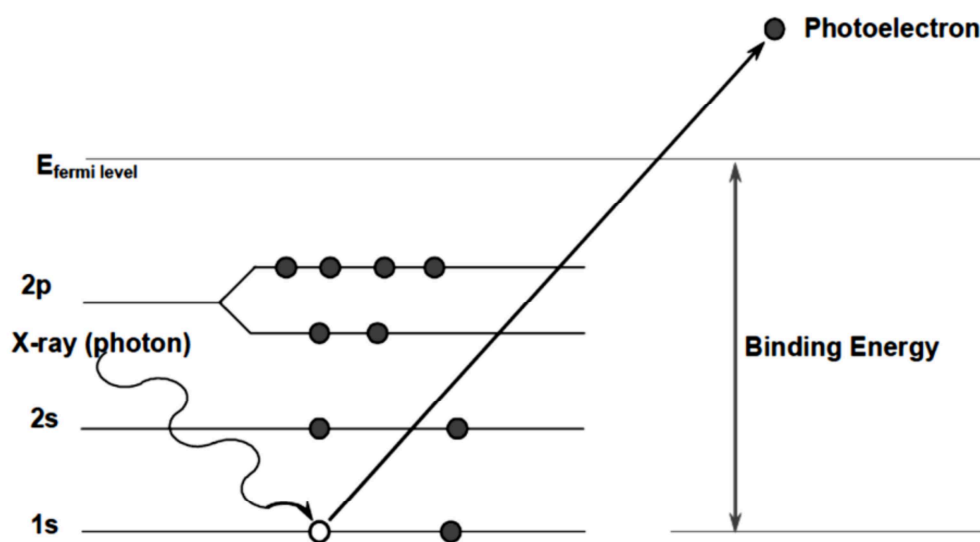
Fig. 2.6 Schematic representation of the X-ray photoelectron process.[8]

If the energy of an X-ray with particular wavelength is known, the electron binding energy of each of the emitted electrons can be determined by using the equation[9] as followes:

$$E_k = h\nu - E_b - \phi$$

Where E_b is the binding energy of the electron, $h\nu$ is the energy of the X-ray photons being used, E_k is the kinetic energy of the electron as measured by the instrument and ϕ is the work function of the spectrometer. Considering that the binding energy is a unique property for each atom, the presence of peaks at different binding energies can be used to identify the elemental composition in the sample.

2.3.6 Nuclear Magnetic Resonance (NMR) Spectroscopy

NMR spectroscopy is a research technique to determine physical and chemical properties of atoms or the molecules in which they are contained.[10,11] There are two kinds of NMR: solution state NMR and solid state NMR. The main parts (Fig. 2.7) of an NMR instrument are the magnet, radio frequency generator and recorder. Usually a superconducting magnet, which generates a strong focused magnetic field running through the center of the instrument, is required. This technique relies on the phenomenon that atomic nuclei absorb electromagnetic radiation at a frequency characteristic of the isotope when placed in a magnetic field. Through exploiting the quantum mechanical magnetic properties of certain atomic nuclei, NMR spectroscopy can provide detailed information about the chemical structure, reaction state and chemical environment of molecules.[12]
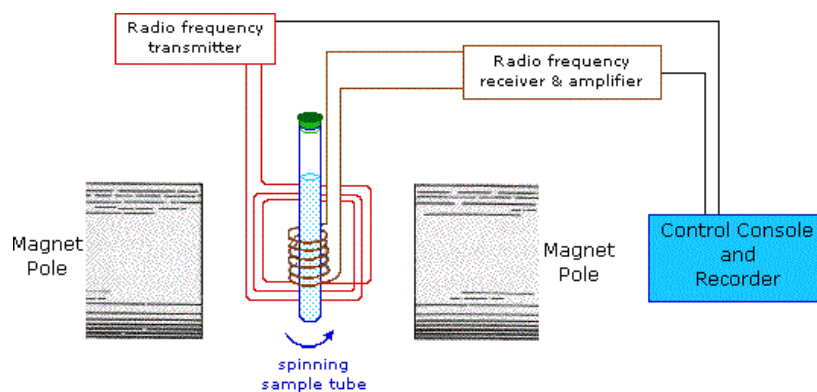
Fig. 2.7 Schematic illustration of the NMR.[12]

To be specific, when a sample is placed into the magnetic field and is subjected to a proper radiofrequency of radiation, the atomic nuclei in the lower energy spin state can be excited to the higher energy spin state. The magnetic moment of the lower energy state is aligned with the external field, but that of the higher energy spin state is opposed to the external field. The energy difference between the two spin states is $\Delta E = \mu B/I$ (μ is magnetic moment, B is magnetic field and I is the characteristic spin). Since the energy difference between the two spin states is proportional to the strength of the external magnetic field, an NMR spectrum for a sample can be gained by varying the magnetic field at a constant frequency radiation or by varying rf radiation with the magnetic field kept constant. The signals are usually reported relative to a reference signal, usually that of TMS (tetramethylsilane), and then the chemical shift (δ) can be obtained:[13]

$$\delta = \frac{\nu_{\text{sample}} - \nu_{\text{TMS}}}{\nu_{\text{TMS}}} \times 10^6$$

Detailed information about the chemical structure, reaction state and chemical environment of molecules can be determined by the chemical shift.

Solution-state NMR spectra were recorded on an Eclipse EX-400 spectrometer (JEOL, 400MHz) and solid state NMR spectra were recorded on a DSX 500 Avance (Brucker) FT-NMR spectrometer with an external magnetic field of 11.4 T at room temperature. The rotation frequencies were 6 KHz or 12 KHz.[14]

2.3.7 FTIR and UV-Vis Spectroscopy

Fourier transform infrared (FTIR) spectroscopy is a technique which is used to obtain an infrared spectrum of absorption of a solid, liquid or gas. An FTIR spectrometer simultaneously collects spectral data in a wide spectral range normally from 400-4000 cm^{-1}. IR spectra of the solids were recorded in reflection geometry using a Spectrum BX II FTIR spectrometer (Perkin Elmer) equipped with a DuraSampler diamond ATR unit at room temperature.

Ultraviolet-visible (UV-Vis) spectrophotometry is a technique used to investigate the ability of a compound to absorb light in the visible, near-UV and near-infrared ranges of the electromagnetic spectrum; typically a range from 800 - 200 nm is covered.[15-17]
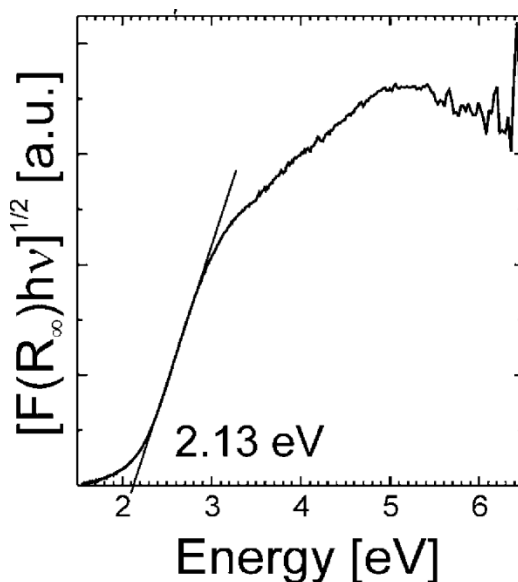
Fig. 2.8 Band gap determination based on the Kubelka-Munk function using $[F(R_\infty) h\nu]^{1/2}$ vs $h\nu$ plots.[18]

For the determination of the optical band gap of a powder sample, normally the Kubelka–Munk function is used.[18,19] Band energy can be determined using the equation $a = A(h\nu - E_g)^n/h\nu$ where a is absorption coefficient, A is a constant, $h\nu$ is the energy of light and n is a constant depending on the nature of the electron transition. Assuming n is some value determined according to the sample and that the absorption coefficient a is proportional to the Kubelka-Munk function $F(R_\infty)$, the band gap energy can be obtained from the plots of $[F(R_\infty) h\nu]^{1/2}$ vs $h\nu$ as the intercept at $[F(R_\infty) h\nu]^{1/2}=0$ of the extrapolated linear part of the plot (Fig. 2.8).

The UV-VIS spectra were recorded on a Hitachi U-3501 UV-Vis spectrophotometer having a resolution of ±0.1 nm for the solid samples. In this double-beam spectrometer, D2 (187 – 340 nm) and W (340 – 3200 nm) lamps are used as the light source. The absorption spectra were observed for the range from 300 nm to 600 nm at room temperature.

2.3.8 Elemental Analysis and Mass Spectrometry

Elemental analysis (EA) for the carbon nitride samples always reference to CHNX analysis—the determination of the mass fractions of carbon, hydrogen, nitrogen, and heteroatoms (X) (halogens, sulfur). This information is important to help determine the structure, as well as to help ascertain the structure and purity of a synthesized compound.

Determination of the elements H, N, C, S and Cl was conducted by the microanalytical laboratory of the Department of Chemistry, LMUMunich. A commercial elemental analyzer system VARIO El was used with He as carrier gas.

Mass spectrometry (MS) is an analytical technique that measures the mass-to-charge ratio of charged particles by ionizing chemical compounds and generating charged molecules or molecular fragments.[20]
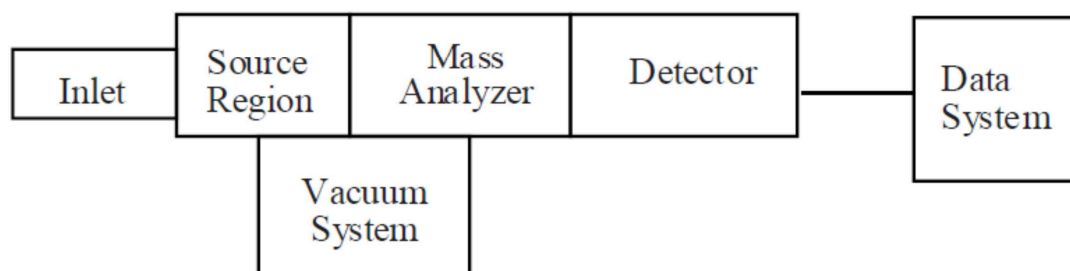
Fig. 2.9 Schematic illustration of the Mass spectrometry process.[20]

The mass spectrometer basically consists of three modules: an ion source, which can convert gas phase sample molecules into ions; a mass analyzer, which sorts the ions by their masses by applying electromagnetic fields; a detector, which measures the value of an indicator quantity and thus provides data for calculating the abundances of each ion present. Typically, the samples are transferred into the vacuum chamber of the mass spectrometer from the inlet. The neutral sample molecules are ionized in the source region and then accelerated into the mass analyzer. The ions are separated in this section by applying electromagnetic fields, either in time or in space, according to their mass-to-charge ratios. After separating, they are detected and signals are transferred to a data system for analysis (Fig. 2.9).

Mass spectra were obtained using a Mstation JMS-700 spectrometer (JEOL) with a mass resolution of $\geq 1ue^{-1}$. Ionization was achieved by fast atom bombardment (FAB), by direct electron impact (DEI) or by direct chemical impact (DCI).

2.4 Chapter References

[1]   W. Friedrich, P. Knipping, von M. Laue, *Sitzungsberichte der Mathematisch-Physikalischen Classe der Königlich-Bayerischen Akademie der Wissenschaften zu München* **1912**.

[2]   J. R. Connolly, *Introduction to x-ray powder diffraction*. **2009**.

[3]   Y. Li, PhD thesis, *LMU München, Munich*, **2012**, p. 31.

[4]   Y. Liu, PhD thesis, *LMU München, Munich*, **2006**, p. 32.

[5]   J. W. S. Hearle, J. T. Sparrow and P. M. Cross, *The use of the scanning electron microscope*, **1972**.

[6]   P. Goodhew, J. Humphreys, and R. Beanland, *Electron microscopy and analysis. Third Edition*. **2000**.

[7]   D. Williams, and C. B. Carter, *Transmission Electron Microscopy. 1 – Basics*, ISBN 0-306-45324-X, **1996**.

[8]   C. D. Wagner. *Handbook of x-ray photoelectron spectroscopy: a reference book of standard data for use in x-ray photoelectron spectroscopy*, **2010**.

[9]   Raaen,S., *Electronspectroscopy*, **2001**.

[10]   J. W. Akitt and B. E. Mann, *NMR and Chemistry, UK: Stanley Thornes*, **2000**.

[11]   J. Keeler, *Understanding NMR Spectroscopy, John Wiley & Sons*, **2005**.

[12]   F. A. Bovey, *Nuclear Magnetic Resonance Spectroscopy, Academic Press In., New York*, **1991**.

[13]   J. Shoolery, *A Basic Guide to NMR, 3rd Edition*, **2008**.

[14]   A. Sattler, PhD thesis, *LMU München, Munich*, **2010**, p. 23.

[15]   D. C. Harris, *Quantitative Chemical Analysis,7th Ed., Freeman, New York,* **2007**.

[16]   J. P. Sibilia, *Materials Characterization and Chemical Analysis, Wiley-VCH, New York*, **1996**.

[17]   D. A. Skoog, F. J. Holler and S. R. Crouch, *Principles of Instrumental Analysis,6th Ed.*, **2004**.

[18]   R. Beranek, H. Kisch, *Photochemistry Photobiological Sciences*,**2007**.

[19]   G. Meichsner, J. Schröder, *Lackeigenschaften messen und steuern*, ISBN 3878707398, **2003**.

[20]   A. Sparkman, O. David, *Mass spectrometry desk reference*. ISBN 0-9660813-2-3, **2000**.

Chapter 3

Insights into the thermal condensation of melem: ''Melem oligomers'' and ultra-long calcined Melamine

3.1 Introduction

Semiconductor photocatalyst development promises a clean, cheap and ethically-sound relief to global energy demands and climate change. Since Fujishima and Honda first reported the decomposition of water on illuminated TiO_2 electrodes in 1972,[1] technologies such as photocatalytic water splitting to produce hydrogen are seeing increasing importance for researchers. Apart from TiO_2, metal-free g-C_3N_4 carbon nitrides are also promising semiconductor photocatalysts. These polymeric semiconductors are easily synthesized, have high thermal stability, are highly functional and show significant visible-light photocatalytic activity.[2,3]

Recently, it has been reported by Antonietti et al.[3] that a polymer semiconductor on the basis of a defective graphitic carbon nitride (g-C_xN_y) was used as a photocatalyst for the splitting of water under visible-light irradiation. Interestingly, Antonietti and coworkers have demonstrated that highly condensed and crystalline carbon nitrides tend to be less active photocatalysts than 'defect-containing' (more hydrogen, less crystallinity) carbon nitrides.[4] Therefore, it is instructive to synthesize different forms of 'defect-containing' carbon nitrides and investigate their photoactivity to see how the activity relates to these structures. Although most research focuses on melon-type materials (one-dimensional, heptazine-based carbon nitrides) due to its rather low band gap (2.7 eV),[3] fewer researchers investigate the photoactivity of the less condensed carbon nitride materials which undergo less condensation than melon but are, on average, more condensed than melem. Herein we have chosen to synthesize these melem oligomers in an open system at relatively low temperatures in order to prevent good crystallization and check whether we can obtain forms of less condensed melon-type materials.

Melem and melon are well studied carbon nitride materials. Melem (2,5,8-triamino-tri-*s*-triazine) $C_6N_7(NH_2)_3$ can be obtained by thermal treatment of simpler, less condensed C-N-H compounds e.g. melamine $C_3N_3(NH_2)_3$, dicyandiamide $H_4C_2N_4$, ammonium dicyanamide $NH_4[N(CN)_2]$, or

cyanamide H_2CN_2 at temperatures up to 450 °C in sealed glass ampoules.[5] Melon ($[C_6N_7(NH)_2(NH_2)]_n)_2$ which is the polymerization product of melem, can be synthesized by thermal treatment of melamine in sealed silica glass ampoules under vacuum at temperatures between 560 and 600 °C for 12 – 36 hours.[6]

As mentioned before, our melem oligomer (melamine calcined sample) is less condensed than melon but it is, on average, more highly condensed than melem, as will be outlined below. These kinds of CN materials likely have larger band gaps than melon as they are less condensed – visible by their lighter color – and also have more defect sites. Literature on this topic describes carbon nitride denoted as $g\text{-}C_xN_y$, and in this work such materials are normally considered to be melon.[3,7,8]

In literature, melon was prepared in vacuum or nitrogen at temperatures between 560 and 600 °C for 12 – 36 h, or in an open system at 490 °C for 72 h. [4][6] Recently, it has been reported by Liu et al.[9] that melon prepared in an open system furnished graphene-like nanosheets by direct thermal oxidation. The resultant nanosheets possess a large surface area and show superior photocatalytic activities compared to bulk melon. Hereby, we have chosen to extend the calcination time at different temperatures in order to get large surface area ultra-long calcined melamine which could possess graphene-like carbon nitride nanosheets.

As the melem oligomers were synthesized in two different synthesis systems which were open to the atmosphere, here these open systems are explained in detail, as shown in Fig. 3.1. The left image displays the sample inside a small glass vial, which was then placed into a larger vial using quartz fiber to block the mouth of the vial. The right image shows a porcelain crucible-based open system.
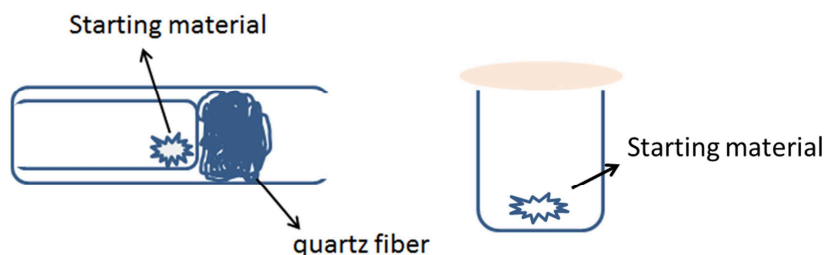
Fig. 3.1 Schematic illustration of the half open glass vials system (left) and open system (right).

3.2 Results and Discussion

Characterizations of the composition and structure, such as by XRD, IR, UV-Vis, XPS, TEM, NMR and so on, are important for material identification. Melem oligomer supposedly is a compound with a condensation degree between that of melem and melon. In the following, the analytical data of melem oligomer will therefore be compared with that of melem and melon. As XRD is the chief method for characterizing the atomic structure of new materials, XRD results will be discussed firstly.

3.2.1 X-ray powder Diffraction
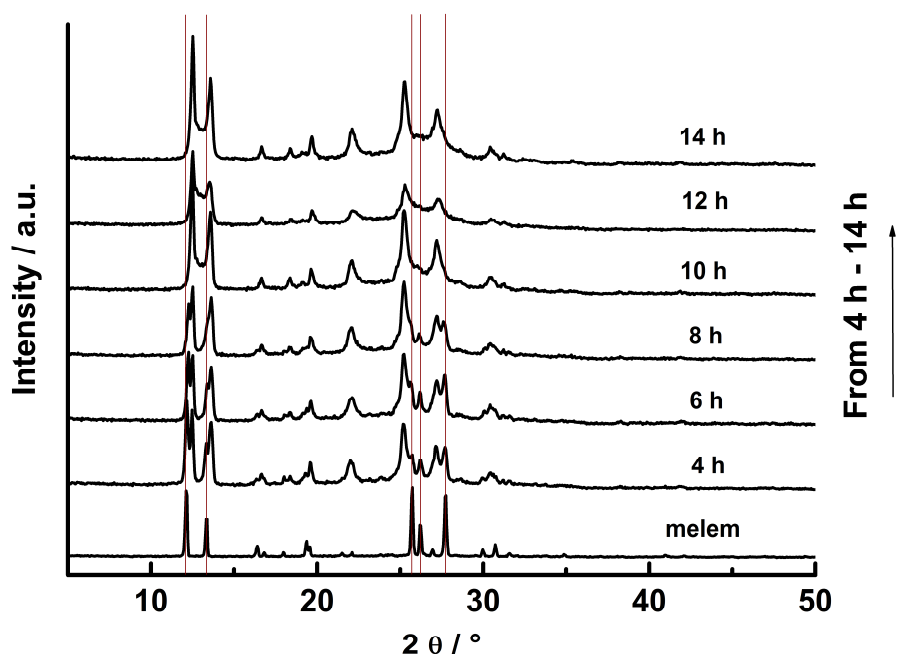
Fig. 3.2 XRD patterns of melamine calcined for 4 – 14 h at 450 °C in an open system compared to melem.
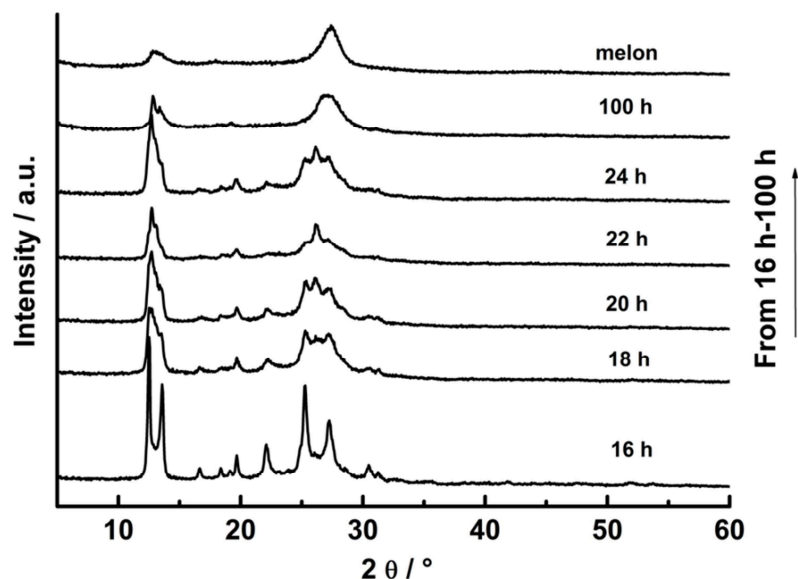
Fig. 3.3 XRD patterns of melamine calcined for 16 – 100 h at 450 °C in an open system, compared to melon (prepared in an open system at 490 °C for 72 h).

Fig. 3.2 and 3.3 show the XRD reflections of melamine calcined at 450 °C in a crucible for various calcination times, together with melem which was prepared in a closed ampoule at the same temperature, and with melon which was prepared in an open system at 490 °C for 72 h. The XRD pattern of melamine calcined for 4 h shows that the sample has two main crystalline phases, and one phase is melem[5] which can be seen in Fig. 3.3. Interestingly, it can be seen that while melem is gradually fading, a new crystalline phase seems to be formed concomitantly which has a similar XRD signature compared to melem. The crystalline melem phase seems to have disappeared after 10 hours calcination, while after 24 hours calcination, the characteristic melon signature is not yet seen (Fig. 3.3). However after 100 hours calcination there is a broad peak observed near the melon characteristic signature at 27.3° 2θ. This indicates that there is a continuous transformation process from the melem phase to the melon-type phase. The peak at around 13° 2θ is split into two peaks, meaning that melamine calcined for 100 h sample is not identical with melon prepared in an open system at 490 °C. One noticeable experimental detail should be pointed out here: The experiments were conducted in the crucible with a loose lid on top (Fig. 3.1 right), which means that the experiments were carried out under close to atmospheric pressure. It is reported that temperature and pressure are crucial factors which can have a significant influence during the carbon nitride formation.[4] Therefore, different polymeric carbon nitrides can be gained with different synthesis procedures.

In the following, the glass vial half open system (Fig. 3.1 left) was used to synthesize calcined melamine samples.
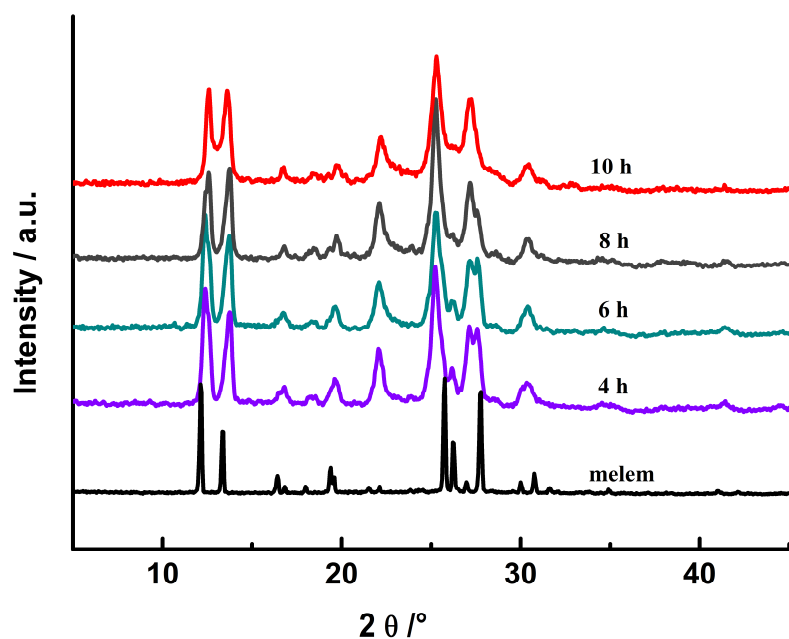
Fig. 3.4 XRD patterns of melamine calcined for 4 – 10 h at 450 °C in the half open glass vial system.
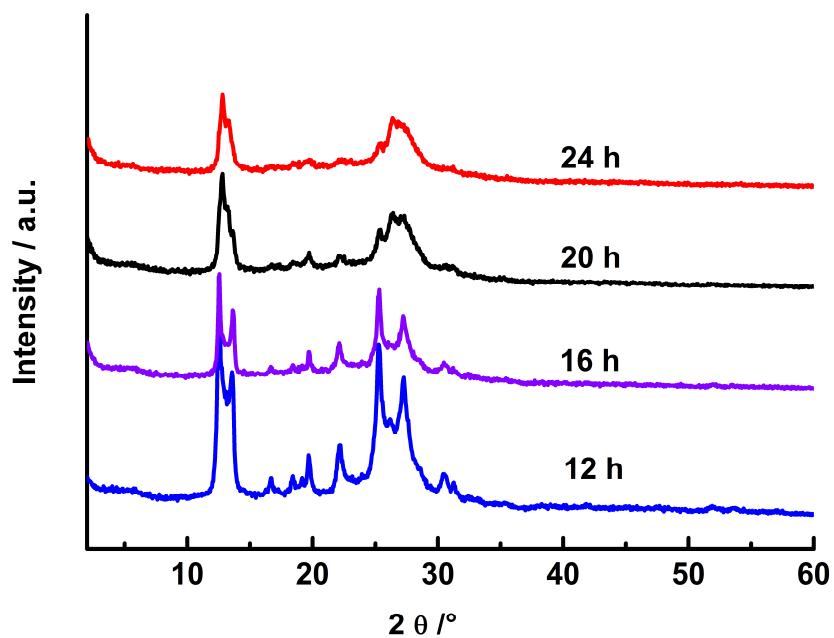
Fig. 3.5 XRD patterns of melamine calcined for 12 – 24 h at 450 °C in the half open glass vial system.

Fig. 3.4 and Fig. 3.5 show the XRD patterns of melamine calcined for 4 – 24 hours at 450 °C in the half open glass vial system. Compared with melamine calcined in the crucible, there are less phases observed. As melem was synthesized in a closed ampule, it was synthesized at high (autogeneous) pressure. Because of the quartz fiber, in the half open glass vial system the pressure should be much lower than in an ampule, but higher than under conditions of atmospheric pressure. According to the XRD patterns, the pressure of the reaction vessel is an important factor determining the crystalline structure of the products. It seems that under high pressure one major crystalline structure can be gained, and multiple crystalline structures are obtained under atmospheric pressure. However, for the half open glass vial system, the pressure of the reaction vial cannot be controlled or detected precisely. Therefore, in this work, we mainly focus on the samples synthesized in a crucible with a loose lid on top, which can be well reproduced.

As for the samples calcined under such conditions, two crystalline phases can initially be seen in the XRD patterns. The XRD patterns of melamine and various melamine-melem adducts[10] were compared with melamine calcined for 4 h. From the XRD comparison (Fig. 3.5), it is obvious that there is no melamine or melamine-melem adduct phase in the calcined sample.
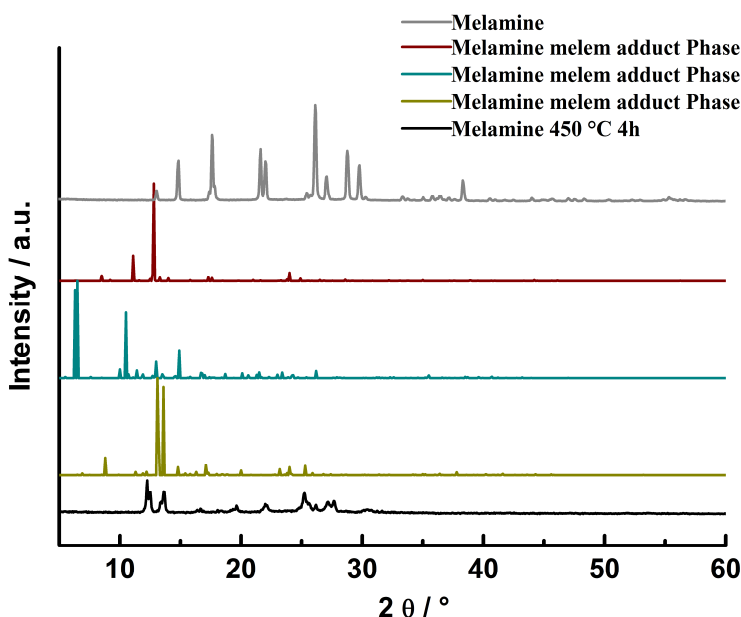
Fig. 3.6 XRD patterns of melamine calcined for 4h at 450 °C in open system together with melamine and melamine-melem-adduct (formula for phase I II III are $2C_3N_3(NH_2)_3 \cdot C_6N_7(NH_2)_3$, $C_3N_3(NH_2)_3 \cdot C_6N_7(NH_2)_3$ and $C_3N_3(NH_2)_3 \cdot 3C_6N_7(NH_2)_3$).
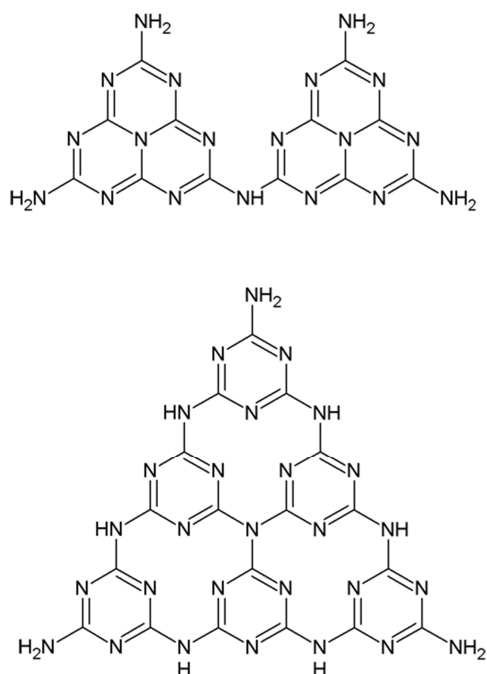
Fig. 3.7 Possible structures of the calcined melamine samples based on heptazine units (dimer, above) and based on triazine units (hexamer, below).

A possible explanation could be that the calcined melamine sample is a polymerized oligomer based on heptazine or triazine units, most probably heptazine (Fig. 3.7). Triazine-based structures obtained at higher temperatures – except for melam – have so far only been observed as products under ionothermal conditions, i.e. syntheses in salt melts (poly(triazine imide) with intercalation of lithium and chloride ions).[11] In the calcination process, multiple crystalline structures could be formed composed of various heptazine units, such as a mixture of melem, a melem dimer as shown in Fig. 3.7 (top), a melem trimer, or even more highly condensed oligomers. The XRD pattern (Fig. 3.2) clearly shows that melem is contained in the sample calcined for 4 hours, and that there is another crystalline phase that could be another unknown modification of melem, or a dimer phase. As melem can be dissolved in hot dimethyl sulfoxide (DMSO),[5][10] hot DMSO could be used to wash away melem and investigate the nature of the residue.

Fig. 3.8 shows the XRD patterns of samples calcined for 4 – 10 h after washing with hot DMSO, together with the calcined 10 h sample, melem and melon. We can see that after washing, the XRD signals of the samples were quite weak and significantly broadened. The XRD pattern of the calcined 10 h sample after DMSO washing was very different from that before washing.

Most of the peaks in the calcined 10 h sample disappeared, only the peak at around 27° is maintained. A new peak at around 13° appears, which is similar with the peak of the melon sample. One possibility is that during the washing procedure, hot DMSO has washed away the crystalline melem phase, and only essentially amorphous structures are left. The other possibility is that hot DMSO not only dissolved melem, but also partly destroyed the crystalline structure of the residue. The 4h sample, which barely shows any XRD signature after washing, may indicate that both crystalline phases present after 4h were washed away by DMSO, thus suggesting that both phases were in fact different modifications of melem and, hence, soluble in DMSO. One noticeable experimental detail should be pointed out here: The amount of the residues is around 50-70 % less than that of the initial material, which is indirect evidence that melem was dissolved. As the DMSO washing solution was too diluted, the liquid NMR did not give any melem signal.
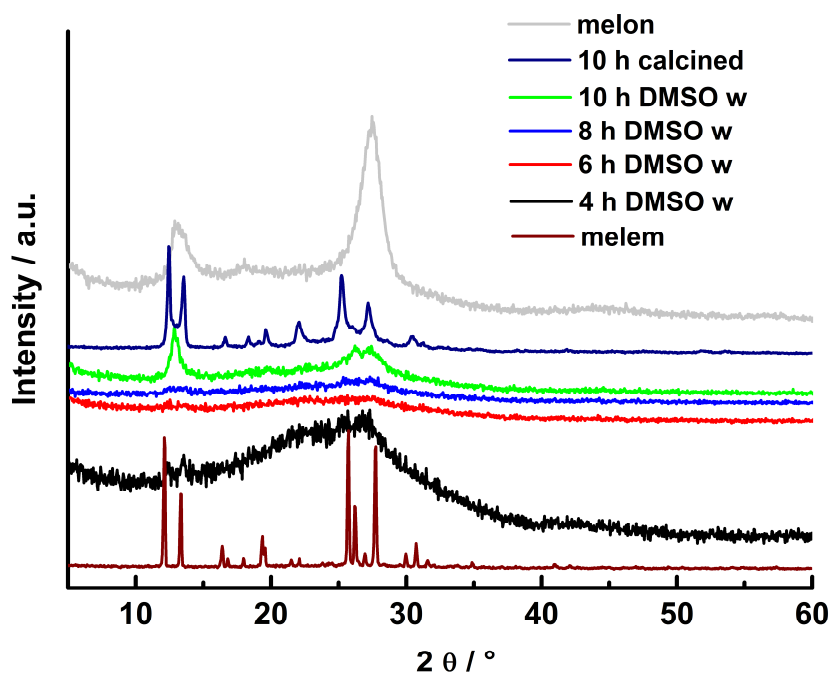
Fig. 3.8 XRD patterns of melamine calcined for 4 – 10 h at 450 °C in an open system after washing with hot DMSO solution, together with melem and melon prepared in an open system.

By increasing the calcination time, the calcined samples transform from melem to a melon-type material. When the calcination time was extended to very long times (160 h), according to the XRD patterns, melon-type materials were gained. It can be seen from Fig. 3.9 that all the samples have an XRD pattern similar to that of melon in Fig 3.8. The XRD pattern of melon

obtained by calcination at 490 °C for 72 h has a major strong peak at 27.6° 2θ which can be indexed as the "graphitic" layer spacing 00l reflection corresponding to a d-spacing of roughly 3.3 Å.[12–15] For these ultra-long calcined samples, we see a reflection at around 26.6 – 27.6° 2θ. However, the positions of these reflections are not exactly the same, but rather shift to higher angles and thus lower d-values with the calcination temperature increasing. This indicates a structural contraction along the layer stacking direction, presumably as a result of a more extended condensation of the carbon nitride chains at elevated temperature.[16] There are several explanations for the peak at 2θ = 13.1°; the 2θ value corresponds to a distance d = 6.75 Å which is typical of more oriented melon.[17] Alternatively, this reflection may relate to an in-plane structural packing motif of the heptazine building block, such as the hole-to-hole distance between two neighboring heptazine rings in the crystal.[4] Interestingly, two reflections can be seen at around 12.7 – 13.3° instead of one when the calcination temperature is not more than 450 °C. This observation could suggest that the ultra-long calcined samples prepared at 430 – 450 °C have at least a partially different crystalline structure with respect to melon prepared at 470 – 490 °C, or there could be some melem left in the ultra-long time calcined samples prepared at 430 – 450 °C. The extra reflection at 13.3° is one of typical reflections for melem sample. Meanwhile, according to the TEM diffraction patterns (Fig. 3.21) melem was found in the ultra-long calcined melamine prepared at 430 °C. For the ultra-long calcined melamine prepared at or below 450 °C there should therefore be a mixture of melem and melon-type phases, and the ultra-long calcined melamine prepared above 450 °C should be mostly composed of a melon-type material.
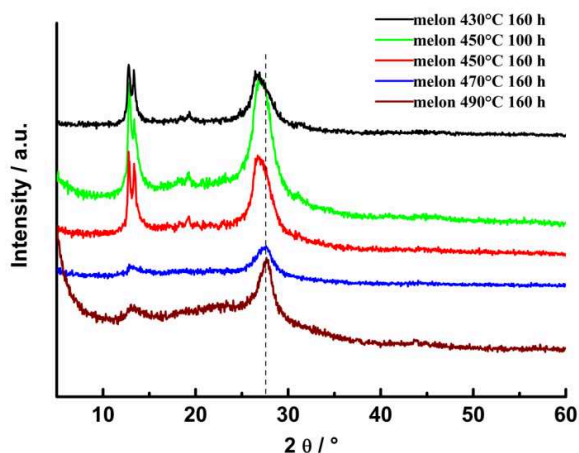

Fig. 3.9 XRD patterns of melamine calcined for 100 or 160 h at 430 – 490 °C in an open system.

41

3.2.2 IR Spectroscopy

The IR spectra of the calcined melamine samples (open system) are displayed in Fig. 3.10 and Fig. 3.11, together with melem and melon as references. The observed wavenumbers, together with a tentative band assignment, are given in Table 3.1. The bands at 3488 cm^{-1} and 3423 cm^{-1} are assigned to the N-H stretching mode v(NH)[5] and are typical bands of melem. The medium intensity and sharp band at around 800 cm^{-1} suggests the materials consists of a non-protonated heptazine or triazine core,[18] but a clear assignment to either of the two is not possible.[19] It can be seen that after 10 hours calcination, the bands at 3488 cm^{-1} and 3423 cm^{-1} are not observed any more, which indicates that the crystalline melem phase has largely disappeared. This phenomenon also corresponds well with the XRD results. After 10 hours calcination, two prominent bands at 1320 cm^{-1} and 1240 cm^{-1} appear, which suggest a C-N single bond stretching vibration of the bridging C-NH-C (or C-N(-C)-C) moiety in carbon nitride polymers.[19] Meanwhile, two medium strong bands are found at 1454 cm^{-1} and 1402 cm^{-1} after 10 hours of calcination. This feature has been observed in several carbon nitride materials with an assumed heptazine-based structure.[14,20,21] After 100 hours calcination a weak band at around 1205 cm^{-1} was found, which is also seen in the hepatzine-based melon-type carbon nitride. The similarity of all the spectra is clearly evidenced by the sharp semicircle ring stretch at around 800 cm^{-1}, which indicates that all the samples are built up from heptazine or triazine units (Fig. 3.7).

Table. 3.1 Vibrational frequencies of melamine calcined for different times. Tentative assignments are given in the right column (v = stretching, δ = in-plane deformation, γ = out-of-plane deformation, ρ = rocking, ω = wagging; vs: very strong, s: strong, ms: medium strong, w: weak, vw: very weak, b: broad).[5]

IR bands	Assignment
3488, 3428, 3152 (*ms,b*)	v(NH$_2$), v(NH)
1633 (*s*)	δ(NH$_2$)
1572 (*ms*)	v(N=C)
1457, 1401 (*s*)	v(N=C)
1313 (*s*)	δ(NH), v(C-N)
1234 (*vs*), 1203 (w)	v(C-N)
1129,1076 (*w*)	ρ(NH$_2$)
1005 (*vw*)	v_{ring}
887 (*w*)	
810 (*m*)	ring sextant bend
775 (*w*)	ω(NH)
731,712 (*vw*)	γ(ring)
646 (*vw*)	ω(NH$_2$)
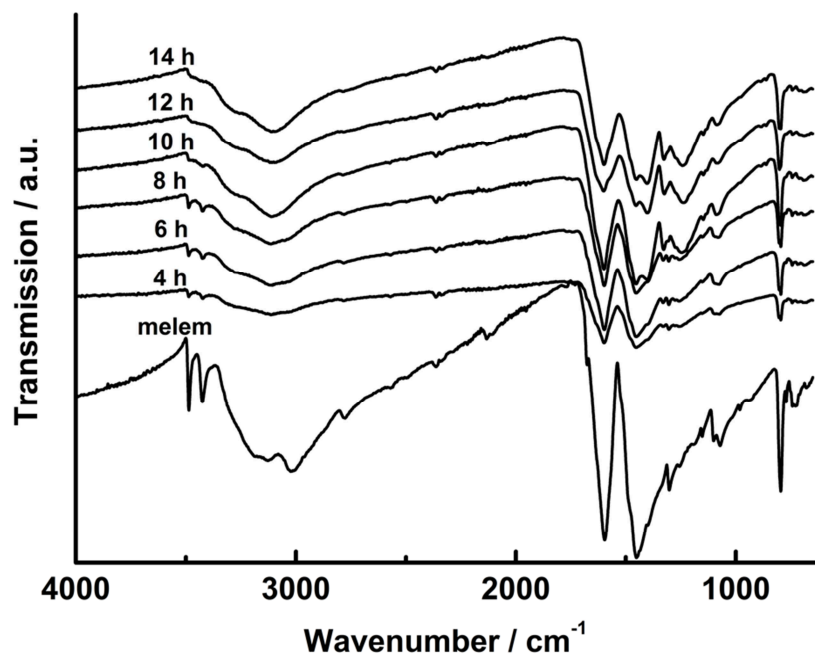
Fig. 3.10 FTIR spectra of melamine calcined for 4 – 14 h at 450 °C in an open system compared to melem.
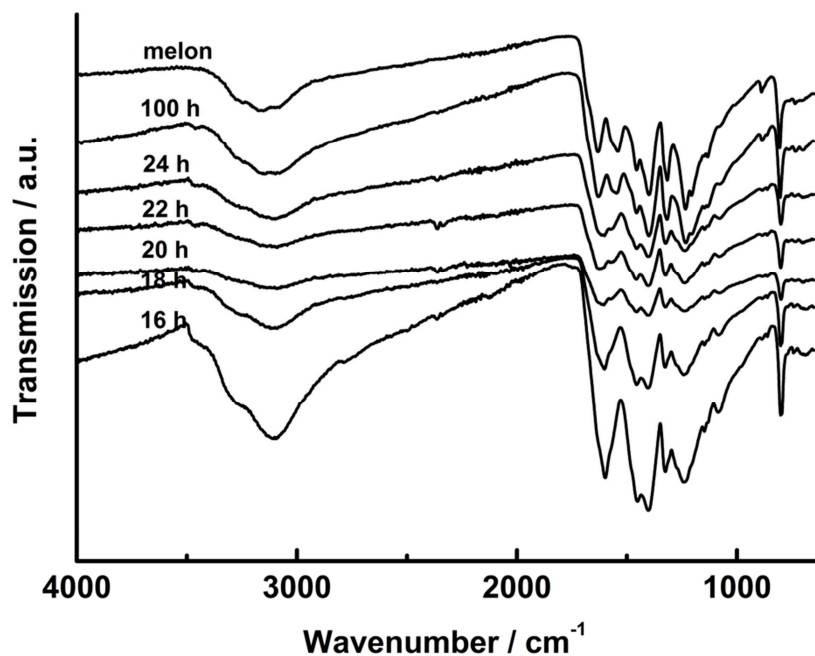
Fig. 3.11 FTIR spectra of melamine calcined for 16 – 100 h at 450 °C in an open system compared to melon prepared in an open system at 490 °C for 72 h.

Fig. 3.12 displays the FTIR spectra of melamine calcined for 4-10 h at 450 °C after washing with hot DMSO, together with the calcined 8 h and 10 h samples, melem and melon. It is clearly seen

43

that the calcined samples after washing with hot DMSO show similar FTIR spectra compared to melon. After washing, the two sharp bands at 3488 cm^{-1} and 3423 cm^{-1} characteristic of melem are missing, which suggests that there is no melem present in the residues. Two prominent bands appear at 1321 cm^{-1} and 1246 cm^{-1}, tentatively assigned to the C-NH-C group, which indicates that after washing the residues should contain some oligomers composed of two or more heptazine units. The initial materials are melem-like and the residues are melon like. This sheds some light on the composition of the calcined samples. A possible composition of the calcined samples could be a mixture of crystalline melem and less crystalline melem oligomers or melon; it also could be a mixture of two types of crystalline melem modifications and amorphous oligomers/polymers. However, so far there is no unambiguous evidence of the exact composition of the calcined samples owing to the insolubility of the oligomeric compounds in any solvent tested. Although we gain some clues as to the structural information of these materials, the complexity and challenge in discovering unambiguous structures of these polymer-like materials is evident.
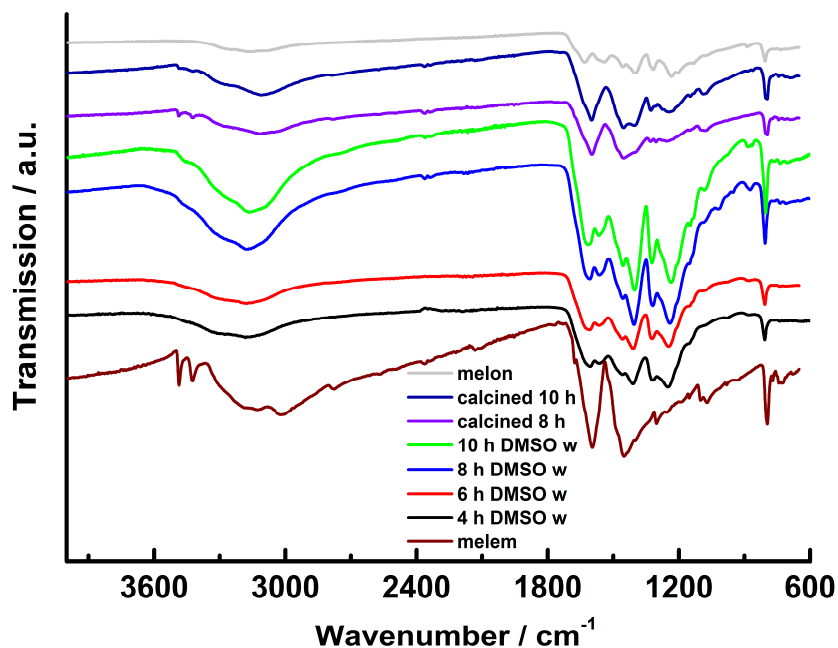
Fig. 3.12 FTIR spectra of melamine calcined for 4 – 10 h at 450 °C in an open system after washing with hot DMSO, together with melem and melon.
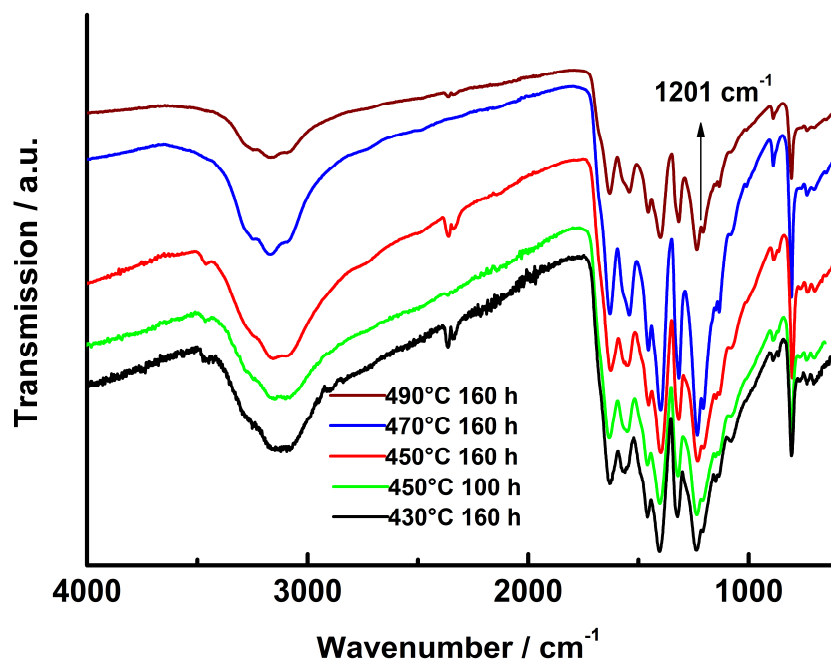
Fig. 3.13 FTIR spectra of melon calcined for 100 or 160 h at 430 – 490 °C in a crucible with a loose lid on the top.

The FTIR spectra (Fig. 3.13) of the ultra-long calcined samples are similar to each other and to that of melon synthesized at 490 °C for 72 hours. The IR spectra are clearly indicative of an at least partially ordered material owing to its well-resolved band structures. The medium intense sharp band at around 805 cm^{-1} suggests the samples consist of triazine or heptazine building blocks; the bands at 1234 and 1313 cm^{-1} indicate the presence of C-NH-C or C-N(-C)-C moieties, which can be inferred for the polymeric material. In principle, the weak band at around 1201 cm^{-1} could indicate the existence of C–N (sp^3) bonds,[22] as in the elusive β-C$_3$N$_4$[23,24][24] or "3D-like"[2,19] heptazine-based g-C$_3$N$_4$ structure obtained by semiempirical structure optimizations at the PM3 level (Fig 3.14).[25] However, the formation of 3D structures with a large fraction of sp^3 bonds or fully condensed graphitic C$_3$N$_4$ structures seems very unlikely in the present case owing to the synthesis conditions which typically furnish melon-type materials. Combining the FTIR and XRD results, the ultra-long calcined samples are polymeric materials likely based on heptazine building blocks and are, hence, melon-like. However, one cannot rule out that higher degrees of condensation appear at such long condensation times, ultimately leading to a graphite-like 2D structure (Fig. 3.15).
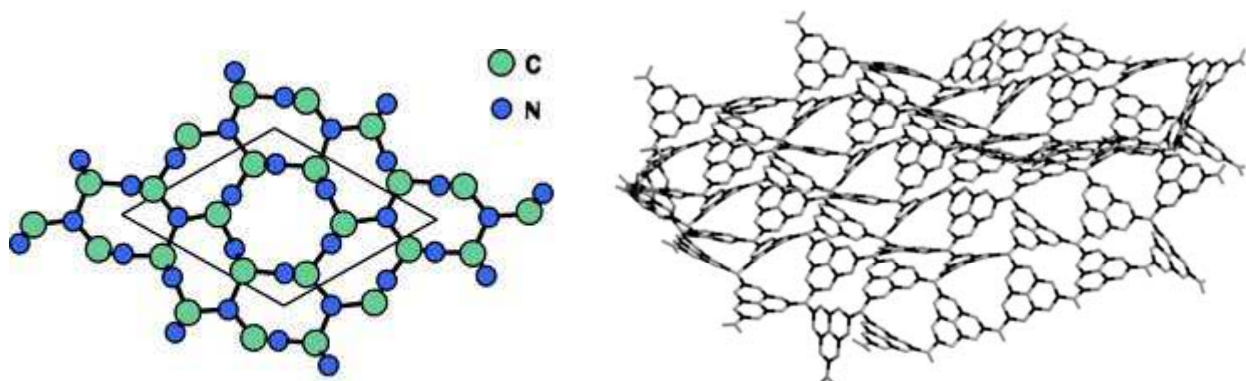
Fig. 3.14 The structure of β-C$_3$N$_4$[29] and a fully condensed heptazine-based g-C$_3$N$_4$ network resulting from semiempirical structure optimizations at the PM3 level of theory.[25]
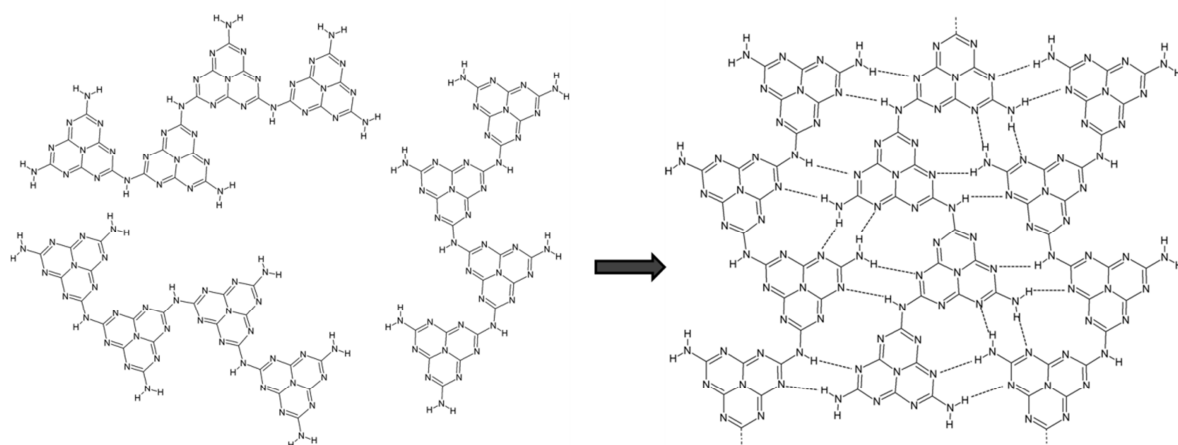
Fig. 3.15 The scheme of melon condensing further at the pending NH$_2$ groups into strongly hydrogen-bonded, quasi 2D arrays.

3.2.3 Transmission Electron Microscopy

As compared to X-ray diffraction, selected area electron diffraction (SAED) provides structural insights into nanometer-sized and polycrystalline materials. A representative TEM image of melamine calcined for 4 hours can be seen in Fig. 3.16. From the image of the edges, it appears that the sample has a layered structure.
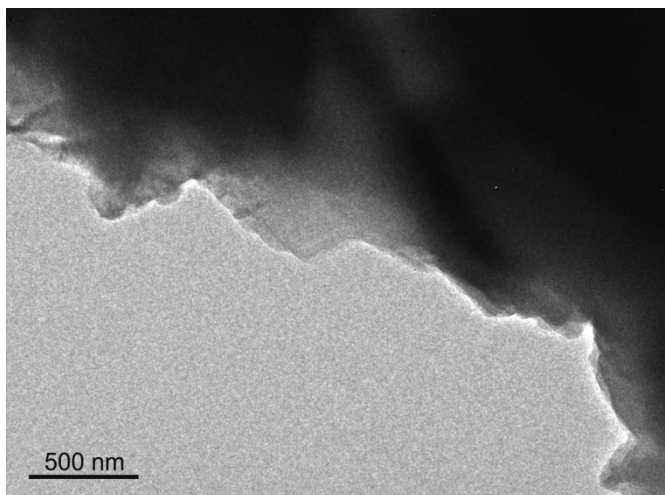
Fig. 3.16 TEM image of melamine calcined for 4 h at 450 °C in an open system.
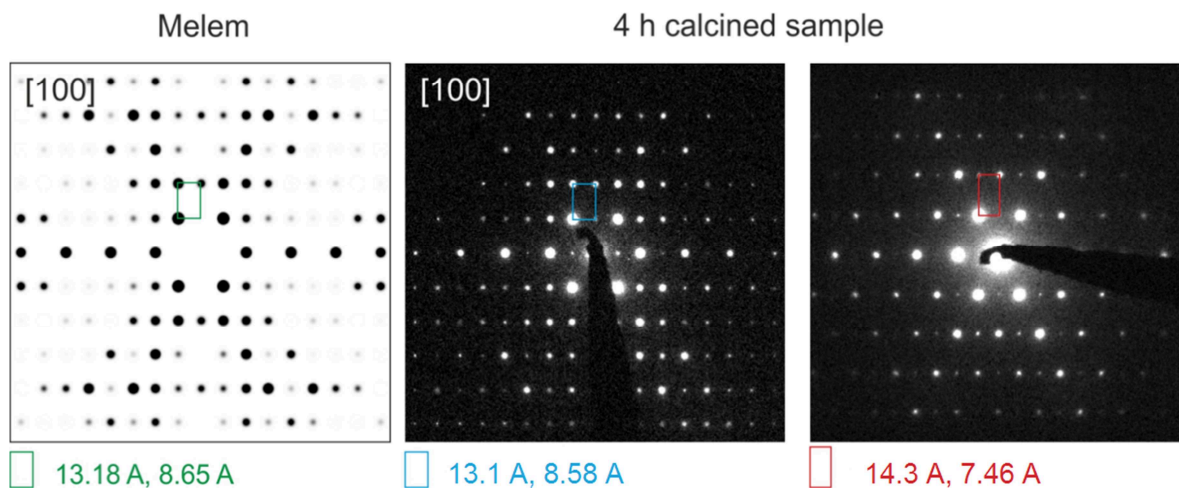
Fig. 3.17 Electron diffraction patterns of melamine calcined for 4 h at 450 °C (middle and right) in an open system, and simulated SAED of the (0*kl*) plane of melem for comparison (left).

Fig. 3.17 shows the simulated diffraction pattern of melem along the [100] zone axis and the experimentally observed diffraction patterns of melamine calcined for 4 h. Two kinds of similar diffraction patterns can be found, one being essentially identical to the simulation based on the melem structure, while the other one shows an almost hexagonal intensity pattern and slightly larger lattice parameters. This is consistent with the XRD diffraction pattern of the same sample calcined for 4h, in which two distinct, yet similar crystalline phases are found (Fig 3.2). The SAED pattern with the larger lattice parameters stems from another crystalline phase, besides melem, in the sample calcined for 4 h. Although the lattice parameters are larger than those for melem, they are still similar and the intensity distribution is also reminiscent of that of melem. Therefore, we conjecture that the second crystalline phase is another, yet unknown modification of melem. Interestingly, it is reported that melem can be self-assembled on Ag(111) under ultra-high vacuum conditions, and one of the observed monolayer polymorphs corresponds to a densely packed row structure symmetry (Fig. 3.18), which has similar lattice parameters ($a = 0.75 \pm 0.1$ nm, $b = 1.45 \pm 0.1$ nm) as those observed in Fig. 3.17 (right).[26] These findings may suggest that the second crystalline phase in the sample calcined for 4 h corresponds to the planar densely packed row structure. Since the densely packed row structure reported in ref. 26 is a planar 2D structure, no conclusions can be drawn with respect to the third dimension of the experimentally observed melem-type crystalline phase.
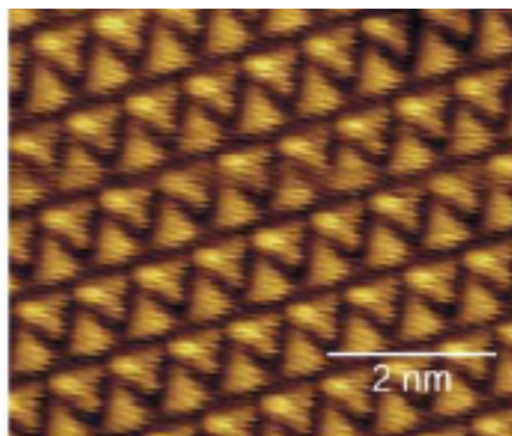
Fig. 3.18 High resolution STM topographs of a melem monolayer polymorph on Ag(111) and tunneling parameters: densely packed row structure polymorph (0.04 V, 75 pA); the experimental lattice parameters are $a = 0.75 \pm 0.1$ nm, $b = 1.45 \pm 0.1$ nm. [26]

According to the metrics obtained by high resolution STM topography in Fig 3.18, the electron diffraction patterns of this densely packed row structure sample were simulated. Unfortunately,

the simulated pattern does not agree well with the SAED pattern of the unknown phase contained in the calcined melamine sample as shown in Fig. 3.19. This suggests that melem may have different crystalline structures, and the 2D structures found by STM are likely different from those found in the bulk.
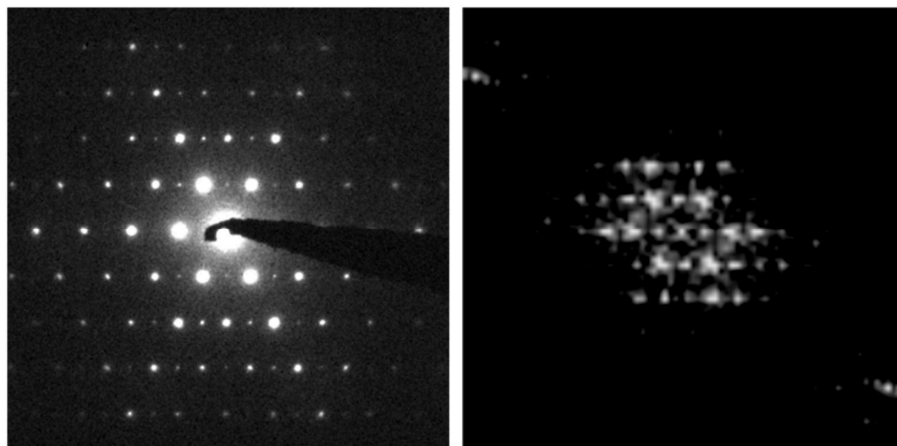
Fig. 3.19 Diffraction pattern of the unknown melem-like phase observed in the melamine sample calcined for 4 h at 450 °C in an open system (left), and the simulated diffraction pattern from densely packed row structure (right).

When the calcination time is increased to 10 hours, two different kinds of intensity distributions can be observed in the electron diffraction patterns. The diffraction patterns of melamine calcined for 10 h is shown in Fig. 3.20. A and B are the diffraction patterns along the zone axes [100] and [101] of melem. Therefore, melem is still present in the sample after 10 h calcination. C and D are the diffraction patterns of the new phase discussed above, whose lattice parameters were calculated as $a = 0.76 \pm 0.1$ nm, $b = 1.49 \pm 0.1$ nm (C) and $a = 0.75 \pm 0.1$ nm, $b = 1.47 \pm 0.1$ nm (D). Hence, the crystalline parts of melamine calcined for 10 h are also a mixture of the two different crystalline phases, which may correspond to different modifications of melem.
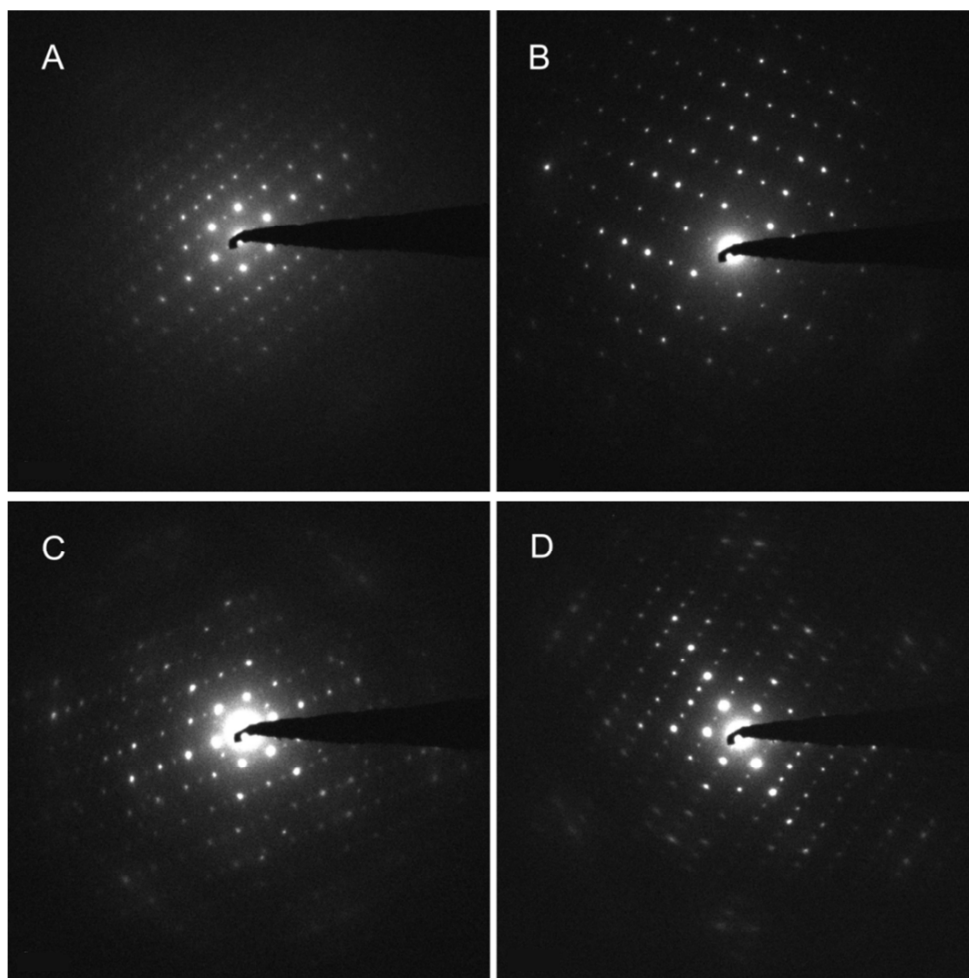
Fig. 3.20 TEM diffraction patterns of two distinct crystalline phases contained in melamine calcined for 10 h at 450 °C in an open system. A and B correspond to melem, whereas C and D correspond to the unknown melem-like modification.

TEM image and electron diffraction patterns of ultra-long calcined melamine at 430 °C are displayed in Fig. 3.21. Again, from the edges of the sample (Fig. 3.21 A) we can see the layer structure as in the samples calcined for shorter times. Fig. 3.21 B and Fig. 3.21 C display the SAED patterns. The middle SAED pattern corresponds to melem, while the other is a diffraction pattern of a poorly crystalline phase, which constitutes the main phase. Combined with the XRD pattern of this sample (Fig. 3.10), the material calcined for 160 h at 430 °C is a mixture of melem and a poorly crystalline, presumably melon-type phase. Therefore, we conclude that temperatures of 430 °C are not high enough to furnish complete conversion of melamine into melon, and melem-type crystalline parts alternate with more highly condensed, poorly crystalline parts in the sample.
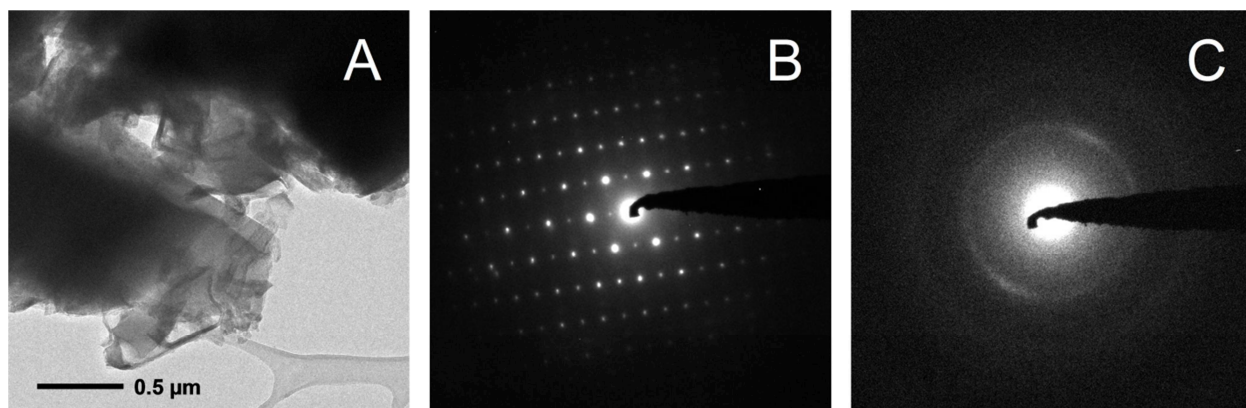
Fig. 3.21 TEM image and diffraction patterns of ultra-long calcined melamine synthesized at 430 °C.
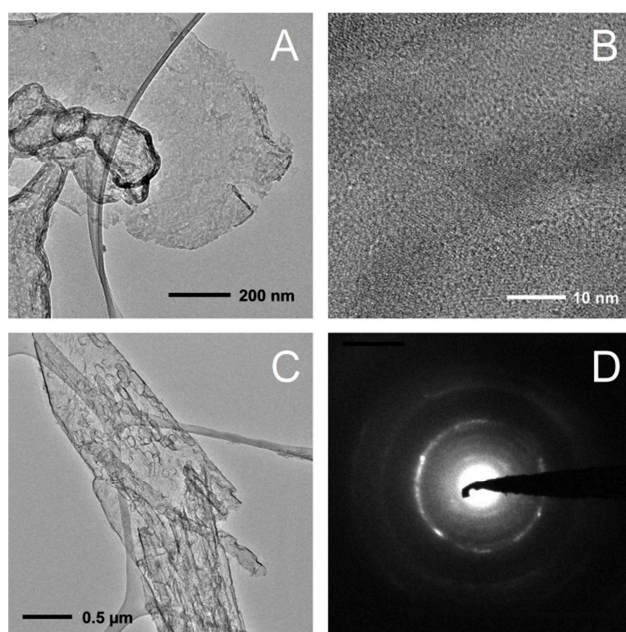
Fig. 3.22 TEM images and diffraction pattern of ultra-long calcined melamine synthesized at 490 °C.

The morphology of the product of the ultra-long melamine calcination at 490 °C is different from that of the ultra-long melamine calcination at 430 °C. As seen in Fig. 3.22 A, the sample seems to be composed of a flaky material, which resembles nanosheets seen in other melon samples.[9] Meanwhile, it seems that the tubular morphology reported in the literature is also observed in Fig. 3.22 C. In Fig. 3.22 B crystalline parts and amorphous parts are clearly distinguishable, where the former can be identified by parallel lattice fringes. According to the diffraction pattern in Fig. 3.22 D, the d value is determined as 3.29 Å, corresponding to the graphitic layer stacking. There are no more SAED patterns corresponding to melem, which indicate that 490 °C is high

enough to furnish complete conversion of melamine into melon. It is worth mentioning that the ultra-long calcined melamine at 490 °C has a BET surface area of 91.7 m^2g^{-1}, which is substantially larger than that of ultra-long calcined melamine at 430 °C (6.47 m^2g^{-1}) according to nitrogen adsorption experiments. The large surface area of the 490 °C sample could be caused by the nanosheet structure which is inferred from the TEM images.

3.2.4 Elemental Analysis Results

Table 3.2 shows the N/C ratio of the series of calcined melamine samples, along with the theoretical ratio for melem and melon. As can be seen in the table, all values for the calcination series are between those for melem and melon. As we mentioned before, the calcined melamine samples could be a mixture of melem and oligomers, hence the ratio obtained could be an average value for a mixture of compounds. Therefore, it was advisable to do a reflux experiment to wash away potentially present melem with hot DMSO.

Table. 3.2 N/C ratio of melamine calcined for different times at 450 °C in an open system, along with that of melem and melon.

Calcin. products / calcin. time	melem*	4 h	6 h	8 h	10 h	12 h	14 h	16 h	18 h	20 h	22 h	24 h	100 h	melon*
N/C ratio	1.94	1.90	1.91	1.89	1.88	1.85	1.84	1.85	1.85	1.84	1.82	1.83	1.78	1.75

* Theoretical N/C ratios for melem and melon[26]

Table 3.3 exhibits the N/C ratio of melamine calcined for 4 – 10 h at 450 °C in an open system after washing with hot DMSO and the according numbers of the heptazine units. The N/C ratios of the residues are quite close, and the numbers of heptazine units are around 3 – 4, indicating that the compositions of the various residues are similar and contain a material having an average degree of condensation of 3-4 heptazine units, which is insoluble in hot DMSO. One noticeable experimental detail should be mentioned here: after DMSO washing, normally water was used to completely remove DMSO. Still, in the elemental analysis results a small amount of sulfur is observed, however less than 1 % (Table 3.3).

We conclude that melamine calcined for 4 – 10 h is composed of both melem and a melem oligomer composed of 3-4 heptazine units, or a mixture of melem and melem oligomers with

higher and lower degrees of condensation. However, since isolation and separation of the oligomeric phases is not possible at this stage due to their insolubility, the exact composition of the material calcined for various times remains a matter at issue.

Table. 3.3 N/C ratio of melamine calcined for 4 – 10 h at 450 °C in an open system after washing (w) with hot DMSO solution, together with melem and melon and the number of condensed heptazine rings calculated from the N/C ratio.

Calcin, products, washed (w) with DMSO	melem*	4 h w	6 h w	8 h w	10 h w	melon*
N/C ratio	1.94	1.81	1.79	1.80	1.79	1.75
S / %		0.30	0.00	0.70	0.34	
Heptazine units	1	3	4	3	4	∞

* The theoretical ratio of melem and melon

The N/C ratios of the ultra-long calcined samples (160 h) are listed in Table 3.4. Theoretically, melon is a hydrogen–containing carbon nitride polymer with idealized formula 'C_2N_3H'. Evidently, the N/C ratios of the ultra-long calcination samples are quite close to that theoretically expected for melon. This suggests that the ultra-long calcined samples should be melon-like. Notably, however, the sums of N, C and H are less than 100%. As mentioned before, the experiments were conducted in an open system in contact with air, implying that oxygen is involved in the reaction. Oxygen determination experiments were carried out to measure the amount of oxygen in the products. Table 3.4 suggests that there is oxygen in the ultra-long calcined products ($\approx$ 3 %). We reason that after the ammonia evolution has ceased, oxygen from the air may be incorporated into the materials at long calcination times. Note that oxygen may act as a "dopant" and may significantly change the electronic and optical properties of the materials, which will be discussed below (Section 3.2.8).

Table. 3.4 N/C ratio of melon-type materials calcined for 160 h at 430 – 490 °C in an open system, along with melon.

Melon-type samples	430 °C	450 °C	470 °C	490 °C	melon*
calcination time	160 h	160 h	160 h	160 h	
N/C ratio	1.78	1.78	1.76	1.75	1.75
$\sum$ N+C+H / %	96.4	96.7	95.0	94.5	
O / %	3.4	2.9	3.3	3.6	

* The theoretical ratio of melon ($C_6N_9H_3$)

3.2.5 Solid-State NMR Spectroscopy

In order to obtain further information on the local structure of the calcined melamine series of samples, ^{1}H, ^{13}C and ^{15}N MAS NMR spectra were recorded. Fig. 3.23 shows the ^{1}H MAS solid-state NMR spectra of melem and the calcined samples, respectively. Two signals peaking at around 4 and 9 ppm can be observed, which are assigned to the NH_2 and NH groups, respectively. Also, we can see that the peak at around 9 ppm becomes gradually larger with the calcination time increasing, indicating an increasingly larger amount of NH moieties upon longer calcination. This is consistent with an increasingly higher degree of condensation, as the NH group is assigned to the C-NH-C moieties, which is the connecting group between two adjacent heptazine units.
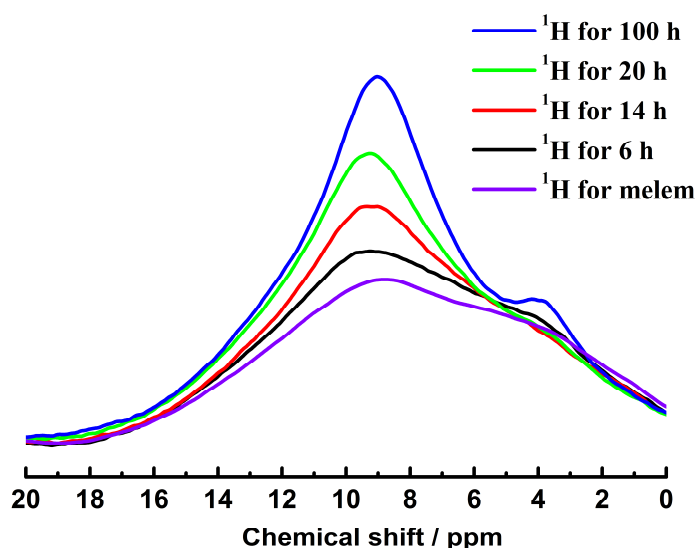
Fig. 3.23 ^{1}H MAS solid-state NMR spectra of melem and melamine calcined for 6, 14, 20 and 100 h at 450 °C in an open system.

In the ^{13}C CP-MAS NMR spectrum shown in Fig. 3.24, two typical signal groups of melem between 153 – 156 and 164 – 166 ppm, respectively, can be observed. Meanwhile, for the melamine sample calcined for 100 h two signal groups are found with peaks at 164.0 and 157.1 ppm,[6] which suggest that the sample also is a melon-type material. Judging from the intensity distribution in Fig. 3.24 the trend can be seen clearly that the obtained phases gradually change from melem-type to melon-type with increasing calcination times. Note that all spectra were measured using the same CP-MAS conditions and rotation speed, therefore allowing for a comparison of the different spectra within a series.
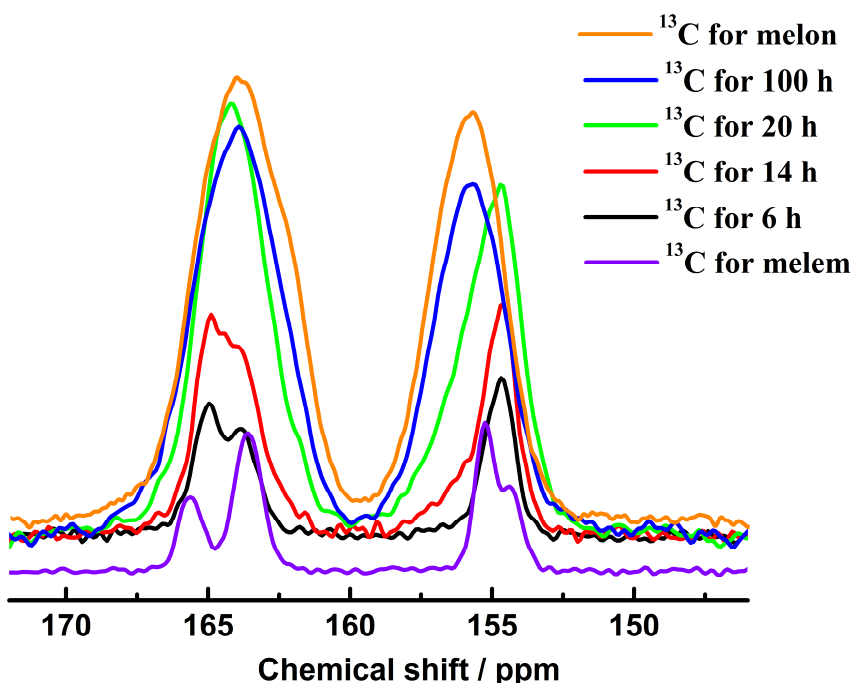
Fig. 3.24 ^{13}C CP-MAS solid-state NMR spectra (spinning frequency 10 kHz) of melem, melon and melamine calcined for 6, 14, 20 and 100 h at 450 °C in an open system.

The ^{15}N NMR spectra suffer from the low sensitivity and natural abundance of the ^{15}N nucleus and the partial disorder of the sample. Therefore, the signals have rather broad lines and insufficient signal intensity. Nevertheless, the ^{15}N signature of the materials is a valuable evidence of the type of building blocks present and the degree of condensation of the sample. Melon-type materials typically show NH signals pertaining to the bridging C-NH-C group. In Fig. 3.25 the signals at δ = -245 ppm and -265 ppm can be assigned as NH and NH_2, respectively.[6] It can be seen that compared with the NH_2 signal the NH signal gets stronger with increasing calcination time, and the NH group is first clearly seen in the sample calcined for

14 h. In general, the spectra become increasingly melon-like at longer calcination times, which can for example be seen by the appearance of tertiary (ring) nitrogen signals between -170 and -200 ppm, which are not present in melem.[5,14] The central nitrogen atom of the heptazine core (N_c) signal at -225 ppm could not be detected in the spectrum of melem because of its low sensitivity. In the samples calcined for a longer period of time, a slight signal may be inferred between -220 and -230 ppm, yet from the ^{15}N spectra no unambiguous evidence for the presence of heptazine building blocks can be extracted from these spectra. However, ^{15}N and ^{13}C spectra taken together are reminiscent of melem and melon-type phases rather than triazine-based materials. Also, the spectra do not evidence whether the calcined materials are single phase or consist of multiple phases of varying crystallinity. In principle, the NMR spectra at intermediate calcination times could be interpreted as either a mixture of melem and different melem oligomers or as a mixture of melem and one particular melem oligomer. However, the data suggest that substantial amounts of oligomeric material can only be found at calcination times longer than 14 h. Below this calcination time, the majority of the material seems to be melem-like, though possibly not identical to the known melem modification.
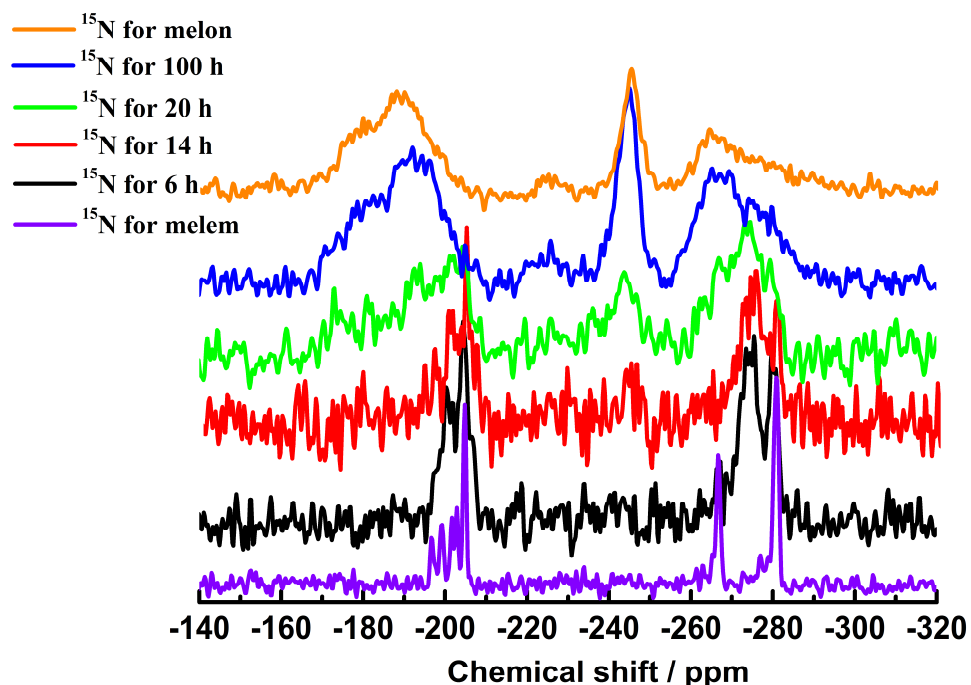
Fig. 3.25 ^{15}N CP-MAS solid-state NMR (spinning frequency 10 kHz) spectra of melem and calcined melamine for 6, 14, 20 and 100 h at 450 °C in an open system.

For the ultra-long calcined melamine samples, ^{13}C and ^{15}N MAS NMR were recorded and are shown in Fig. 3.26 and Fig. 3.27. Two signal groups at 155.8 and 164.0 ppm can be easily distinguished in the spectra which are similar to those of melon[6].
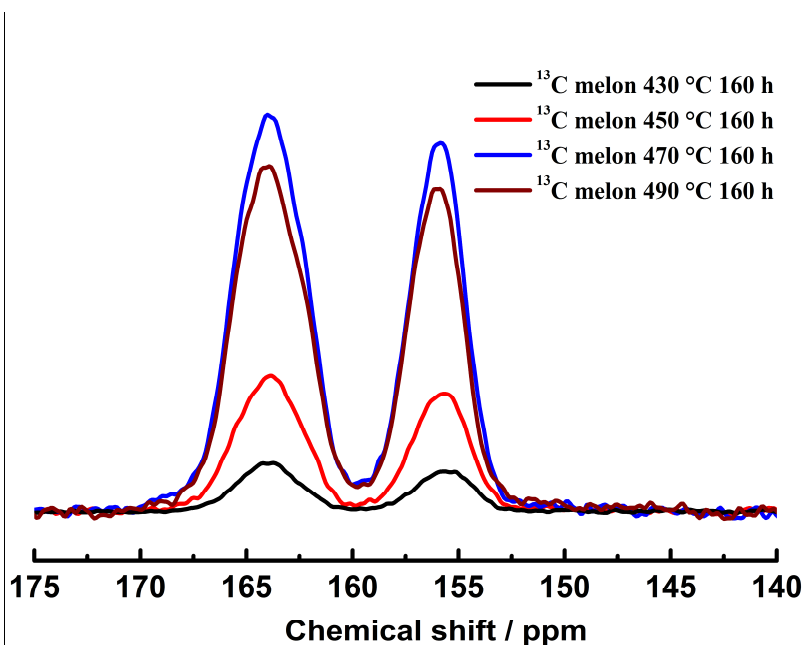
Fig. 3.26 ^{13}C CP-MAS solid-state NMR spectra (spinning frequency 10 kHz) of ultra-long calcined melamine at 430 – 490 °C for 160 h in an open system.
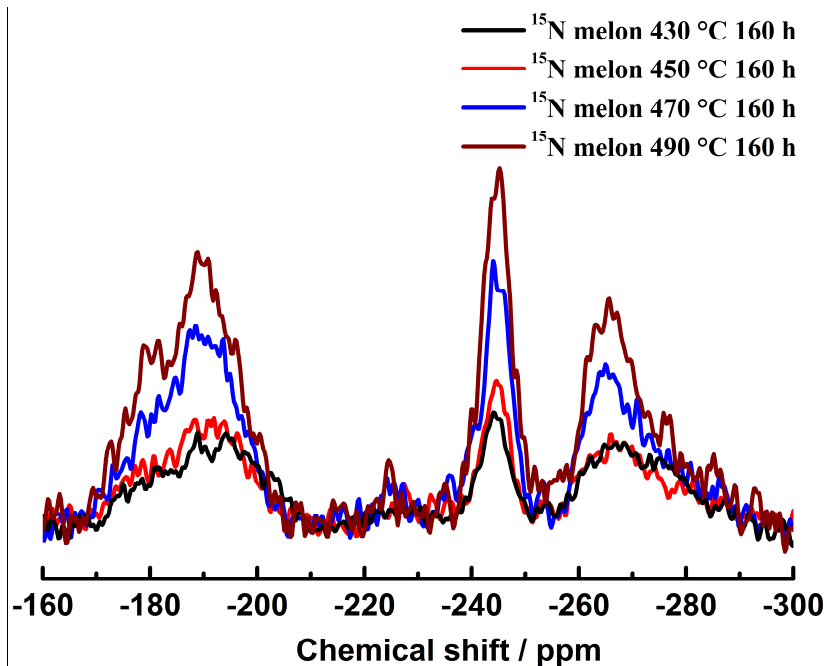
Fig. 3.27 ^{15}N CP-MAS solid-state NMR spectra (spinning frequency 10 kHz) of ultra-long calcined melamine at 430-490 °C for 160 h in an open system.

Likewise, the ^{15}N NMR is reminiscent of that of melon; the signals between -177 and -198 ppm can be assigned as the tertiary ring nitrogen atoms N_{tert}.[6] The quite weak signal at around -225 ppm suggests the presence of the central nitrogen atom of the hepatzine core.[6] As mentioned before, elemental analysis indicates that oxygen is present in the products. However, the amount of oxygen is too small to have a pronounced effect on the NMR signals of the adjacent ^{13}C and ^{15}N atoms. The signals at -245 and -265 ppm can be assigned as NH and NH_2, respectively. In brief, the ultra-long calcined samples have the characteristic features of melon, meanwhile the samples also contain oxygen. Therefore, the samples may be considered as lightly oxygen-doped variants of melon.

3.2.6 UV-Vis Absorption Properties

UV-Vis gives information about the ability of samples to absorb light in the visible and near-UV range of the electromagnetic spectrum. As we can see in Fig. 3.28, the absorption edge of the calcination series of melamine is around 450 nm. The Kubelka–Munk function[27] corresponding to $[F(R_\infty)\ hv]^{1/2}$ is introduced to calculate the optical band gap from the diffuse reflectance spectra (Table 3.4). The band gaps of the series of samples are roughly the same, and all of them have band gaps a little larger than that of melon. This again suggests that the calcined melamine samples should be less condensed than melon samples synthesized at higher temperatures.
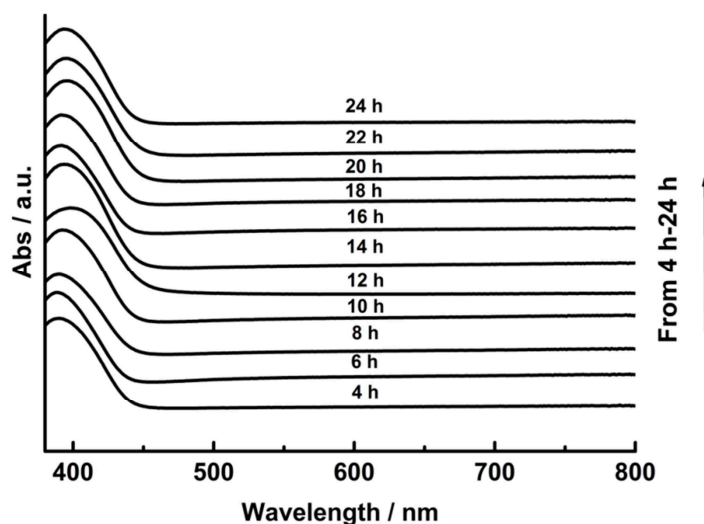
Fig. 3.28 UV-Vis diffuse reflectance spectra of the melem oligomers at 450 °C for 4 – 24 h in an open system.

Table. 3.4 Band gaps (extracted based on the Kubelka-Munk function) of melamine calcined at 450 °C for 4 – 24 h in an open system, together with that of melon.

Calcin. products (calc. time)	4 h	6 h	8 h	10 h	12 h	14 h	16 h	18 h	20 h	22 h	24 h	Melon (490 °C)
Band gap / eV	2.79	2.80	2.79	2.81	2.78	2.80	2.79	2.80	2.79	2.79	2.80	2.63

3.2.7 Solubility

Above we have suggested that melamine calcined for 4 to 20 h are a mixture of melem and melem oligomers composed of roughly 3– 5 hepatzine units. Therefore, if the samples can be dissolved in some appropriate solvent, in principle more information about the structure of the samples will be accessible. Many solvents were tested in order to dissolve the calcined melamine samples, shown in Table 3.5. Three kinds of solvents (non-polar, polar aprotic and polar protic solvents) were used in the experiments. As a result, the samples are insoluble in most of the solvents. Only DMSO, which has a large dipole moment of 16.4 D, can dissolve the samples to some extent. Obviously, DMSO dissolves the melem portion of the sample, while the oligomers remain insoluble. We also tried to use all kinds of solvents to dissolve the samples at high temperature. However, heating is also not effective in dissolving the sample completely. As it is known that melem is already quite difficult to dissolve, the calcined melamine samples will likely be even more difficult to dissolve, which is in line with our solubility studies as shown in Table 3.5.

Table. 3.5 Solubility investigation of melamine calcined at 450 °C for 4 and 16 h.

Calcin. products / solvents	Melamine calcined 4 h	Melamine calcined 16 h
Tetrahydrofuran (THF)	No	No
Dimethylformamide (DMF)	No	No
Dimethyl sulfoxide (DMSO)	Slightly	Slightly
Dichloromethane (DCM)	No	No
Acetonitrile (MeCN)	No	No
Toluene	No	No
Benzene	No	No
Chloroform	No	No
Pentane	No	No
Hexane	No	No
Acetic acid	No	No
Ethanol	No	No
Methanol	No	No
n-Butanol	No	No
n-Propanol	No	No
Water	No	No

3.2.8 Photocatalytic Activity

Photocatalytic activity experiments were all carried out in our group by Brian Tuffy. In order to test the photocatalytic activities of the carbon nitride samples discussed above, hydrogen evolution reaction experiments were carried out. As a sacrificial electron donor was added, oxygen evolution will not occur in this experiment. Typically, 1 mg mL^{-1} aqueous suspension of carbon nitride catalyst were prepared and dispersed with an ultrasonic bath for 30 min. Triethanolamine (TEoA) was used as a sacrificial electron donor and H_2PtCl_6 (8 wt% in H_2O) was used as the Pt co-catalyst precursor which was photo-reduced during the reaction. Suspensions with 10 vol% TEoA and 6 μL H_2PtCl_6 (2.3 wt% Pt) were illuminated in 24 mL glass vials in an argon atmosphere with PTFE/Teflon septa. Samples were side-illuminated with a 10 W Biolux lamp (visible light) for a whole week. The evolved gas was measured by gas chromatography with argon as carrier gas, dosing injector system and thermal conductivity detector.

Fig. 3.29 Photocatalytic activities of various calcined melamine samples for the hydrogen evolution reaction driven by visible light.

Fig. 3.29 shows the photocatalytic activity of various calcined melamine samples for the hydrogen evolution reaction. It is immediately evident that all samples are active photocatalysts, although only visible light was used for irradiation. However, according to the results shown in Fig. 3.29, the amount of evolved H_2 is quite random and no unambiguous trend of the photocatalytic activities of these samples is visible. The possible reason could be that there is

leakage of the hydrogen through the septa during the long illumination time. Generally speaking, all samples show similar photocatalytic activities for the hydrogen evolution reaction. Most of them produce 2 μmol g^{-1} h^{-1} of H$_2$. As expected from the higher degree of condensation, the accordingly lower band gap and more pronounced absorption of melon in the visible range, melon produced around 5 μmol g^{-1} h^{-1} of H$_2$. From these results a generally lower activity of the samples containing a higher amount of melem and oligomers with a low condensation degree is inferred. The most likely reason for this observation is the low absorption of these species in the visible part of the electromagnetic spectrum.

Hydrogen production experiments were also conducted for the ultra-long calcined melamine samples. The experimental procedure was similar to that used for the samples calcined for shorter times, except for the light source and illumination time. Samples were side-illuminated with a 300 W Xenon lamp with a water filter and dichroic mirror blocking wavelengths < 420 nm. The evolved gas was measured by gas chromatography with an online injection system, using a thermal conductivity detector with argon as carrier gas.
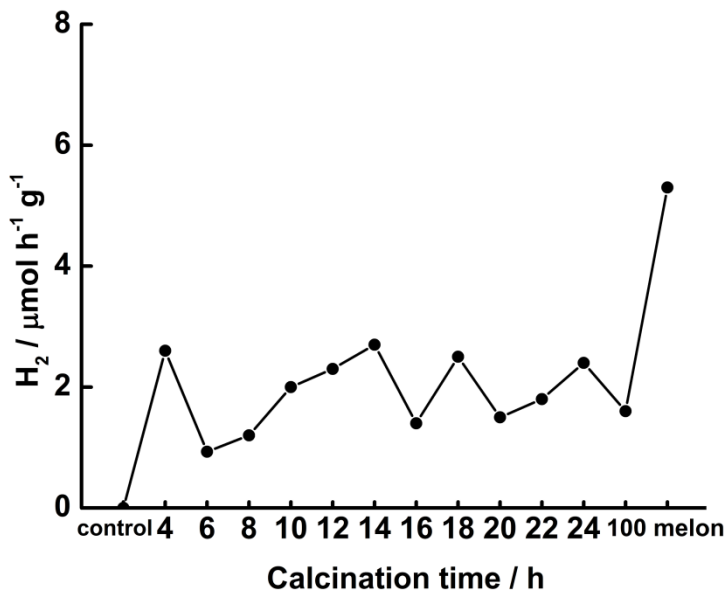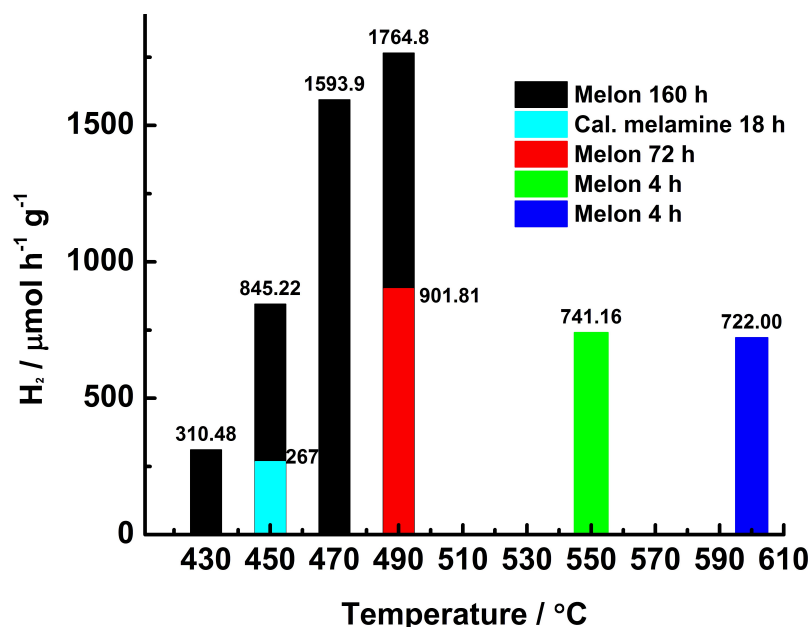

Fig. 3.30 Photocatalytic activities of ultra-long calcined melamine samples for the hydrogen evolution reaction driven by visible light, compared to those of standard melon samples synthesized at different temperatures.

Fig. 3.30 shows the photocatalytic activites of the ultra-long calcined melamine samples, together with standard melon which was prepared under three different conditions. As the series of calcined melamine samples shows similar photocatalytic activities for the hydrogen evolution

reaction, one representative sample (calcined melamine 18 h) was tested under the 300 W Xenon lamp illumination. This sample still shows smaller photocatalytic activity as compared to melon obtained under various synthesis conditions. When the calcination time is 160 h, the photocatalytic activites increase significantly with increasing calcination temperature. When the calcination temperature is 490 °C, melon calcined for 72 h is only half as active as the melon sample calcined for 160 h at the same temperature. One possible reason for this activity enhancement could be changes in the morphology of the sample at long calcination times, as the material becomes increasingly flaky and nanosheet-like compared to bulk melon (see TEM part 3.2.3).[9] This material has an accordingly higher surface area of 91.7 m^2 g^{-1}, which exposes more photocatalytically active spots. Another reason could be oxygen doping which may become more relevant at longer calcination times in air. Recently, Schwinghammer et al. reported that carbon and oxygen doped PTI shows quite high photocatalytic activities.[28] As demonstrated in the elemental analysis section, around 3 % oxygen were incorporated in the ultra-long calcined samples. In a paper published by Antonietti et al. melon was prepared at 550 °C and 600 °C for 4 h. These melon samples show lower photocatalytic activities as compared to ultra-long calcined melamine in this thesis.

3.3 Conclusion

In summary, a series of low condensed carbon nitride materials based on heptazine units were synthesized showing photocatalytic activity for the hydrogen evolution reaction. Though we were not able to unambiguously elucidate the composition and structure of the melamine samples calcined for an increasing period of time, we have accumulated evidence that the calcined samples are mixtures of melem and melem oligomers. TEM analysis of the samples calcined for a short period of time as well as for intermediate times invariably shows the presence of melem in the samples. However, another crystalline phase was observed which likely is another modification of melem, possibly a planar structure. The melem oligomers presumably resemble melon on a local level as well as with respect to their planar layered structure, but seem to be essentially amorphous. Nevertheless, the solubility of the calcined samples is quite low. Three kinds of solvents (non-polar, polar aprotic and polar protic solvents) were tested, but only DMSO slightly dissolves parts of the samples which contain melem. The photocatalytic activities of these calcined melamine samples in the hydrogen evolution reaction are smaller than that of melon.

When extending the calcination time to 160 h at 430 – 490 °C, melon-type materials can be obtained. The samples calcined for very long times (160 h) at less than or 450 °C are a mixture of melem and melon, possibly also melem oligomers. No melem was detected when the ultra-long calcined samples were synthesized at temperatures higher than 450 °C. The morphology of the ultra-long calcined melamine prepared at 490 °C is flaky and sheet-like and the sample exhibits a surface area of 91.7 m^2g^{-1}. Interestingly, the ultra-long calcined samples show good photocatalytic activites for the hydrogen evolution reaction driven by visible light. Especially the flaky melon shows the best photocatalytic activites, which is superior to most of the undoped melon-type samples reported in the literature.[3,28] This strongly suggests that the morphology and polymerization degree of carbon nitrides should have a significant influence on the hydrogen evolution reaction.

3.4 Chapter References

[1]   A. Fujishima, K. Honda, *Nature* **1972**, *238*, 37–38.

[2]   J. Gracia, P. Kroll, *Journal of Materials Chemistry* **2009**, *19*, 3013–3019.

[3]   X. Wang, K. Maeda, A. Thomas, K. Takanabe, G. Xin, J. M. Carlsson, K. Domen, M. Antonietti, *Nature materials* **2009**, *8*, 76–80.

[4]   A. Thomas, A. Fischer, F. Goettmann, M. Antonietti, J.-O. Müller, R. Schlögl, J. M. Carlsson, *Journal of Materials Chemistry* **2008**, *18*, 4893–4905.

[5]   B. Jürgens, E. Irran, J. Senker, P. Kroll, H. Müller, W. Schnick, *Journal of the American Chemical Society* **2003**, *125*, 10288–300.

[6]   B. V Lotsch, M. Döblinger, J. Sehnert, L. Seyfarth, J. Senker, O. Oeckler, W. Schnick, *Chemistry (Weinheim an der Bergstrasse, Germany)* **2007**, *13*, 4969–4980.

[7]   B. Yue, Q. Li, H. Iwai, T. Kako, J. Ye, *Science and Technology of Advanced Materials* **2011**, *12*, 034401.

[8]   X. Wang, K. Maeda, X. Chen, K. Takanabe, K. Domen, **2009**, 1680–1681.

[9]   P. Niu, L. Zhang, G. Liu, H.-M. Cheng, *Advanced Functional Materials* **2012**, *22*, 4763–4700.

[10]   A. Sattler, S. Pagano, M. Zeuner, A. Zurawski, D. Gunzelmann, J. Senker, K. Müller-Buschbaum, W. Schnick, *Chemistry (Weinheim an der Bergstrasse, Germany)* **2009**, *15*, 13161–13170.

[11]   E. Wirnhier, M. Döblinger, D. Gunzelmann, J. Senker, B. V Lotsch, W. Schnick, *Chemistry (Weinheim an der Bergstrasse, Germany)* **2011**, *17*, 3213–3221.

[12]   E. Kroke, *Coordination Chemistry Reviews* **2004**, *248*, 493–532.

[13] B. V Lotsch, W. Schnick, *Chemistry of Materials* **2005**, *17*, 3976–3982.

[14] B. V. Lotsch, W. Schnick, *Chemistry of Materials* **2006**, *18*, 1891–1900.

[15] I. Alves, G. Demazeau, B. Tanguy, F. Weill, *Solid State Communications* **1999**, *109*, 697–701.

[16] Y. Cui, J. Zhang, G. Zhang, J. Huang, P. Liu, M. Antonietti, X. Wang, *Journal of Materials Chemistry* **2011**, *21*, 13032–13039.

[17] Q. Guo, Y. Xie, X. Wang, S. Lv, T. Hou, X. Liu, *Chemical Physics Letters* **2003**, *380*, 84–87.

[18] F. Parmigiani, E. Kay, H. Seki, *Journal of Applied Physics* **1988**, *64*, 3031–3036.

[19] B. V. Lotsch, *LMU München Ph.D thesis* **2006**.

[20] T. Komatsu, T. Nakamura, *Journal of Materials Chemistry* **2001**, *11*, 474–478.

[21] T. Komatsu, *Macromolecular Chemistry and Physics* **2001**, *202*, 19–25.

[22] J. Wei, P. Hing, Z. Q. Mo, *Surface and Interface Analysis* **2000**, *211*, 208–211.

[23] P. Instrumentation, E. P. Detector, *Science* **1992**, *261*, 337–337.

[24] D. M. Teter, R. J. Hemley, *Science* **1996**, *271*, 53–55.

[25] J. Sehnert, *Universit Bayreuth Ph.D thesis* **2007**.

[26] J. Eichhorn, S. Schlögl, B. V. Lotsch, W. Schnick, W. M. Heckl, M. Lackinger, *CrystEngComm* **2011**, *13*, 5559–5565.

[27] H. Kisch, S. Sakthivel, M. Janczarek, D. Mitoraj, *Journal of Physical Chemistry C* **2007**, *111*, 11445–11449.

[28] K. Schwinghammer, B. Tuffy, M. B. Mesch, E. Wirnhier, C. Martineau, F. Taulelle, W. Schnick, J. Senker, B. V Lotsch, *Angewandte Chemie (International ed.)* **2013**, 1–6.

[29] D. M. Teter, R. J. Hemley, *Science* **1996**, *271*, 53–55.

Chapter 4

Carbon Nitride doped Titanates

4.1 Introduction

Since Fujishima and Honda first reported the decomposition of water on illuminated TiO_2 electrodes in 1972,[1] technologies such as photocatalytic water splitting to produce hydrogen and reduction of CO_2 to solar fuels are seeing increasing importance for researchers. As well as TiO_2, titanates are also employed as photocatalysts but suffer from larger band gaps of around 3.8 eV (*vs* 3.2 eV for TiO_2); therefore titanates have not been studied as intensely for photocatalysis as TiO_2. However, layered titanates have a broad compositional range, unique structural, morphological and electrical features which could lead to new physical and chemical properties and offer an enhanced tailorability of their property profile. Recently, it was shown that titanates can be chemically modified to reduce their band gap, such as by modification with nitrogen or doping with cations such as gold[2], niobium[3], and many more.[4–7]

One very recent direction to address the large band gaps in these materials is to introduce carbon nitride materials to enhance light absorption and photocatalytic performance. Kisch et al. found that calcining melamine or urea with TiO_2 resulted in a material with high photocatalytic activity.[8–12] It is worth mentioning that Kisch is the first to put forward carbon nitride doping. Many researchers have done N-doping of titanates and TiO_2 (depending on the dopant), putting forward the explanation that N is doped into the TiO_x lattice. However, Kisch realized that upon using specific N-dopants such as urea and other small molecular carbon nitrides the dopant seems to be in fact polymeric carbon nitride rather than atomic nitrogen. Recently, a hybrid photocatalyst of g-C_3N_4 and TaON with visible light response was prepared by a milling heat-treatment method and was used for photodegradation of rhodamine B.[13] The good performance in photooxidation resulted from suitably matching the conduction and valance band levels which improved the separation efficiency of photogenerated electron–hole pairs.

In this thesis we mostly focus on the synthesis of layered Lepidocrocite-type titanates (Fig. 4.1) and the "doping" of layered titanates with carbon nitrides in order to enhance their photoactivity, targeting the hydrogen evolution reaction from water.
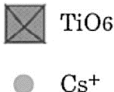
Fig. 4.1 Crystal structure of Lepidocrocite-type cesium titanate $Cs_xTi_{(2-x/4)}\square_{x/4}O_4$.[14]

The carbon nitride material presented here is a species that was mentioned in chapter 3 (melamine calcined for various periods of time at 450 °C). Calcined melamine samples have a slightly larger band gap than melon, but as it is less condensed and therefore chemically more reactive, it may give rise to stronger interactions with semiconductors such as TiO_2 or titanates owing to more versatile surface condensation reactions *via* the terminal NH_2 groups.[15] In the literature, photoactive carbon nitrides are typically referred to as "graphitic carbon nitride, *g*-C_3N_4", corresponding to the most fully condensed graphitic carbon nitride species. However, from the presented data it gets evident that most of these carbon nitrides are identical with the 1D polymer melon.[16–18] In our work we report a calcined melamine / cesium titanate (CTO) hybrid which is a promising photocatalyst material for the hydrogen evolution reaction.

4.2 Results and Discussion

4.2.1 X-ray powder Diffraction
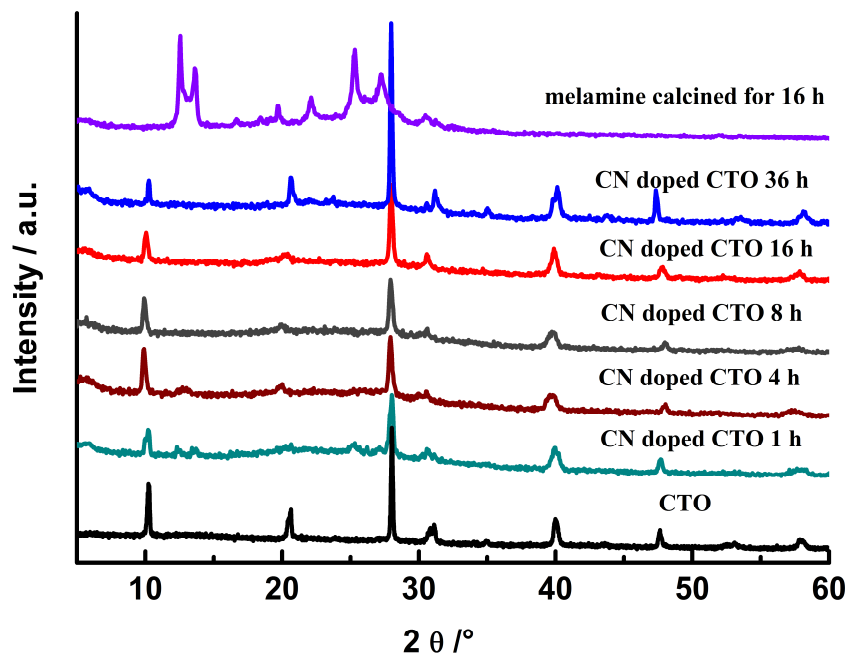
Fig. 4.2 Powder XRD patterns of cesium titanate (CTO), calcined melamine (16 h) and CN-doped CTO for different calcination times at 450 °C (the initial weight ratio of melamine and CTO was 1:1).

Fig. 4.2 shows the powder XRD patterns of CTO, melamine calcined for 16 h and CN-doped CTO materials. Pronounced reflections were found in all samples, which can be assigned to $Cs_xTi_{2-x/4}\square_{x/4}O_4$ (x = 0.67).[3] A broad reflection at $2\theta \approx 27°$ at low calcination times may indicate the formation of a layered structure with rather poorly defined, graphite-like interlayer spacing.[19] For the hybrid samples with increasing calcination times, the two peaks at 12.4 and 13.6°, assigned to the carbon nitride species, are decreasing. This trend suggests that the amount of semicrystalline calcined melamine is decreasing gradually as the calcination time increases. The doped samples present a two-phase composition: CTO and carbon nitride. It is interesting to note that when the calcination time is 1 – 16 h, the 040 and 060 reflections at 20.6° and 31.2° get broader and shorter in the hybrid material, while after calcining for 36 h the reflection turns sharp again.

70

4.2.2 IR Spectroscopy
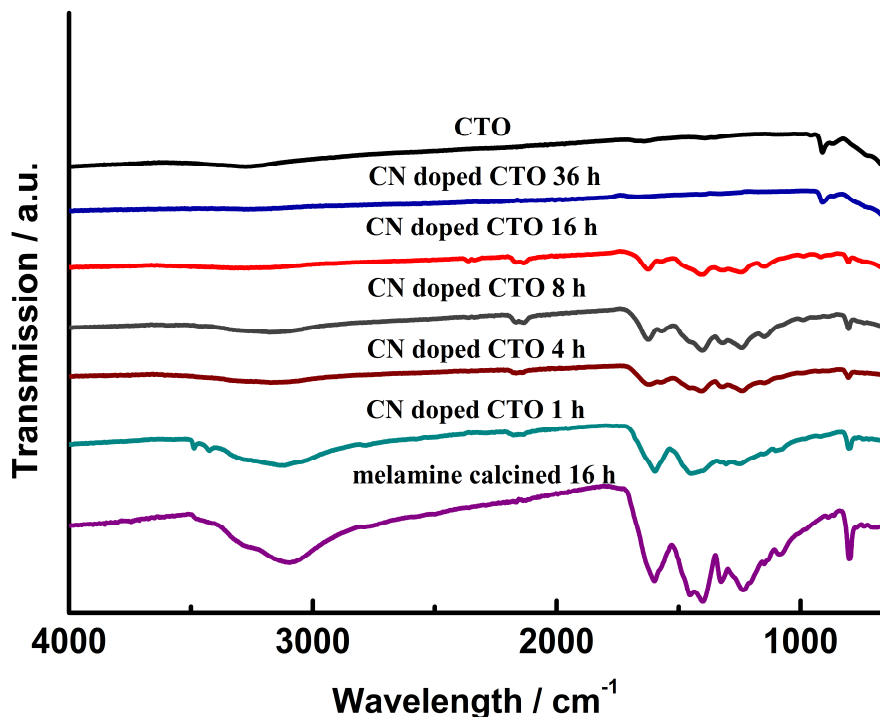
Fig. 4.3 FTIR spectra of CTO, calcined melamine (16 h) and CN-doped CTO for different calcination times at 450 °C (the initial weight ratio of melamine and CTO was 1:1).

Fig. 4.3 shows the IR spectra of CTO, melamine calcined for 16 h and CN-doped CTO materials. The IR spectra of melamine calcined for 16 h shows features very similar to that of melem,[20] especially the two strong bands at 1605 and 1460 cm^{-1} as well as the sharp heptazine semicircle ring stretch at 804 cm^{-1}.[20] However, the two bands at 1322 and 1235 cm^{-1}, which are absent in the melem spectrum, correspond to the v(C-N) and δ(NH)[19] vibrations indicative of NH-bridged heptazine units and thus, a higher degree of condensation than in melem. The band at 1399 cm^{-1} is attributed to an aromatic C–N stretching vibration.[21] A broad band near 3140 cm^{-1} corresponds to the stretching modes of N–H species such as terminal NH_2 or NH groups.[22] The spectrum after 1h calcination time shows two sharp N-H stretches just below 3500 cm^{-1}, which is indicative of the presence of melem in this sample.[20] For the CN-doped CTO samples, the trend shows that the bands lose intensity as the calcination time increases. This indicates that the amount of carbon nitride species decreases during the calcination process. The presence of CTO most likely facilitates the condensation and also decomposition process of the carbon nitride

precursor by action of its acidic terminal Ti-OH groups.[11] The two bands at 2167 cm^{-1} and 2136 cm^{-1} are due to C≡N groups, which points to terminal –CN groups resulting from the depolymerization of the melamine or heptazine rings catalyzed by the TiO$_x$ surface.[23–25] This is the reason why the hybrid materials get more CTO-like with increasing calcination time as the carbon nitride species is broken up into gaseous products and removed from the hybrid.

4.2.3 UV-Vis Absorption Properties

The optical properties of the samples were investigated by UV-Vis diffuse reflectance spectroscopy. Fig. 4.4 shows the UV-Vis absorption spectra of CTO, melamine calcined for 16 h and CN-doped CTO materials. The absorption edge of the CTO sample occurs at around 370 nm, and the band gap energy is estimated to be about 3.5 eV as obtained by the Kubelka-Munk function (Table 4.1). After carbon nitride doping of CTO, the absorption edge shifts to the lower energy region. We can also see that the absorption edges of the doped samples shift remarkably to longer wavelengths with increasing calcination times. However, the calcination time should not be too long, as the absorption edge of the hybrid significantly shifts back to lower wavelengths below 420 nm when the calcination time is as long as 36 hours. Table 4.1 shows the band gap of CTO, melamine calcined for 16 h and CN doped CTO materials. The table suggests that the doped materials exhibit lower band gaps than CTO, even lower than that of calcined melamine alone. Therefore, the hybrid materials can absorb more visible light and this property will be advantageous for photocatalysis because of the extra availability of photons.

Table. 4.1 Band gap of CTO, calcined melamine, and various CN-doped CTO sanples.

| Sample	CTO	CN doped CTO 1h	CN doped CTO 4h	CN doped CTO 8h	CN doped CTO 16h	CN doped CTO 32h	Melamine calcined 16 h
Band Gap (eV)	3.52	2.57	2.51	2.50	2.48	3.25	2.80
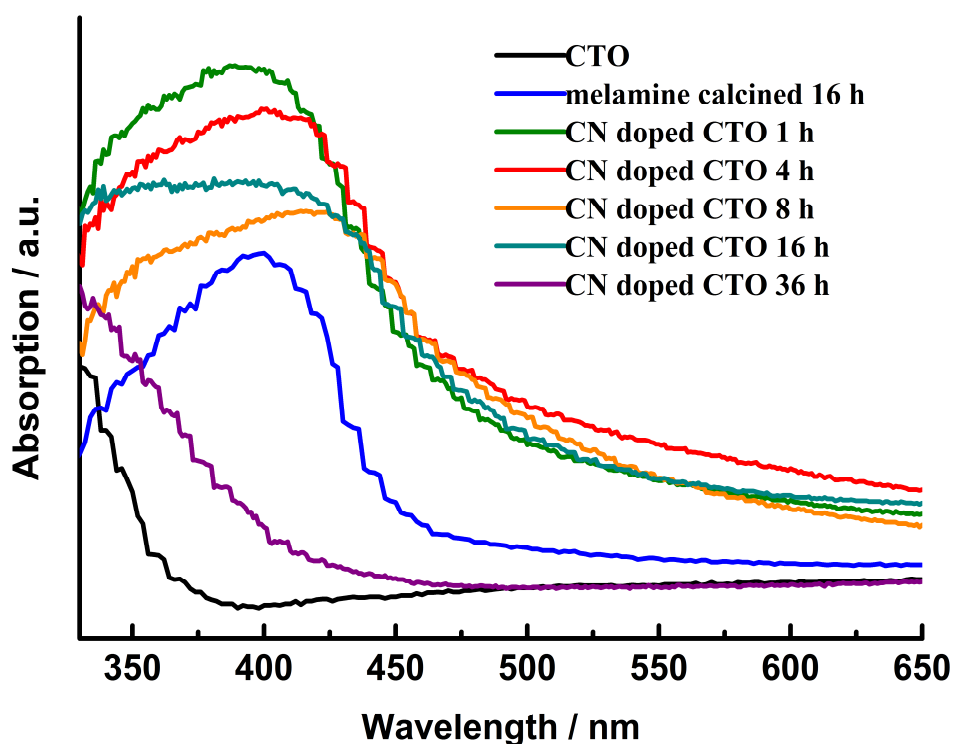
Fig. 4.4 UV-Vis absorption spectra of CTO, melamine calcined for 16 h and CN-doped CTO for different calcination times at 450 °C (the initial weight ratio of melamine and CTO was 1:1).

4.2.4 Elemental Analysis Results

Table 4.2 shows the elemental analysis results of the CN doped CTO samples with 1 – 36 h. The N/C ratios of the CN-doped CTO samples are decreasing with increasing calcination time. It suggests that the samples calcined for a longer time should be melon-like. As expected from the presence of oxygen and titanium in the hybrid materials, the sums of N, C and H are significantly less than 100 % and decrease with increasing calcination time, as the formed extended melon-type carbon nitride is continuously broken up into gaseous products and removed from the hybrid samples.

Table. 4.2 Elemental analysis results of CN doped CTO samples calcined for various times.

samples	CN-doped CTO, 1 h	CN-doped CTO, 4 h	CN-doped CTO, 8 h	CN-doped CTO, 16 h	CN-doped CTO, 36 h
N / %	22.98	17.23	14.04	7.33	0.18
C / %	12.54	9.85	8.12	4.37	0.05
H / %	0.87	0.71	0.42	0.33	0.02
N/C / %	1.83	1.74	1.72	1.67	3.6
Sum N+C+H / %	36.36	27.79	22.58	12.03	0.25

4.2.5 Solid-State NMR Spectroscopy
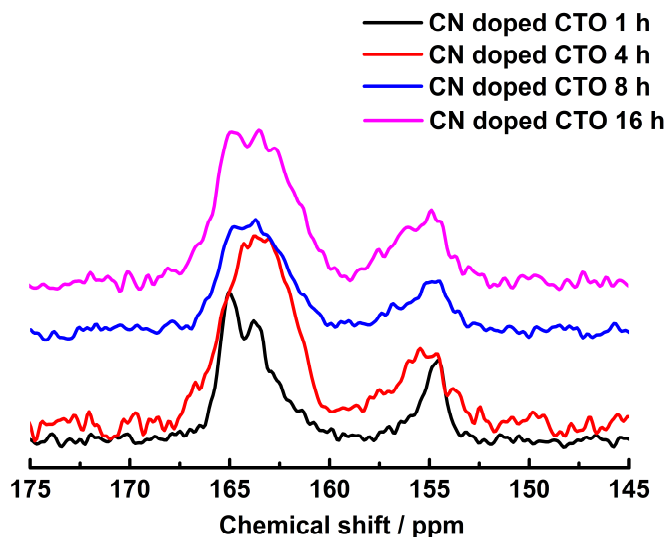
Fig. 4.5 ^{13}C CP-MAS solid-state NMR spectra (spinning frequency 10 kHz) of CN-doped CTO calcined for 1-16 h at 450 °C (the initial weight ratio of melamine and CTO was 1:1).

Solid-state NMR spectroscopy is a valuable tool for probing the structure of semi-crystalline or amorphous materials on local and intermediate length scales, as it is not dependent on the long-range order in contrast to diffraction techniques. The ^{13}C CP-MAS solid-state NMR spectra of the CN-doped CTO 1 – 16 h samples are displayed in Fig. 4.5. The spectra of CN-doped CTO 4-16 h samples show similarities with those of melem and melon. Two signal groups are found

with peak maxima around δ = 164 and 156 ppm. In melon, two groups of carbon resonances are observed at δ = 164 and 157 ppm[19] and in melem two groups of carbon resonances are observed at δ = 164.3/166.4 and 155.1/156.0 ppm, respectively, where the low-field signals (δ = 164 – 166 ppm) are assigned to the carbon positions adjacent to the amino groups and the high-field signals (δ = 155.1/156.0 ppm) are assigned to the carbon positions adjacent to the CN_3 groups[20]. For the CN-doped CTO 1 h sample, there are two signal groups in the range 163 – 165 ppm, which is similar to those of melem rather than melon. Consistent with the IR results, this signal pattern suggests that a substantial carbon nitride part of CN-doped CTO 1 h is melem, whereas the CN-doped CTO 4 – 16 h samples are rather of the melon type.
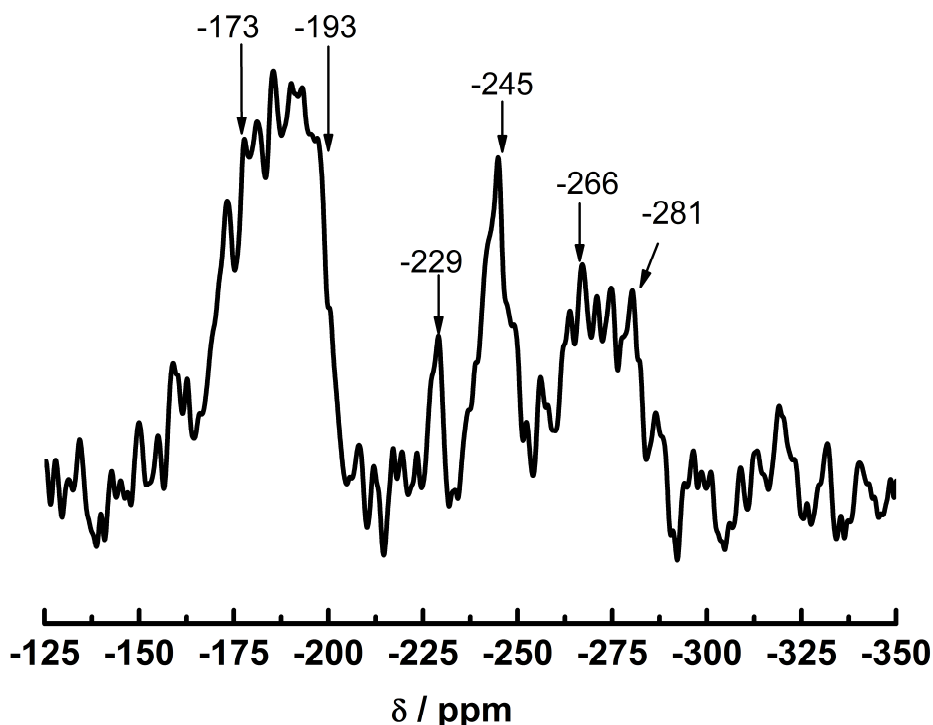
Fig. 4.6 ^{15}N CP-MAS solid-state NMR spectrum (spinning frequency 10 kHz) of CN-doped CTO calcined for 4 h at 450 °C (the initial weight ratio of melamine and CTO was 1:1).

Generally speaking, for the ^{15}N CP-MAS solid-state NMR spectrum, four types of N signals can be distinguished in carbon nitride samples: NH_2, NH, NC_3 and NCN(NH)/NCN(NH$_2$). Fig. 4.6 shows the ^{15}N CP-MAS solid-state NMR spectrum of CN-doped CTO 4 h, where three types of

N signals are observed. As from the elemental analysis results it is evident that the carbon nitride content in the CN-doped CTO calcined for 8 – 36 h samples is rather low, here only the ^{15}N NMR result of the CN-doped CTO 4 h sample is shown. The signals at -266, -245 and -229 ppm are assigned to the NH_2, NH and NC_3 groups of melon, respectively[19]. The signals between -173 and -197 ppm are assigned to the tertiary nitrogen atoms $NCN(NH)/NCN(NH_2)$. It is worth mentioning that the signal δ = -229 ppm of NC_3 is between the NC_3 signals of melem (δ = -234.4 ppm) and melon (δ = -225 ppm). This may indicate that the carbon nitride dopant has a degree of condensation intermediate between that of melem and melon.

4.2.6 Transmission Electron Microscopy
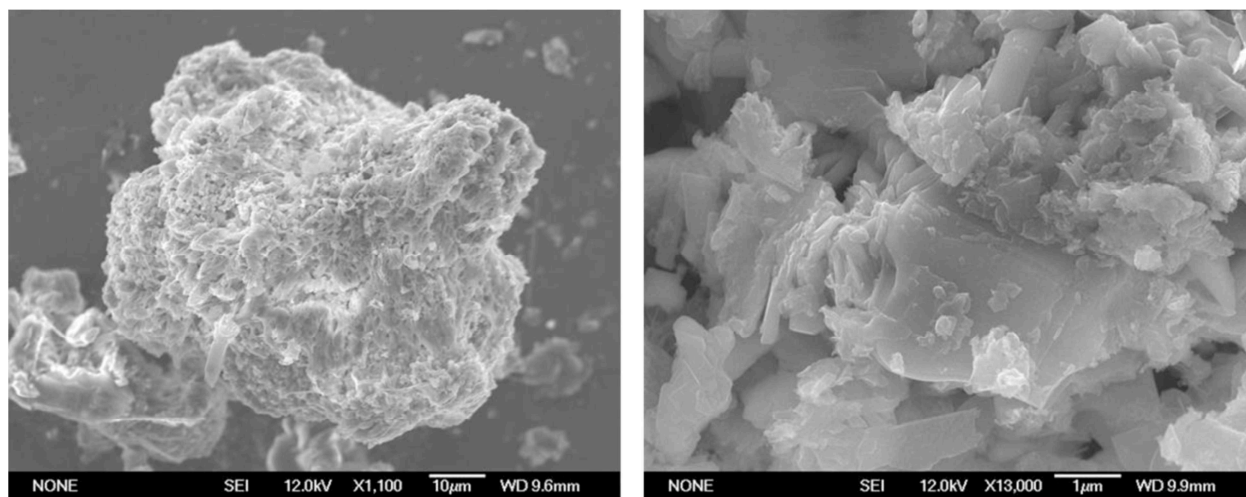
Fig. 4.7 SEM images of CN-doped CTO 4 h calcined at 450 °C (the initial weight ratio of melamine and CTO was 1:1).

The SEM image shows the surface morphology of the CN-doped CTO 4 h sample. It gets evident that part of the sample has a layered structure as steps can be seen near the edges. The particle sizes are not very uniform.
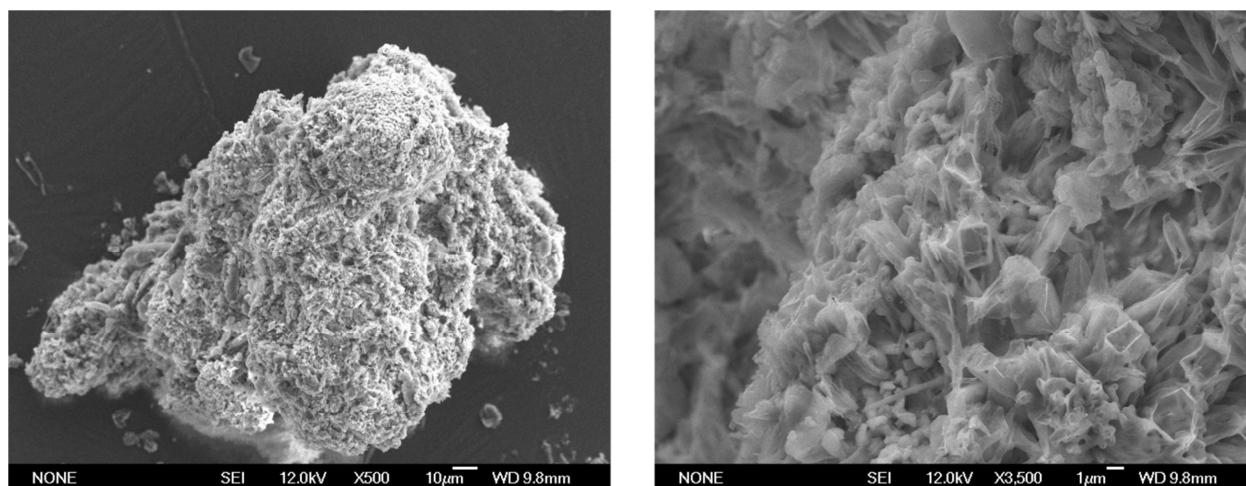
Fig. 4.8 SEM images of CN-doped CTO 16 h at 450 °C (the initial weight ratio of melamine and CTO was 1:1).

The morphology of the CN-doped CTO 16 h is shown in Fig. 4.8. The SEM images indicate that the sample morphology is different from that of the CN-doped CTO 4 h sample, as the layer structure is less evident. However, rectangular structures with a fibrous morphology structures can be seen. However, the particle sizes remain around 60 – 70 μm.

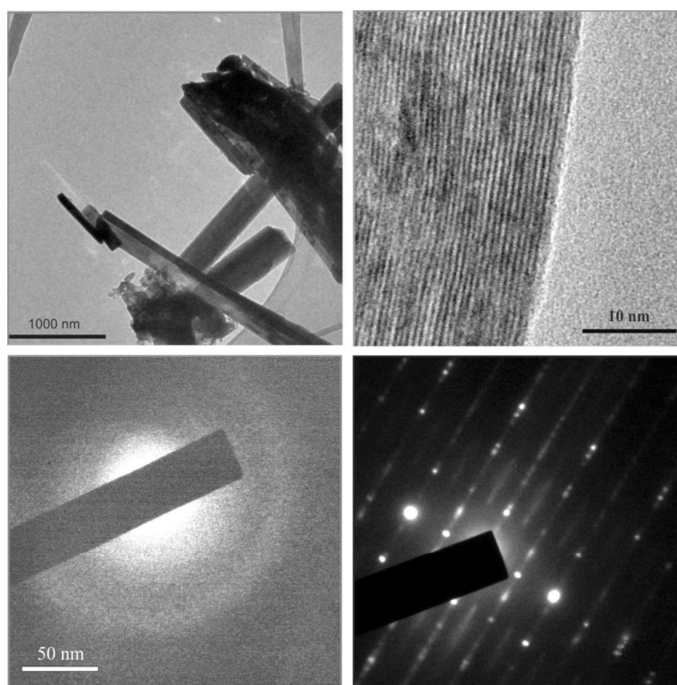**Fig. 4.9** TEM images and diffraction patterns of CN-doped CTO 4 h at 450 °C (the initial weight ratio of melamine and CTO was 1:1).

TEM images of CN-doped CTO 4 h sample are shown in Fig. 4.9. Two kinds of phases can be observed; one is quite densely packed with plate-like shape and the other one consists of small particles without a regular shape. It can be easily distinguished that the plate-like shaped phase is cesium titanate, which has a well-defined layered structure (Fig. 4.9 right top) [25] and the small, ill-defined particles are carbon nitride. Also, it is evident that the carbon nitride material is intimately mixed with the cesium titanate. However, it is not possible to ascertain with this technique whether the two phases interact (i.e. are bonded) chemically. Two diffraction patterns can be observed at the bottom of Fig 4.9, where the left one showing a diffuse ring pattern is indicative of an amorphous structure and belongs to carbon nitride, and the one showing a highly crystalline structure belongs to cesium titanate.

4.2.7 X-ray Photoelectron Spectroscopy
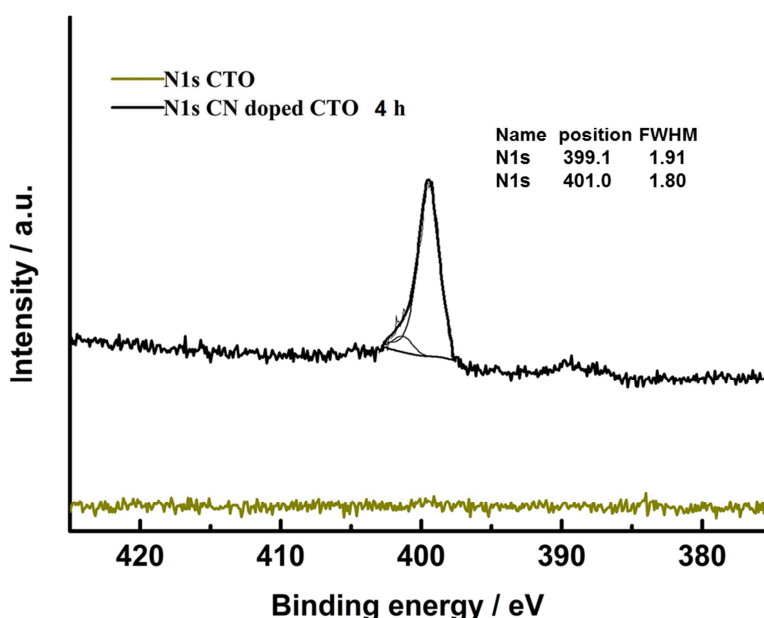
Fig. 4.10 N1s XPS spectra of CTO and CN-doped CTO 4 h (the initial weight ratio of melamine and CTO was 1:1).

Via XPS we can investigate the chemical state of the elements in the samples, albeit only that of the surface portion of the material. Therefore, XPS measurements were conducted to check whether there is a possible interaction of the two phases – carbon nitride and CTO – at their interface through chemical bonding. The chemical states of nitrogen before and after carbon nitride doping of cesium titanate was determined. Fig. 4.10 shows the high-resolution N1s XPS spectra of CTO and CN-doped CTO 4 h. Generally speaking, nitrogen with binding energy at

396 eV is considered to be atomic β-N[26] and indicates the formation of Ti-N bonds in the network of Ti-O-Ti. Interestingly, there is no peak at ~396 eV in our samples. For CN-doped CTO 4 h peak at ~399 eV are observed which can be ascribed to N-H moieties.[11] The shoulder of the two peaks at ~401 eV is assigned to a C=N−C group.[11][27] These data suggest the existence of carbon nitride in the sample. Fig. 4.11 displays the changes of the N1s peak upon sputtering with Ar$^+$ ions so as to remove possible contaminations from the surface of the material. The sputtering procedure results in broader peaks and a very weak shoulder peak is observed around ~397 eV. This peak could point to the presence of nitridic nitrogen as observed in TiN.[28] These results may indicate that a very small fraction of Ti-N bonds is present, which could be either due to classical nitrogen-doped TiO_xN_y with nitrogen on oxygen sites, or due to Ti-N bonds between CN_x and the TiO_x surface.
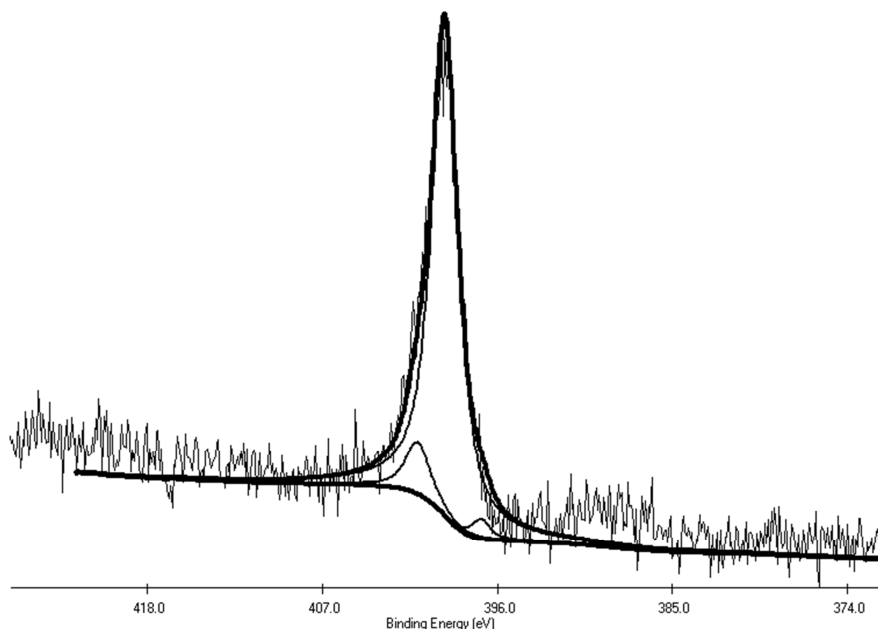
Fig. 4.11 N1s XPS spectra of the CN-doped CTO 4 h sample (the initial weight ratio of melamine and CTO was 1:1) after sputtering with Ar$^+$ ions to remove the top layer and probe the sample interior.
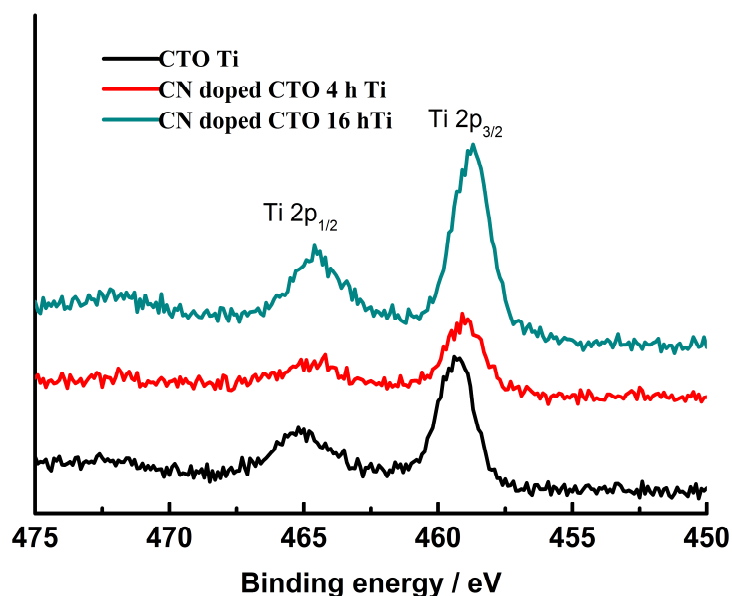
Fig. 4.12 Ti XPS spectra of CTO and CN-doped CTO 4 h and 16 h (the initial weight ratio of melamine and CTO was 1:1).

Fig. 4.12 shows Ti XPS spectra of CTO and CN-doped CTO 4 h and 16 h. Two peaks which are assigned as Ti $2p_{3/2}$ and Ti $2p_{1/2}$, respectively, can be seen for all of these samples. The Ti $2p_{3/2}$ and Ti $2p_{1/2}$ peaks of the doped samples are at around 464.6 eV and 458.8 eV, and are therefore shifted to lower energies compared with that of CTO (465.2 eV and 459.2 eV). The shift to lower binding energies suggests that some Ti^{4+} atoms are partially reduced to a lower oxidation state, presumably due to the nitrogen species bound to Ti or to a higher amount of oxygen vacancies.[9]

4.2.8 Photocatalytic Activity

In order to test the photocatalytic properties of these carbon nitride-doped CTO samples, hydrogen evolution reaction experiments were carried out. The procedure is similar to that of chapter 3; the only difference is the type of illumination. In this chapter, UV light was used as the light source, rather than visible light. UV light at 255 and 366 nm illuminated the samples for 3 hours.

Fig. 4.13 Hydrogen production under UV irradiation (3h) of calcined melamine samples at different calcination times and CN-doped CTO materials.

Fig. 4.13 shows the comparison of UV-driven hydrogen production for calcined melamine materials and CN-doped CTO materials. It can be seen that in the same illumination time, the hydrogen amount is gradually increasing with increasing calcination times up to 16 h. Notably, the melamine sample calcined for 16 h shows a quite high hydrogen evolution capability compared to the others. Quite likely, the 16 h calcined sample is the most highly condensed carbon nitride, or it shows a higher efficiency owing to a higher degree of 'defect-containing' sites which may assist charge recombination.[16] UV hydrogen production for the pure CTO sample results in negligible H_2 after 3 h illumination, which suggests that the pure CTO is not active in H_2 evolution under the conditions used. After CN-doping, most of the samples show

less hydrogen production than the pure carbon nitride samples. For the CN-doped CTO 32 h sample, there is too little carbon nitride present (0.25%) to substantially increase the photocatalytic hydrogen evolution of CTO. According to the EA results, the composition of the CN-doped CTO 16 h sample is only 12% C+N+H and 88 % CTO. Assuming the active material is carbon nitride, Fig. 4.14 displays the calculated photocatalytic activites of CN-doped CTO compared with calcined melamine samples having the same weight of carbon nitride. Then, all CN-doped CTO samples exhibit better hydrogen production efficiency than the pure carbon nitride samples, meanwhile the CN-doped CTO 16 h sample still shows the best activity. This suggests that CN-doped CTO 16 h samples are not a true composite mixture of CN and CTO, but it may be a heterojunction-type material with a large amount of CTO – carbon nitride interfaces. After exciton formation, charge separation at these interfaces is facilitated by the presence of interfaces, and, hence, fast charge recombination is hindered. According to the XPS results the presence of Ti-N bonds cannot be excluded; however non-covalent interactions between the carbon nitride dopant and the titanate are more likely to be responsible for the good photocatalytic activity.

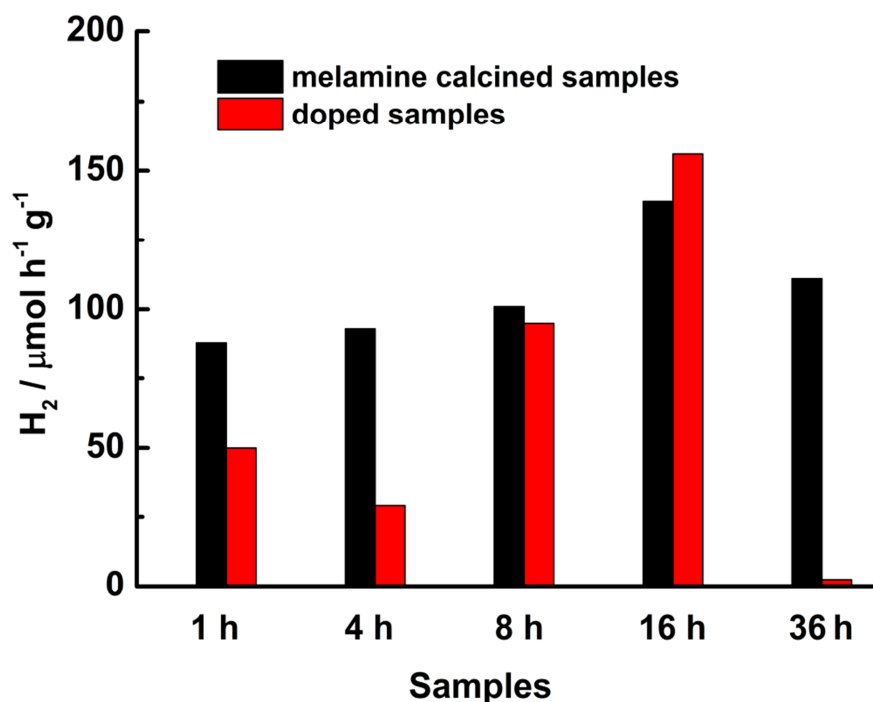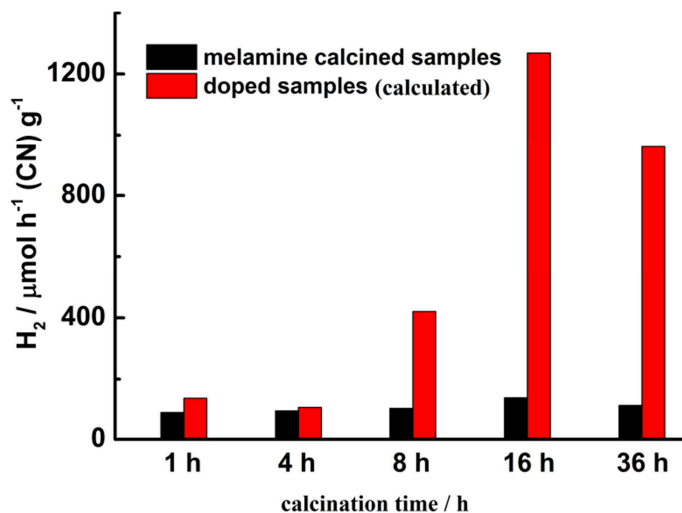**Fig. 4.14** Hydrogen production under UV irradiation (3h) of calcined melamine samples at different calcination times and CN-doped CTO materials (calculated based on the same weight of carbon nitride, see text).

The morphology of the CN-doped CTO 16 h sample could also influence the photocatalytic properties. As seen in the SEM images (Section 4.2.6), the CN-doped CTO 16 h sample has a large amount of rectangular, tube-like structures within a fibrous matrix, and its surface may be more irregular and thus larger than that of the CN-doped CTO 4 h sample.

4.3 Conclusion

In summary, a series of CN-doped CTO materials with low band gaps were prepared by calcining melamine in the presence of CTO at 450 °C for different times in a half open system. Promising visible light absorption was ascertained from the UV-Vis spectra with band edges at around 440 nm. XPS spectra illustrate the binding situation between the CTO and carbon nitride materials for the doped materials after Ar^+ polishing. Comparing the same amounts of photocatalysts, the CN-doped materials do not show significantly higher photocatalytic activities in hydrogen evolution experiments under UV light illumination as compared to the pure carbon nitride samples. Only the CN-doped CTO 16 h sample, which is a mixture of 12 % CN and 88% CTO, produced more hydrogen than the corresponding melamine sample calcined for 16 h. However, the calculated hydrogen production of all CN-doped CTO samples is higher than those of the pure carbon nitrides samples when equal absolute amounts of carbon nitride where inferred for the photocatalyst. Presumably, the carbon nitride and CTO form a heterojunction-type architecture which facilitates charge separation and, hence, increases the photocatalytic activity.

4.4 Chapter References

[1]   A. Fujishima, K. Honda, *Nature* **1972**, *238*, 37–38.

[2]   Y. Ide, M. Matsuoka, M. Ogawa, *Journal of the American Chemical Society* **2010**, *132*, 16762–16764.

[3]   Z. J. Chen, B. Z. Lin, B. H. Xu, X. L. Li, Q. Q. Wang, K. Z. Zhang, M. C. Zhu, *Journal of Porous Materials* **2010**, *18*, 185–193.

[4]   J. Geng, D. Yang, J. Zhu, D. Chen, Z. Jiang, *Materials Research Bulletin* **2009**, *44*, 146–150.

[5]   F. Sastre, Y. Bouizi, V. Fornés, H. Garcia, *Journal of Colloid And Interface Science* **2010**, *346*, 172–177.

[6]   S. Mozia, E. Borowiak-Paleń, J. Przepiórski, B. Grzmil, T. Tsumura, M. Toyoda, J. Grzechulska-Damszel, A. W. Morawski, *Journal of Physics and Chemistry of Solids* **2010**, *71*, 263–272.

[7]   N. Miyamoto, K. Kuroda, M. Ogawa, *The Journal of Physical Chemistry B* **2004**, *108*, 4268–4274.

[8]   R. Beranek, H. Kisch, *Angewandte Chemie (International ed.)* **2008**, *47*, 1320–1322.

[9]   R. Beranek, H. Kisch, *Photochemical & photobiological sciences* **2008**, *7*, 40–48.

[10]   D. Mitoraj, H. Kisch, *Angewandte Chemie (International ed. in English)* **2008**, *47*, 9975–9978.

[11]   D. Mitoraj, H. Kisch, *Chemistry A European Journal* **2010**, *16*, 261–269.

[12]   H. Kisch, S. Sakthivel, M. Janczarek, D. Mitoraj, *Journal of Physical Chemistry C* **2007**, *111*, 11445–11449.

[13] S. C. Yan, S. B. Lv, Z. S. Li, Z. G. Zou, *Dalton transactions (Cambridge, England : 2003)* **2010**, *39*, 1488–1491.

[14] T. Sasaki, M. Watanabe, Y. Michiue, Y. Komatsu, F. Izumi, S. Takenouchi, *Society* **1995**, 1001–1007.

[15] D. Mitoraj, R. Beránek, H. Kisch, *Photochemical & photobiological sciences : Official journal of the European Photochemistry Association and the European Society for Photobiology* **2010**, *9*, 31–38.

[16] X. Wang, K. Maeda, A. Thomas, K. Takanabe, G. Xin, J. M. Carlsson, K. Domen, M. Antonietti, *Nature materials* **2009**, *8*, 76–80.

[17] B. Yue, Q. Li, H. Iwai, T. Kako, J. Ye, *Science and Technology of Advanced Materials* **2011**, *12*, 034401.

[18] M. R. Bayati, R. Molaei, a. Z. Moshfegh, F. Golestani-Fard, *Journal of Alloys and Compounds* **2011**, *509*, 6236–6241.

[19] B. V Lotsch, M. Döblinger, J. Sehnert, L. Seyfarth, J. Senker, O. Oeckler, W. Schnick, *Chemistry (Weinheim an der Bergstrasse, Germany)* **2007**, *13*, 4969–4980.

[20] B. Jürgens, E. Irran, J. Senker, P. Kroll, H. Müller, W. Schnick, *Journal of the American Chemical Society* **2003**, *125*, 10288–10300.

[21] F. Zimmermann, T. Lippert, C. Beyer, J. Stebani, O. Nuyken, A. Wokaun, *Applied Spectroscopy* **1993**, *47*, 986–993.

[22] H. Yan, Y. Huang, *Chemical Communications* **2011**, *47*, 4168-4171.

[23] J. Kaufman, S. Metin, D. Saperstein, *Physical Review B* **1989**, *39*, 13053–13060.

[24] F. Alvarez, N. M. Victoria, P. Hammer, F. L. Freire, M. C. dos Santos, *Applied Physics Letters* **1998**, *73*, 1065–1067.

[25] I. E. Grey, I. C. Madsen, J. A. Watts, M. Chemistry, P. Melbourne, L. A. Bursill, J. Kwiatkowska, *journal of solid state chemistry* **1985**, *58*, 350–356.

[26] R. Asahi, T. Morikawa, T. Ohwaki, K. Aoki, Y. Taga, *Science (New York, N.Y.)* **2001**, *293*, 269–271.

[27] T. Komatsu, T. Nakamura, *Journal of Materials Chemistry* **2001**, *11*, 474–478.

[28] N. C. Saha, H. G. Tompkins, *Journal of Applied Physics* **1992**, *72*, 3072–3079.

Chapter 5

The synthesis and characterization of "OH-melem"

5.1 Introduction

OH-melem is short for oxo-diamino heptazine (or hydroxy-diamino heptazine), which refers to the different tautomers of the compound 2-oxo-6,10-diamino-*s*-heptazine (Fig. 5.1 A). As yet, not much has been reported concerning such compounds. So far, well-characterized heptazine derivatives are mostly substituted with three identical functional groups[1] as shown in Fig. 5.1 B. However, there are two different functionalities in OH-melem, which may open up avenues to overcome the synthetic limitations of heptazines. The synthesis of OH-melem by a careful alkaline hydrolysis of melon has been reported by Finkel'shtein et al.[2] The reactivity has been claimed to be tunable by adjusting the concentration of hydroxide base and reaction time.

R=NH, NH$_2$, H, Cl, N$_3$,
OK, (NCN)K, OH etc.
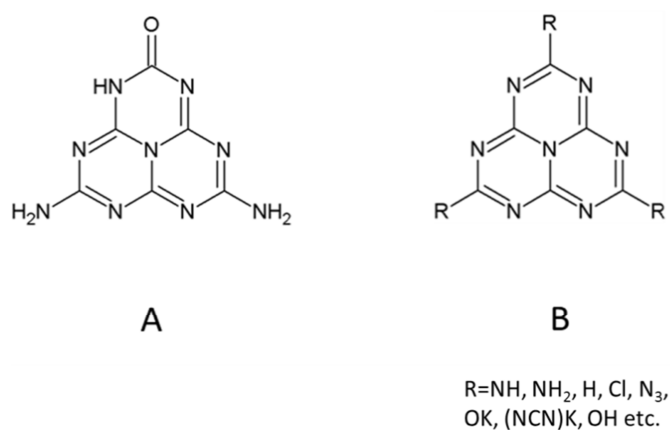
Fig. 5.1 (A) 2-Oxo-6,10-diamino-*s*-heptazine and (B) general structure of heptazine derivatives.[1]

In A. Sattler's Ph.D thesis OH-melem was also mentioned, yet he was unable to reproduce these oxo-amino heptazines.[3] It was claimed that the 2-oxo-6,10-diamino-*s*-heptazine is possibly only mixtures of cyameluric acid with unreacted starting material. These findings suggest that the synthesis of OH-melem is difficult to control. In this thesis, we try to use a strong oxidizing acid for the hydrolysis of calcined melamine samples to produce OH-melem.

5.2 Results and Discussion

5.2.1 X-ray powder Diffraction

Fig. 5.2 Powder XRD patterns of OH-melem prepared with different starting materials (4 mL H_2SO_4 and hydrolysis temperature of 80 °C).

The procedure of preparing OH-melem has many variables; such as starting material, amount of oxidizing agent H_2SO_4, temperature and time etc., which can influence the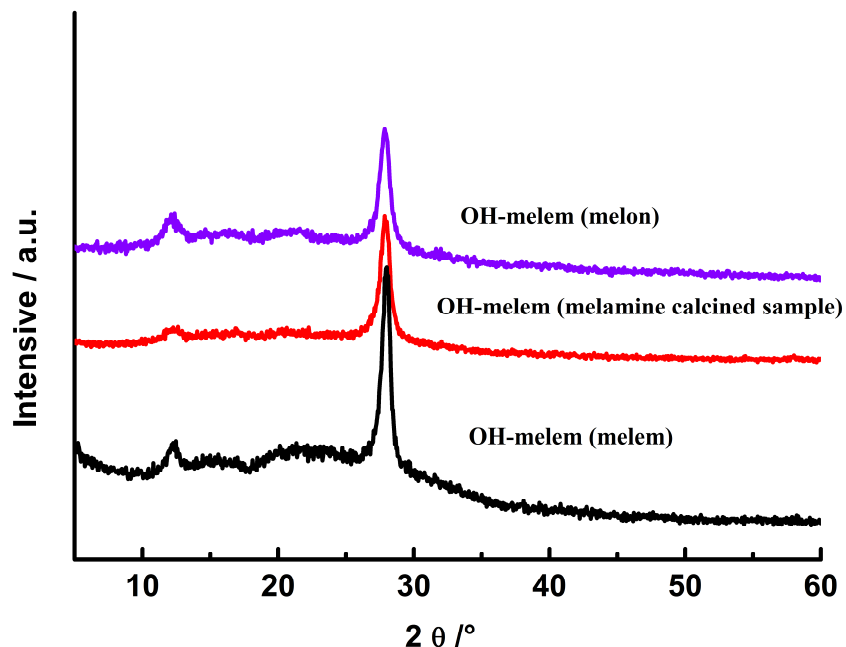 final experimental products. Therefore, many experiments were carried out to investigate these factors. Fig. 5.2 shows the powder XRD patterns of OH-melem, which were prepared with different starting materials (4 ml H_2SO_4, hydrolysis temperature 80 °C). It can be seen that these XRD patterns are similar, with a main peak at around $2\theta = 27.8$ ° and a small shoulder peak at around $2\theta = 12.2$ ° which is different from melem and the calcined melamine sample. The XRD pattern of OH-melem is reminiscent of melon.[4] Melon also has a characteristic signature at $2\theta = 27.3°$ indicating the stacking layer distance. It suggests that OH-melem has a similar (pseudo-) layered structure like melon with a stacking distance around 3.20 Å, and the type of starting material is not a crucial factor in the OH-melem synthesis.
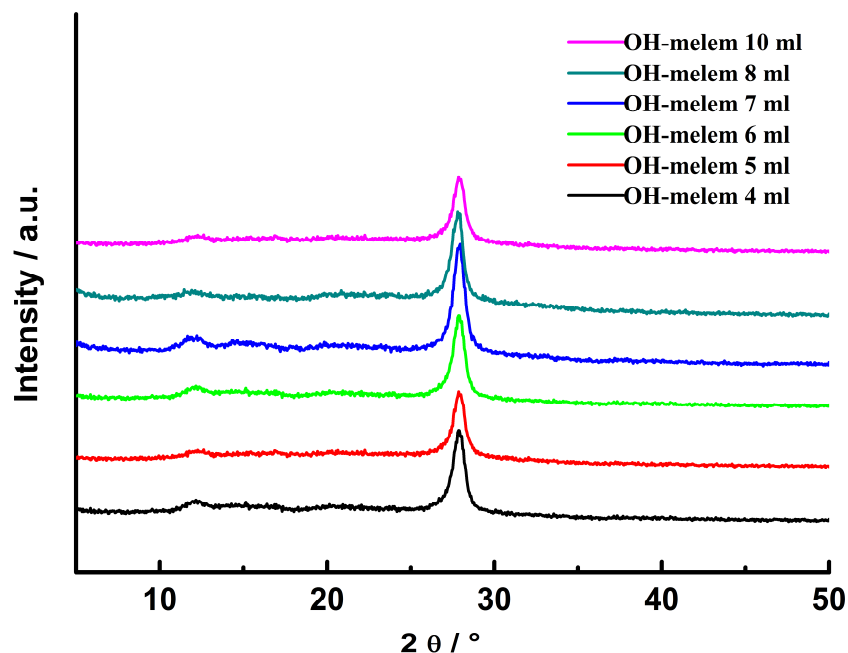
Fig. 5.3 Powder XRD patterns of OH-melem prepared with different amounts of H_2SO_4 (hydrolysis temperature is 80 °C and calcined melamine as starting material).

In order to investigate the influence of the strongly oxidizing acid in the preparation of OH-melem, different amounts of H_2SO_4 were added to hydrolyze the calcined melamine sample. Fig. 5.3 shows the XRD patterns of OH-melem prepared with different amounts of H_2SO_4 (starting material: calcined melamine, hydrolysis temperature 80 °C). It can be seen that all the XRD patterns are similar with a main peak at around $2\theta = 27.9°$ and a small peak at around $2\theta = 12.2°$. We speculate that changing the amount of acid does not have a visible influence on the XRD signature of the products.
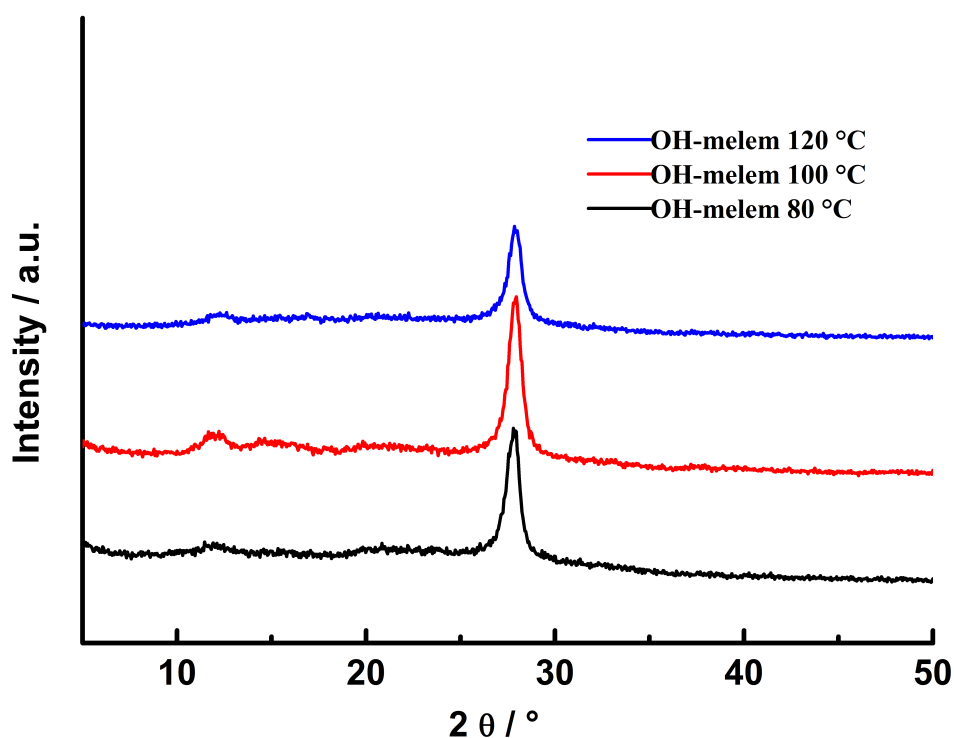
Fig. 5.4 Powder XRD patterns of OH-melem prepared with different hydrolysis temperatures (4 mL H_2SO_4 and calcined melamine as starting material).

The influence of the hydrolyzing temperature was also investigated. As seen in Fig. 5.4 the XRD patterns of OH-melem synthesized at different temperatures are very similar with the main peaks at around $2\theta = 27.9°$. Therefore, the influence of the hydrolyzing temperature also does not seem to be very pronounced.

We also did a comparison between the starting materials and OH-melem. As all of the OH-melem XRD patterns are similar, only one sample was chosen for the comparison. Fig. 5.5 shows the XRD comparison of the product with all the starting materials. It is evident that the XRD pattern of OH-melem is different from that of all the starting materials themselves, although the XRD pattern of OH-melem is similar to that of melon.

Fig. 5.5 Powder XRD patterns of OH-melem together with all the starting materials.

These data suggest that all these factors do not have much influence on the XRD patterns of the OH-melem samples and there is no starting material left in the OH-mele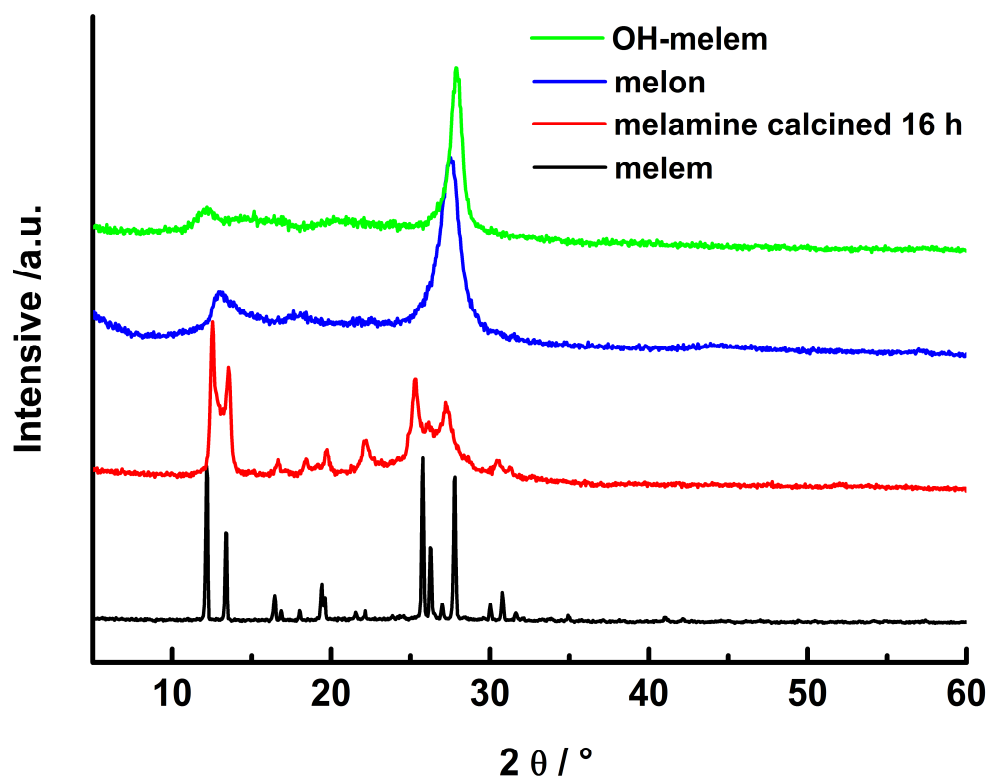m product. However, the OH-melem samples do not possess good crystallinity, so only the graphitic layer structure can be seen in the XRD patterns.

5.2.2 IR Spectroscopy
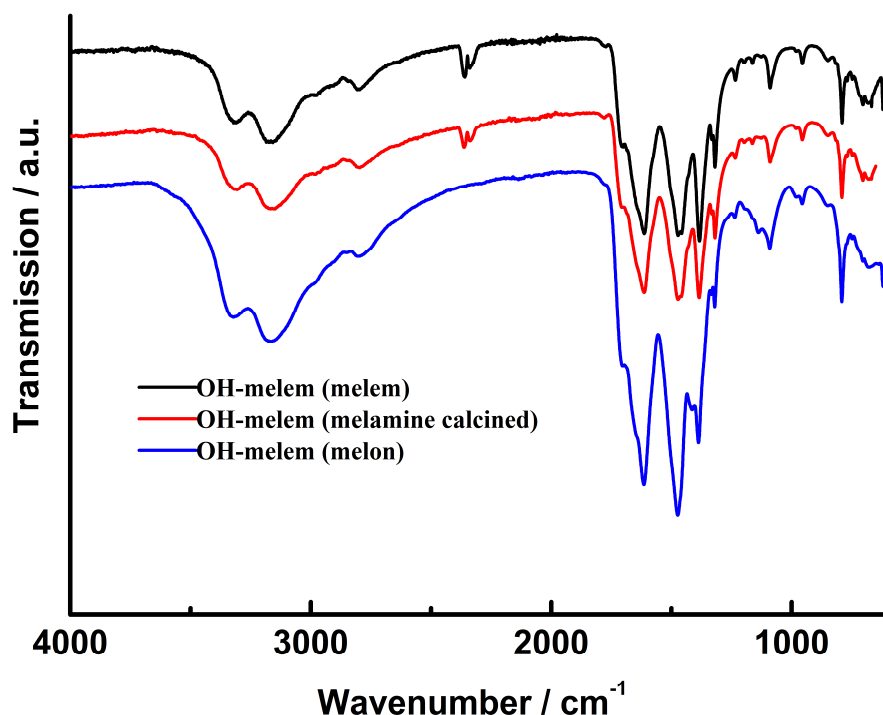
Fig. 5.6 FTIR spectra of OH-melem prepared with different starting materials (melem, calcined melamine sample and melon).

The IR spectra of the OH-melem samples with different starting materials are displayed in Fig. 5.6. It can be seen that all three of these samples have very similar IR spectra with the bands almost coinciding. The IR spectra of OH-melem display the absorption bands for NH_2 or NH at 3323 cm^{-1}, 3172 cm^{-1} and possibly 2801 cm^{-1}.[5][6] The low intensity, small band at 1710 cm^{-1} and 1646 cm^{-1} are indexed as the C=O stretching[5]. The medium intensity, sharp band at around 800 cm^{-1} suggests that the materials consist of a cyameluric core[4]. Meanwhile, three medium strong bands are found at 1612 cm^{-1}, 1475 cm^{-1} and 1382 cm^{-1} for all of the OH-melem samples. This feature has been observed in several carbon nitride materials with an assumed heptazine-based structure.[1,7–10] As for OH-melem there could be different tautomeric forms as shown in Fig 5.7. No obvious bands pertaining to the OH group are visible in the IR spectra. This may suggest that OH-melem has a molecular structure as shown in Fig. 5.1 (A).
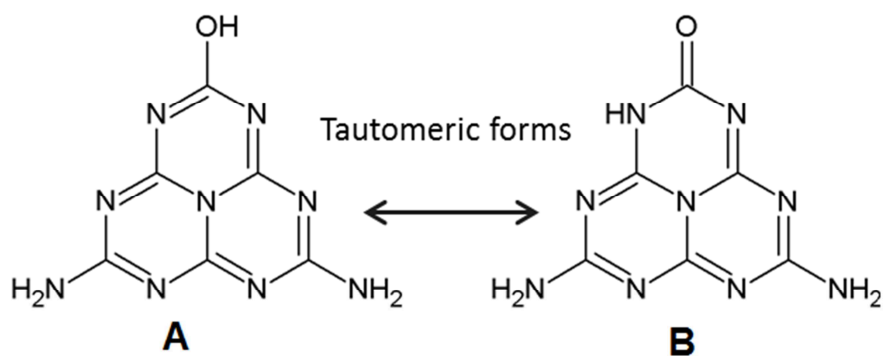
Fig. 5.7 Tautomeric forms of OH-melem.

When different amounts of H_2SO_4 are added to hydrolyze the starting material at 80 °C, very similar IR spectra of the OH-melem products are obtained as shown in Fig. 5.8. The broad bands at around 3323, 3172 and 2801 cm^{-1}, the small and weak bands at around 1710 and 1646 cm^{-1} together with the sharp band at approximately 800 cm^{-1} appear in all IR spectra. This suggests that changing the amount of the H_2SO_4 does not have much influence on the formation of the OH-melem products.
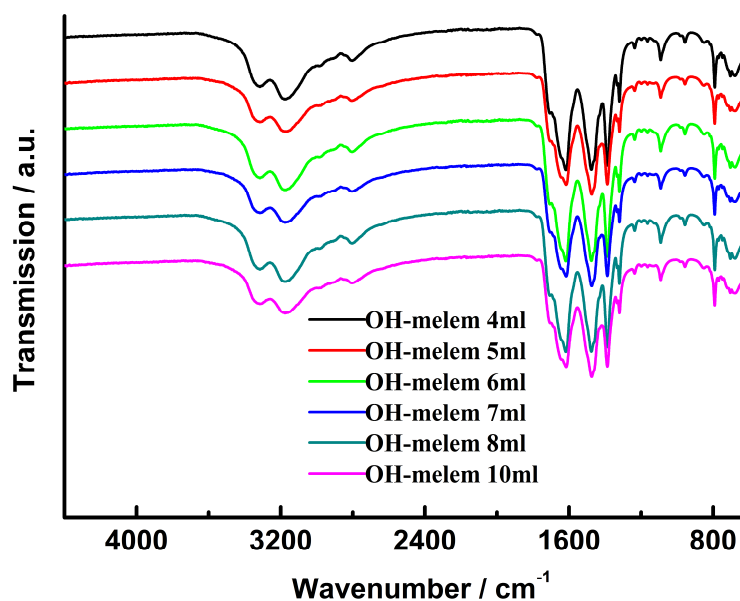
Fig. 5.8 FTIR spectra of OH-melem prepared with different amounts of H_2SO_4 (hydrolysis temperature is 80 °C and starting material is calcined melamine).
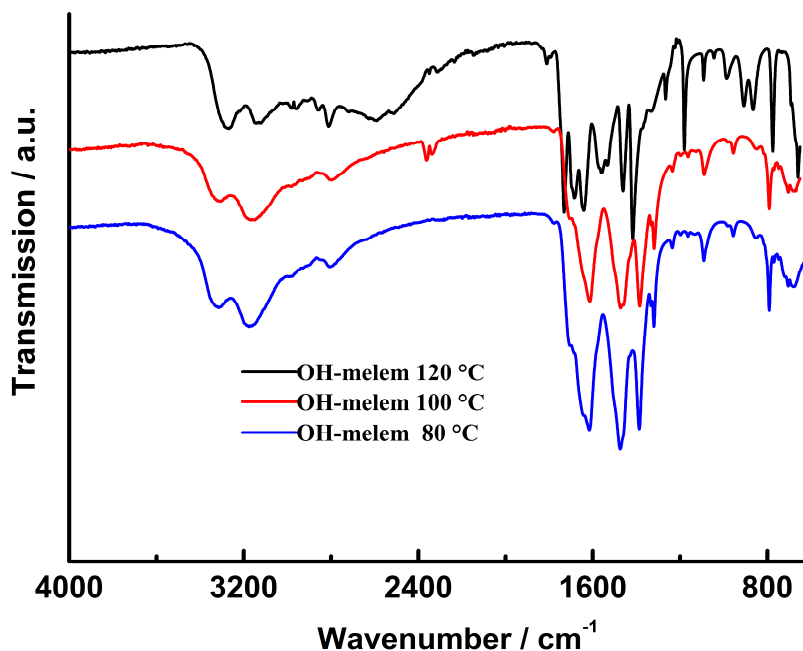
Fig. 5.9 FTIR spectra of OH-melem prepared at different hydrolysis temperatures (4 ml H_2SO_4 and calcined melamine as starting material).

The IR spectra of the OH-melem samples prepared at different hydrolyzing temperatures are displayed in Fig. 5.9. When the hydrolyzing temperatures were 80°C and 100 °C, similar IR spectra of the OH-melem products are obtained with the major bands being at almost the same positions. However, when the temperature was raised to 120 °C, some different and extra bands were found. The sharp band at around 800 cm^{-1} was left-shifted to 774 cm^{-1}, which can be due to the formation of cyameluric acid or cyanuric acid or it may indicate the protonation of the heptazine ring.[3][12] Two sharp peaks can be seen at 1455 cm^{-1} and 1417 cm^{-1}, which can be indexed as NH deformation.[13] There is another strong band at 1180 cm^{-1}, which may be attributed to HSO_4^-,[14] resulting from a heptazine- or triazine-based sulfate or hydrogen sulfate salt.

5.2.3 Elemental Analysis Results

In order to obtain more information about the composition of OH-melem, elemental analysis was conducted to determine the amount of C, N and H in the material. Table 5.1 shows the elemental analysis results of OH-melem synthesized from different starting materials (synthesis condition: 4 ml H_2SO_4, hydrolyzing temperature 80 °C). As outlined above, there is almost no difference in XRD and FTIR results for the OH-melem obtained from different starting materials. However, there are some differences in the elemental analysis results. When the starting materials are calcined melamine, the N/C ratios of OH-melem are close to the theoretical ratio of 1.76. The N/C ratio of OH-melem obtained from melon is far away from the theoretical one. One possible reason could be that the basic units of melon have decomposed or have been overoxidized by H_2SO_4 as melon needs a long time to be totally dissolved in the H_2SO_4 solution. The elemental composition of OH-melem prepared with calcined melamine and melem as starting materials is close to the theoretical content of OH-melem•$0.8H_2O$; meanwhile the N/C ratio is also similar to the theoretical one.

Table 5.1 Elemental analysis results for OH-melem prepared with different starting materials (4 mL H_2SO_4 and hydrolysis temperature 80 °C).

Samples (starting materials)	OH-melem (melon)	OH-melem (c.m.[&] sample)	OH-melem (melem)	OH-melem*	OH-melem•$0.8H_2O$*
N / %[#]	49.54	53.59	54.31	57.50	53.98
C / %[#]	27.17	30.15	30.68	32.90	30.85
H / %[#]	3.29	3.13	2.96	2.30	2.49
Rest / %[#]	20.00	13.13	12.05	7.3	12.68
N/C	1.82	1.78	1.77	1.75	1.75

* calculation from theoretical molecular formular; [#]: weight percentage, &: c.m. is short for calcined melamine at 450 °C for 16 h

When different amounts of H_2SO_4 were added to hydrolyze the starting material at 80 °C, elemental analysis was also conducted. Table 5.2 shows the elemental analysis results of the OH-melem prepared with different amounts of H_2SO_4. The nitrogen, carbon, and hydrogen weight percent of all OH-melem samples are around 54%, 30% and 3.1% respectively. The composition

of the rest in Table 5.2 should be oxygen, which is the main part, and sulfur. All the samples have a similar content of N, C and H, which indicates that changing the amount of the H_2SO_4 does not have much influence on the OH-melem products.

Table 5.2 Elemental analysis results of OH-melem prepared with different amounts of H_2SO_4.

Samples (H$_2$SO$_4$ / ml)	OH-melem (4 ml)	OH-melem (5 ml)	OH-melem (6 ml)	OH-melem (7 ml)	OH-melem (8 ml)	OH-melem (10 ml)
N / %	53.59	53.87	53.81	54.83	53.49	53.82
C / %	30.15	30.17	29.65	30.24	29.65	30.32
H / %	3.13	3.05	3.39	3.15	3.21	3.08
rest / %	13.13	12.91	13.15	11.78	13.65	12.78
N / C	1.78	1.79	1.81	1.81	1.80	1.77

The elemental analysis results of the OH-melem samples obtained at different hydrolyzing temperatures are displayed in Table 5.3. When the hydrolyzing temperatures were 80 °C and 100 °C, similar elemental compositions of OH-melem can be inferred. However, when the temperature reached 120 °C, the nitrogen weight percentage and the N/C ratio go down. A possible reason is that when the hydrolyzing temperature is 120 °C, the starting material is overoxidized and "2OH-melem" (dioxo-amino-heptazine), cyameluric acid or even cyanuric acid is obtained. Oxygen determination experiments were also carried out for OH-melem (synthesis condition: calcined melamine as starting material, 4 ml H_2SO_4, hydrolyzing temperature 80 °C). Around 10% oxygen is found in the sample. The theoretical amount of oxygen in OH-melem should be 7.3%, thus indicating that there may be some water of crystallization by analogy to melem, which quite easily forms melem hydrate in water.[15] The OH-melem•0.8H$_2$O is close to the experimental results, however further investigations need to be done.

Table. 5.3 Elemental analysis results of OH-melem prepared at different hydrolysis temperatures (starting material: calcined melamine and 4 mL H_2SO_4).

Samples (temperature / °C)	OH-melem (80 °C)	OH-melem (100 °C)	OH-melem (120 °C)	2OH-melem*
N / %	53.59	53.34	43.56	50.9
C / %	30.15	30.20	28.00	32.7
H / %	3.13	3.14	3.48	1.8
Rest / %	13.13	13.12	34.96	14.5
N / C	1.78	1.77	1.55	1.55

* calculation from theoretical molecular formular

5.2.4 Solid-state NMR Spectroscopy

Solid-state NMR spectroscopy was used to probe the local structure of the OH-melem material, of which no single crystal could be obtained. ^{1}H, ^{13}C and ^{15}N CP-MAS NMR spectra were recorded. Fig. 5.10 shows the ^{1}H MAS solid-state NMR spectra of OH-melem and melem. OH-melem was prepared by hydrolyzing calcined melamine at 80 °C with 4 ml H_2SO_4. Two broad signals peaking at around 4 and 12 ppm can be observed. This suggests there are at least two different types of protons in the sample and the hydrogen pattern is distinct from that in melem. The peak at around 4 ppm can be assigned to the NH_2 group; the peak at around 12 ppm can be assigned to OH or NH groups. As can be seen, the signal at around 12 ppm is very broad, which may result from the presence of different functional groups and from structural disorder.

Fig. 5.10 ^{1}H MAS solid-state NMR spectra of OH-melem and melem.
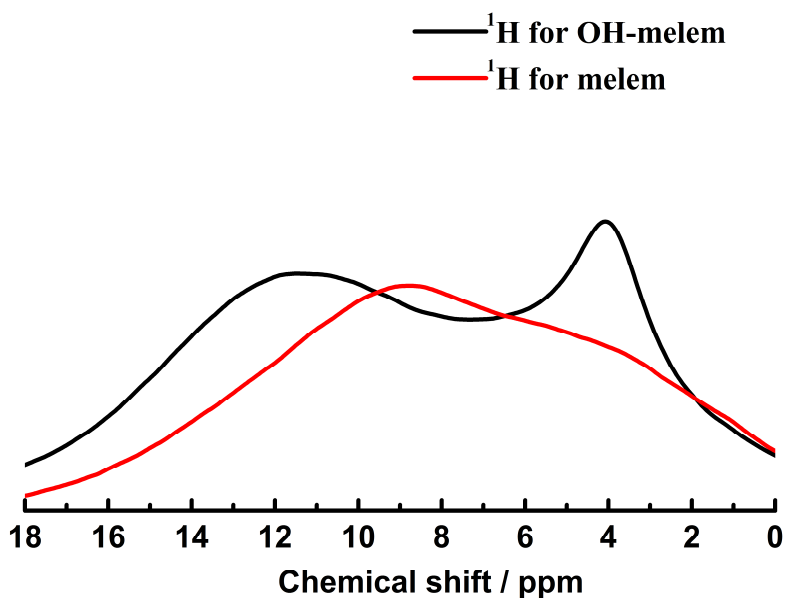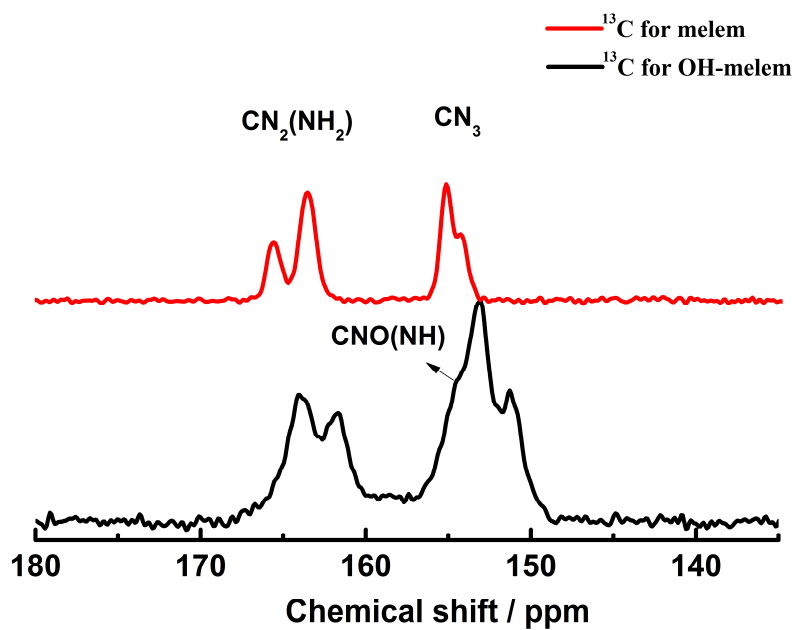

Fig. 5.11 ^{13}C MAS solid-state NMR spectra of OH-melem and melem.

In the ^{13}C NMR spectrum shown in Fig. 5.11, two typical signal groups of melem at around 153 – 156 ppm and 164 – 166 ppm can be observed, which belong to the CN_3 and $CN_2(NH_2)$ groups, respectively. Two similar groups are also observed in the spectrum of OH-melem. The signal

group at around 161 – 164 ppm belongs to the $CN_2(NH_2)$ groups. In contrast, however, the carbon atoms $CN_2(NH_2)$ in melem are shifted downfield; the carbon atoms CNO(NH) in cyameluric acid are slightly shifted upfield with respect to those in OH-melem (152 – 156 ppm).[16] A shoulder signal at around 154 ppm can be seen, which should belong to the CNO(NH) group. The signal group of OH-melem at around 151 – 153 ppm belongs to the CN_3 group of the cyameluric nucleus. This signal group is also shifted upfield compared with that of melem.[16] These findings suggest that OH-melem has the molecular structure as shown in Fig. 5.1(A).

Meanwhile, ^{15}N CP-MAS NMR spectra of melem and OH-melem were recorded (Fig. 5.12). In the spectrum of melem, resonances of the outer ring tertiary nitrogen atoms (N_{tert}) are observed between -197 and -205 ppm with five different signals. For the central nitrogen atom N_c, the intensity of the peak is too low and so this particular resonance cannot be found. The signals arising at -267 and -281 ppm originate from the NH_2 groups.[17] In the spectra of OH-melem, the signal group around -199 to -213 ppm can be assigned to the N_{tert}. The resonance arising at -269 ppm can be assigned to NH_2 groups. A sharp signal at around -246 ppm can be seen clearly, which should belong to the NH group.[4] This corroborates that OH-melem has the molecular structure shown in Fig. 5.1(A). Interestingly, the small sharp signal at -238.4 ppm can be observed which should originate from the central nitrogen atom N_c. The shift of N_c is quite characteristic. In melem the shift of N_c is -234.2 ppm, in cyameluric acid it is -245 ppm. As with the amount of oxygen increasing the shift decreases, we infer a linear dependence of the resonance of N_c on the amount of covalently bonded oxygen per molecule. Fig. 5.13 depicts this relationship, which gives an oxygen amount per molecule of 1.16 when the shift of N_c is -238.4 ppm, which is quite close to 1. This can be seen as another piece of indirect evidence that there is in fact one oxygen in the sample we assume to be OH-melem.
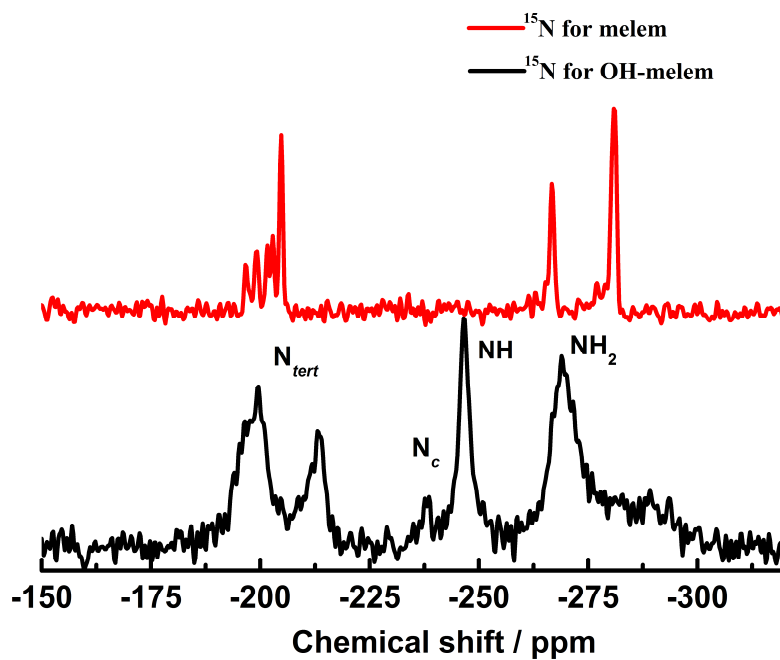
Fig. 5.12 ^{15}N CP-MAS solid-state NMR spectra of OH-melem (starting material: calcined melamine, hydrolysis temperature 80°C and 4 mL H_2SO_4) and melem.
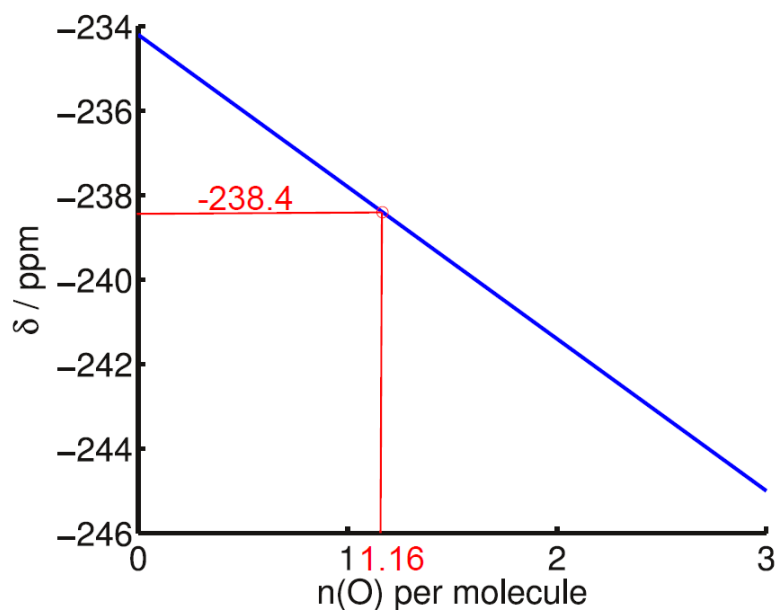

Fig. 5.13 A linear relationship between the amount of oxygen per melem molecule (given in atoms per molecule) and the chemical shift of the central nitrogen of the heptazine ring, N_c.

5.2.5 Mass Spectrometry Results

In order to confirm the identity of OH-melem based on its molecular formula, mass spectrometry experiments (DEI$^+$) were carried out. Most of the OH-melem samples show very similar mass spectrometry results. Here only a few mass spectrometric data are shown. As seen in Fig. 5.14 and Fig 5.15, the peak at *m/z* 219 representing the molecular mass peak of OH-melem (M_w = 219.10 g/mol) can be observed in both spectra. Some main fragments are assigned as follows: 178 (OH-melem$^+$ – CNO), 127 ([C3N6H7]$^+$), 68 ([C2N3H2]$^+$), 43 ([CN2H3]$^+$).[17][18]
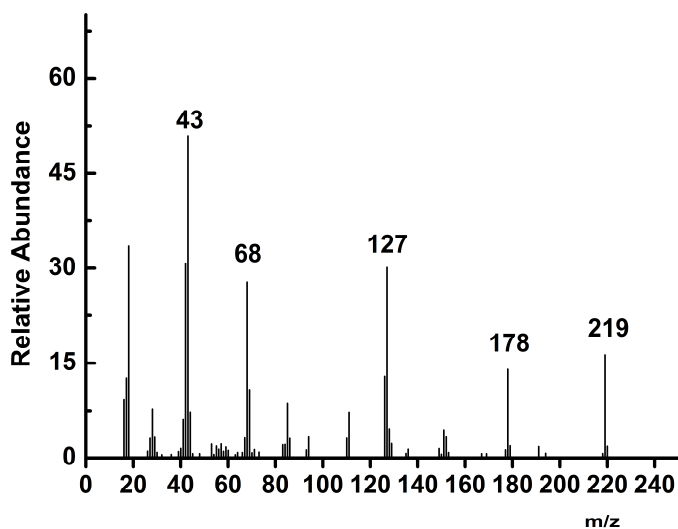
Fig. 5.14 Mass spectrometry result (DEI$^+$) for OH-melem prepared with melon as starting material.
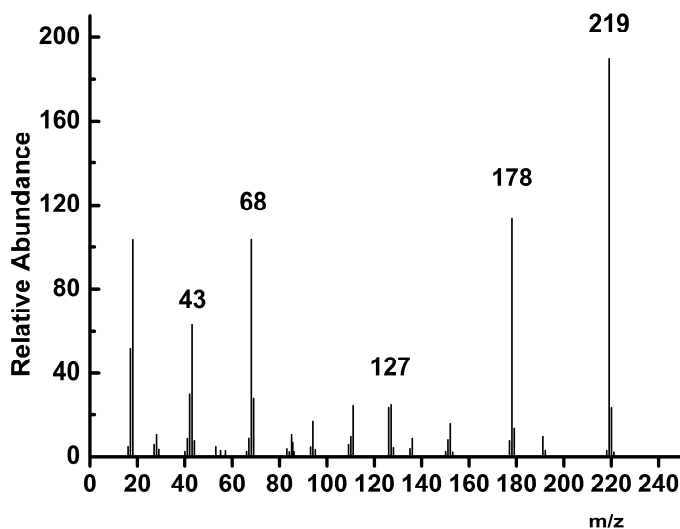
Fig. 5.15 Mass spectrometry result (DEI$^+$) for OH-melem prepared with calcined melamine as starting material.

As seen from the above FTIR and elemental analysis results, when the hydrolyzing temperature is 120 °C, a distinctly different product was obtained. Fig. 5.16 shows the mass spectrum of OH-melem prepared at the hydrolyzing temperature 120 °C. No peak at m/z 219 representing OH-melem can be observed. However, the peak at m/z 128 represents dihydroxy-amino-triazine, which apparently is a hydrolysis product of OH-melem formed under these conditions.
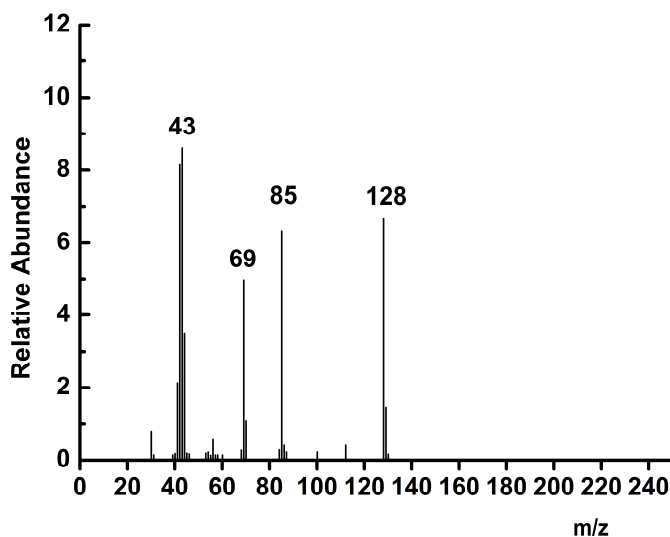
Fig. 5.16 Mass spectrometry result (DEI$^+$) for OH-melem prepared at the hydrolysis temperature at 120 °C.

5.2.6 X-ray Photoelectron Spectroscopy
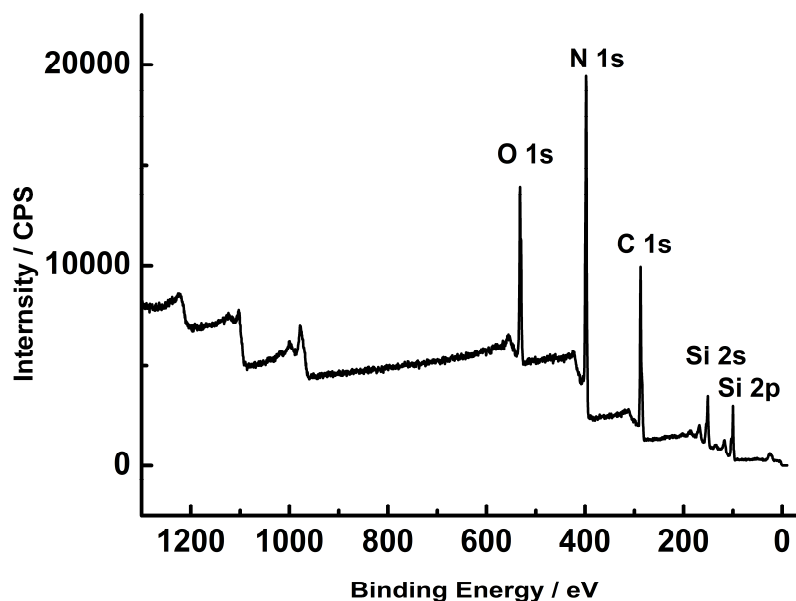
Fig. 5.17 XPS spectra of OH-melem (synthesis condition: calcined melamine sample as starting material, 4 ml H_2SO_4, hydrolysis temperature 80 ℃)

XPS probes the chemical state of the elements in the surface region of the sample, thus XPS measurements were carried out for OH-melem synthesized with 4 mL H_2SO_4 at hydrolysis temperature 80 °C from calcined melamine. A full range XPS spectrum of OH-melem is shown in Fig. 5.17. The binding energies of C, N, O and Si can be observed clearly. The chemical states of the elements (C, N and O) can also be determined.
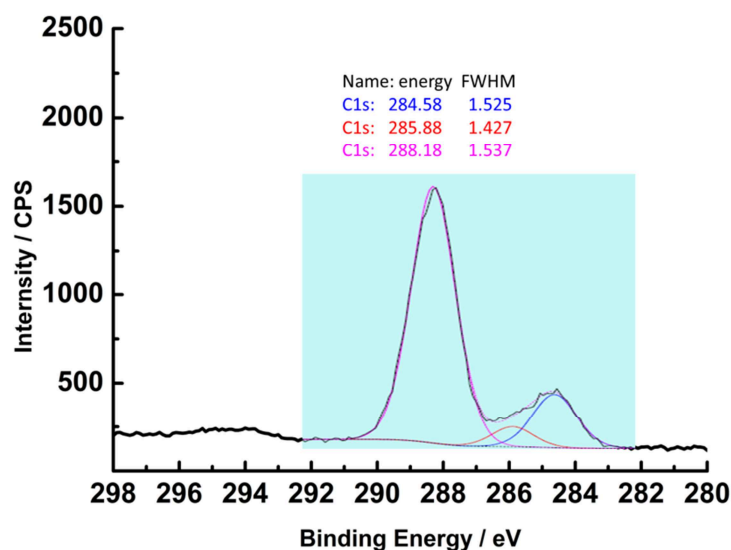
Fig. 5.18 C1s XPS spectrum of OH-melem.

Fig. 5.18 shows the high-resolution C 1s XPS spectrum of OH-melem together with the XPS fitting. The C 1s binding energy shows mainly two carbon species with two binding energies centering at 288.2 eV and 284.6 eV. The binding energy of 284.6 eV corresponds to an ubiquitous carbon contamination; the binding energy of 288.2 eV corresponds to a C-N-C coordination.[19] However, it may also correspond to a C=O group.[20] In addition, a weak signal at 285.9 eV can be inferred, which corresponds to the C–NH$_2$ amino group.[21]
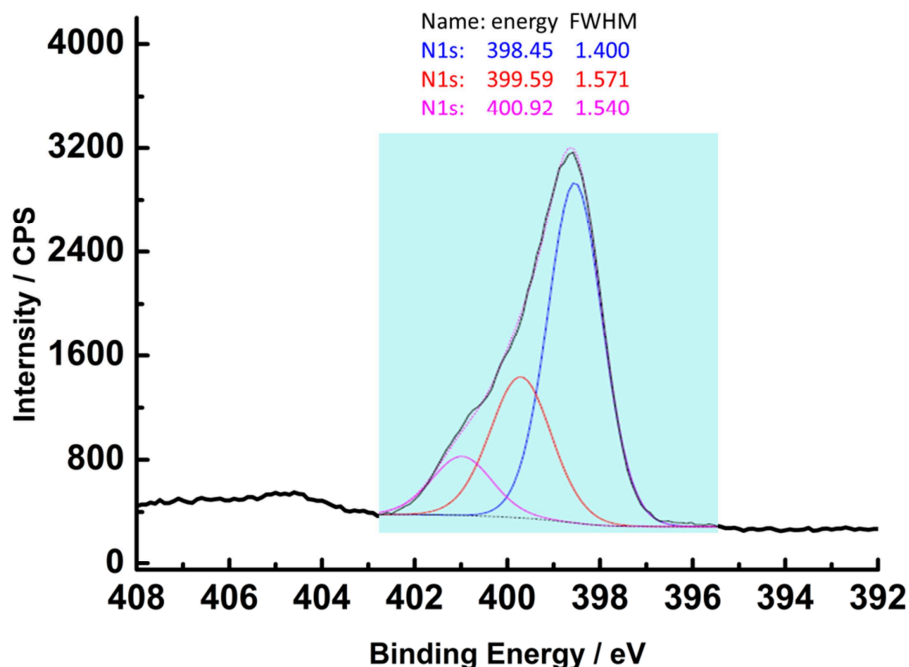
Fig. 5.19 N1s XPS spectrum of OH-melem.

In the N 1s spectrum (Fig. 5.19) several binding energies can be inferred by deconvolution of the main signal around 398 eV. The main signal shows the occurrence of C–N–C groups at 398.4 eV and tertiary nitrogen N–(C)$_3$ groups at 399.6 eV.[22] A weak signal around 401 eV can also be inferred, indicative of amino functions carrying hydrogen (C–N–H).[19]

In the O 1s spectra (Fig. 5.20) two oxygen species can be observed with signals at 530.8 eV and 533.2 eV, respectively. The signal at 533.2 eV[23] corresponds to the Si–O groups (as the specimen was prepared on a silicon wafer), while the signal at 530.8 eV indicates the presence of C=O groups.[21][24] Taken together, the XPS results further confirm the assumed identity of OH-melem as shown in Fig. 5.1 A.
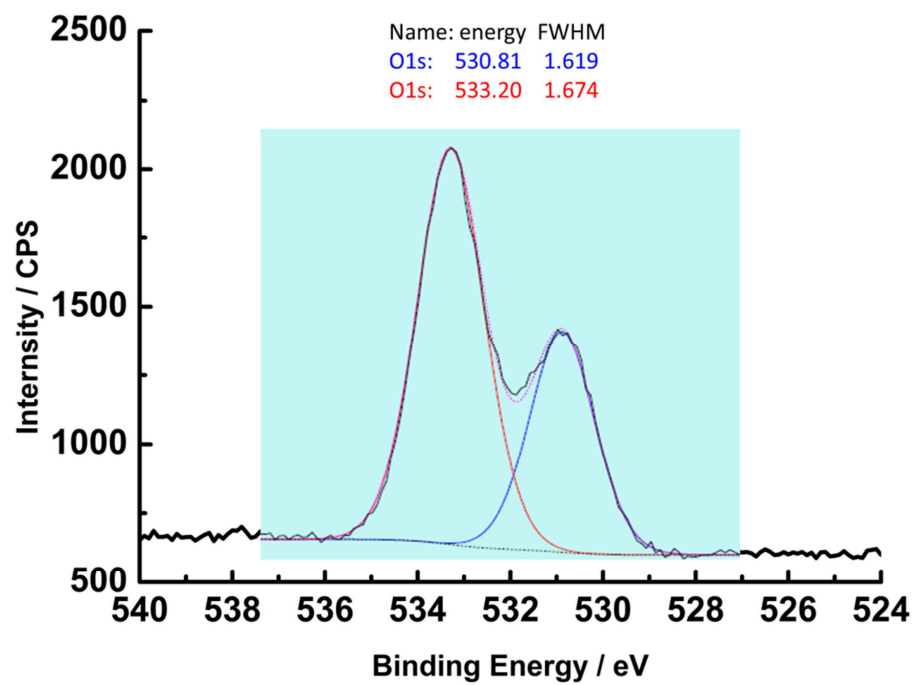
Fig. 5.20 O1s XPS spectra of OH-melem.

5.2.7 Transmission Electron Microscopy
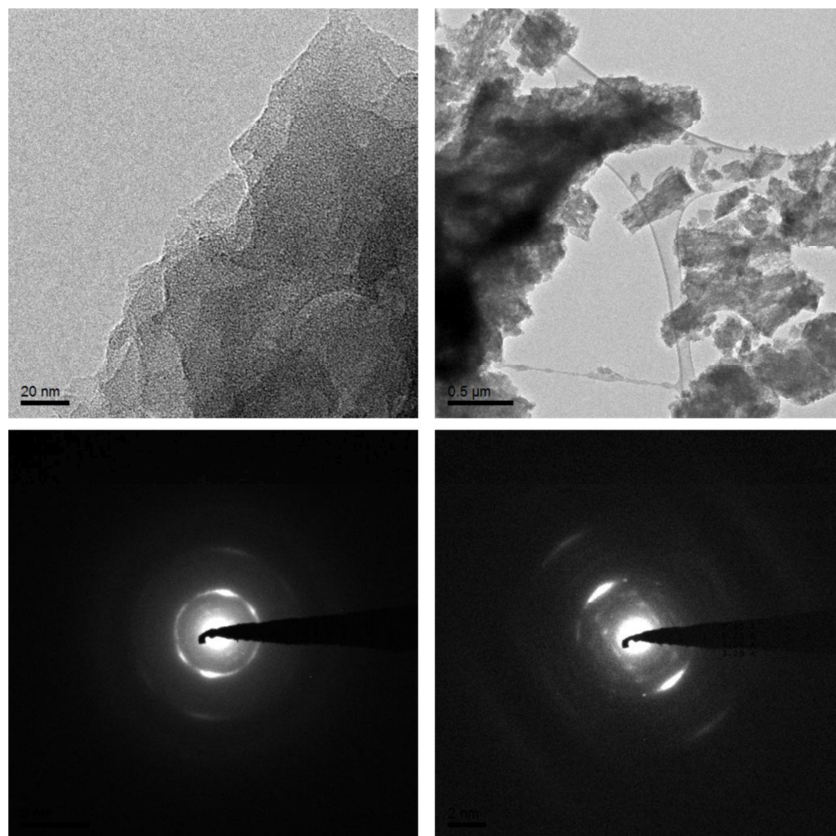
Fig. 5.21 TEM images and diffraction patterns of OH-melem (starting material: calcined melamine, hydrolysis temperature 80°C and 4 mL H_2SO_4).

TEM were carried out to get structural insights into nanometer-sized and polycrystalline structure of the OH-melem sample. Representative TEM images of OH-melem sample are displayed in Fig. 5.21(top). From the image of the edges, it is clearly seen that the sample has a layered structure. The diffraction patterns of OH-melem are shown in the bottom of Fig. 5.21. Some rings and dots can be seen, however, no clear diffraction patterns of nanocrystalline sample regions can be observed, indicating the poor crystallinity of OH-melem.

5.3 Conclusions

In summary, OH-melem can be prepared by hydrolyzing melon, calcined melamine or melem at 80 – 100 °C with concentrated H_2SO_4 in aqueous solution. It turned out that calcined melamine and melem are more suitable as starting materials than melon. Apparently, as melon is a highly condensed carbon nitride polymer, it will take a longer time to dissolve it with H_2SO_4. At the end of this process, parts of the material may be hydrolyzed beyond the state of OH-melem, possibly leading to cyanuric acid derivatives. Furthermore, it seems that the amount of concentrated H_2SO_4 is not a crucial factor to influence the final product. However, the hydrolysis temperature is quite important and should not be too high. At a reaction temperature of 120 °C, side products will form that have not been identified yet, however a cyanuric acid-based structure is likely, as well as the presence of a sulfate species in the side product. The crystallinity of OH-melem is rather low according to the XRD and TEM results. Only one obvious reflection can be observed in the XRD pattern for all OH-melem samples, which is indicative of a stacking distance at around 3.20 Å. In the FTIR spectra, the band around 800 cm^{-1} indicates the presence of either the triazine or heptazine nucleus and the shoulder band at 1710 cm^{-1} suggests the presence of C=O groups, which is consistent with the carbonyl-tautomer of OH-melem (Fig 5.7). Elemental analysis shows that the N/C ratio of OH-melem is quite close, yet does not exactly correspond to the theoretical ratio. Oxygen determination experiments confirm that there is oxygen in the synthesized OH-melem, however since the experimentally found oxygen amount is higher than the theoretical value, it is likely that either traces of 2OH-melem (dioxo-amino-heptazine) are present or the material is obtained as a hydrate. The NMR spectra of OH-melem are different from melem or cyameluric acid. Assuming a linear dependence of the N_c signal shift on the amount of oxygen per molecule and according to the N_c shifts of melem and cyameluric acid, the calculated N_c shift of OH-melem closely agrees with one covalently bonded oxygen per molecule and, hence, OH-melem. By employing mass spectrometry, the molecular mass peak *m/z* 219 is observed, which is also a strong evidence for the presence of OH-melem. Finally, the XPS O 1s spectra exhibit a signal at 530.8 eV, which indicates the presence of C=O groups. All these results are strong evidence for the successful synthesis of OH-melem, which apparently is furnished in the carbonyl tautomeric structure rather than as hydroxyl tautomer as suggested in Figure 5.1 A.

5.4 Chapter References

[1]   E. Horvath-Bordon, E. Kroke, I. Svoboda, H. Fuess, R. Riedel, S. Neeraj, A. K. Cheetham, *Dalton transactions* **2004**, 3900–39088.

[2]   A. Finkel'shtein, *Zhurnal Obshchei Khimii* **1962**, *32*, 3403–3406.

[3]   A. Sattler, *Ph.D thesis LMU* **2010**.

[4]   B. V Lotsch, M. Döblinger, J. Sehnert, L. Seyfarth, J. Senker, O. Oeckler, W. Schnick, *Chemistry (Weinheim an der Bergstrasse, Germany)* **2007**, *13*, 4969–4980.

[5]   M. R. Mahmoud, H. M. F. Madkour, M. M. Habashy, A. M. El-Shwaf, *American Journal of Organic Chemistry* **2012**, *2*, 39–47.

[6]   X. H. Xu, G. L. Ren, J. Cheng, Q. Liu, D. G. Li, Q. Chen, *Journal of Materials Science* **2006**, *41*, 4974–4977.

[7]   X. Wang, K. Maeda, A. Thomas, K. Takanabe, G. Xin, J. M. Carlsson, K. Domen, M. Antonietti, *Nature materials* **2009**, *8*, 76–80.

[8]   H. Yan, H. Yang, *Journal of Alloys and Compounds* **2011**, *509*, 26–29.

[9]   B. Yue, Q. Li, H. Iwai, T. Kako, J. Ye, *Science and Technology of Advanced Materials* **2011**, *12*, 034401.

[10] N. E. a. El-Gamel, J. Wagler, E. Kroke, *Journal of Molecular Structure* **2008**, *888*, 204–213.

[11] E. Horvath-Bordon, E. Kroke, I. Svoboda, H. Fuess, R. Riedel, S. Neeraj, A. K. Cheetham, *Dalton transactions (Cambridge, England : 2003)* **2004**, 3900–3908.

[12] B. Y. K. Newman, *Journal of the American Chemical Society* **1952**, *74*, 3545–3548.

[13] I. The, T. Iupac, *Asian Journal of Chemistry* **2010**, *22*, 5049–5056.

[14] S. T. Martin, D. Salcedo, L. T. Molina, M. J. Molina, *The Journal of Physical Chemistry B* **1997**, *101*, 5307–5313.

[15] S. J. Makowski, P. Köstler, W. Schnick, *Chemistry (Weinheim an der Bergstrasse, Germany)* **2012**, *18*, 3248–3257.

[16] L. Seyfarth, J. Sehnert, N. E. A. El-gamel, W. Milius, E. Kroke, J. Breu, J. Senker, *Journal of Molecular Structure* **2008**, *889*, 217–228.

[17] B. Jürgens, E. Irran, J. Senker, P. Kroll, H. Müller, W. Schnick, *Journal of the American Chemical Society* **2003**, *125*, 10288–300.

[18] K. Chingin, R. H. Perry, S. D. Chambreau, G. L. Vaghjiani, R. N. Zare, *Angewandte Chemie (International ed. in English)* **2011**, *50*, 8634–8637.

[19] A. Thomas, A. Fischer, F. Goettmann, M. Antonietti, J.-O. Müller, R. Schlögl, J. M. Carlsson, *Journal of Materials Chemistry* **2008**, *18*, 4893–4905.

[20] T. I. T. Okpalugo, P. Papakonstantinou, H. Murphy, J. McLaughlin, N. M. D. Brown, *Carbon* **2005**, *43*, 153–161.

[21] F. Truica-Marasescu, M. R. Wertheimer, *Plasma Processes and Polymers* **2008**, *5*, 44–57.

[22] E. Raymundo-Piñero, D. Cazorla-Amorós, A. Linares-Solano, J. Find, U. Wild, R. Schlögl, *Carbon* **2002**, *40*, 597–608.

[23] J.-W. He, X. Xu, J. S. Corneille, D. W. Goodman, *Surface Science* **1992**, *279*, 119–126.

[24] J. Zhang, X. Liu, R. Blume, A. Zhang, R. Schlögl, D. S. Su, *Science* **2008**, *322*, 73–77.

Chapter 6

Conclusions and Outlook

The main focus of this thesis was the synthesis and characterization of various carbon nitrides (incompletely condensed melon, carbon nitride doped cesium titanate, ultra-long calcined melon, and OH-melem). Those carbon nitrides were tested with regard to their photocatalytic properties. However, OH-melem was excluded, since OH-melem was synthesized as a precursor for further condensation (not part of this thesis).

In Chapter 3, the mechanism of the condensation reaction from melamine to melon is discussed. Therefore, the precursor melamine was heated for $4 - 100$ h at a reaction temperature of 450 °C in an open system at near to ambient pressure. When the calcination time is not higher than 10 h, two obviously different crystalline structures of melem and some amorphous residues are obtained. Those residues could be dimer, trimer or even melon-type material. By increasing the calcination time, the properties of the calcined products get closer and closer to melon. However, from the XRD result (Section 3.2.1) the end stage (calcined for 100 h) is not totally equal with melon prepared at 490 °C for 72 h in an open system. This interesting phenomenon leads us to the ultra-long calcined melamine samples synthesized at $430 - 490$ °C for 160 h in an open system. From the TEM and MS results (Section 3.2.3), a melem phase can still be observed when the calcination temperature is not higher than 450 °C. It indicates that during the condensation reaction, temperature is a crucial factor. When the temperature is not higher than 450 °C, melem obviously cannot undergo further condensation to melon. The TEM images also display interesting morphologies for ultra-long calcined melamine at 490 °C. This sample possesses a layered nanosheet structure which could be caused by thermal oxidation. The thermal oxidation can also introduce oxygen dopant into the ultra-long calcined products, which can be proven by elemental analysis (Section 3.2.4). In photocatalytic activity testing (hydrogen evolution reaction in water splitting experiments), calcined melamine samples exhibit less activity than melon prepared at 490 °C for 72 h in an open system. Ultra-long calcined melamine at 490 °C shows the best photocatalytic activity in the hydrogen evolution reaction experiment of all the samples. Since it has a layered nanosheet structure with high surface area, this suggests that the morphology is an important factor for the photocatalytic activity.

In Chapter 4, carbon nitride doped cesium titanate samples were synthesized in a half open system at 450 °C for 1 – 36 h. Carbon nitride doping can decrease the band gap of the titanate, which was demonstrated by UV-Vis spectroscopy (Section 4.2.3). Although the band gap of the carbon nitride doped cesium titanates decreased, it did not exhibit as good a photocatalytic activity as expected. However, when the carbon nitride doped sample was calcined at 450 °C for 16 h, the product showed better photocatalytic activity for the hydrogen evolution under UV light illumination than the pure carbon nitride calcined at 450 °C for 16 h under the same conditions. As the pure cesium titanate results in negligible H_2 evolution, this indicates that the carbon nitride or carbon nitride/titanate hybrid is the active part in H_2 evolution. When referencing to equal weight of carbon nitride in the doped and pure carbon nitride samples, the calculated hydrogen production of all hybrid compositions are higher than those of the pure carbon nitrides. This indicates that carbon nitride doping of titanates can enhance the photocatalytic activity in the hydrogen evolution reaction.

In Chapter 5, a new method was established to synthesize OH-melem, which could be a good precursor for oxygen doped carbon nitride materials. In contrast with the previous method, which hydrolyzed melon with an alkaline solution by carefully adjusting the concentration of hydroxide base and reaction time, various amounts of concentrated H_2SO_4 were utilized to hydrolyze the calcined melamine sample at different temperatures. After neutralizing the solution, OH-melem was obtained. The starting materials, the hydrolysis temperatures and the amount of concentrated H_2SO_4 were investigated to check which of them influence the final product. It turned out that calcined melamine and melem are more suitable as starting materials than melon, and that the hydrolysis temperature should not be higher than 100 °C. However, the amount of concentrated H_2SO_4 is not very important. The molecular structure of OH-melem was studied by a range of analytical techniques, and the results point to the carbonyl tautomeric structure in Fig. 5.1 A.

The investigations into these carbon nitride materials carried out in this thesis can lead us to synthesize an optimized material which would possess enhanced photocatalytic properties. As known from Chapter 3, the melamine calcined samples were prepared in two different open systems which are different with respect to the pressure in the system. The pressure of the system apparently is a crucial factor in the synthesis of carbon nitrides, which is often neglected. Investigating the synthesis of carbon nitrides as a function of ambient pressure and type of

atmosphere may be an important future direction. The ultra-long calcined melon samples have good photocatalytic activity for hydrogen evolution from water, but the calcination temperature was only investigated up to 490 °C. In the future, further synthesis temperatures should be investigated. Likewise, the calcination time can also be adjusted to longer and shorter times to check which time is most suitable for optimum photocatalytic activity.

OH-melem (Chapter 5) may serve as a precursor for further polymerization, for example polymerization with melamine, melem, or with itself. Meanwhile, various temperatures and calcination times can be probed in open or closed systems.

In summary, this work puts forward investigations deeper into the material chemistry and photocatalytic properties of various carbon nitride compounds, which could show great potential in the future as photocatalysts, organic semiconductors, covalent organic frameworks and photovoltaic materials.

Chapter 7

Appendix

Synthetic Procedures

''Melem oligomers'':

Melem oligomers were synthesized in two different open systems. Typically, 4 g of melamine were transferred into the porcelain crucible or into the small glass vial. The crucible or glass vials were placed into a muffle furnace and heated to 450 °C (5 °C min^{-1}), at which the temperature was held for 4 – 100 hours. The cooling rates did not affect the crystallinity of the products, so the sample was directly moved out of the muffle furnace, which cooled to room temperature within 1 h. As the calcination time increased from 4 – 100 h, the color of the yellowish product changed from beige to deep yellow (Fig.1).

Fig. A.1 Melem oligomers were prepared at 450 °C in open system for 6, 14, 20 and 100 h.

Melem:

Melem was synthesized by heating melamine at 450 °C in a closed ampule. Typically, 200 mg of melamine was filled into a glass ampule under vacuum (outer diameter, 16 mm; inner diameter,

12 mm). The ampule was sealed at a length of 120 mm and heated to 450 °C (heating rate: 1 °C min^{-1}). After keeping this temperature for 5 h, the ampule was slowly cooled to room temperature (cooling rate: 2 °C min^{-1}). The sample was then isolated by carefully breaking the ampule, and a significant amount of ammonia was released.

Melon:

Melon was synthesized by heating melamine at 490 °C in an open system. Typically, 6 g of melamine was placed into a crucible with a loose lid on top. The crucible was transferred into a muffle furnace and heated at 490 °C (heating rate: 5 °C min^{-1}) for 72 h then cooled down to room temperature.

Ultra-long calcined melon type material:

Ultra-long calcined melon type material was prepared by heating melamine at 430 – 490 °C in an open system (Fig. 3.1 right) for 160 h. Typically, 6 g of melamine were placed into a crucible with a loose lid on top. The crucible was put into a muffle oven and heated at 430 – 490 °C (heating rate: 5 °C min^{-1}), keeping this temperature for 160 h then cooled down to room temperature.

Hybrid materials:

The cesium titanate (CTO) powder was prepared by calcining a mixture of TiO_2 and Cs_2CO_3 at 800 °C (the molar ratio of TiO_2 to Cs_2CO_3 was 5:1). After calcination for 20 h, the powder was ground carefully and then calcined for another 20 h. $Cs_xTi_{2-x/4}\square_{x/4}O_4$ (x = 0.67) was obtained. Then the CTO was mixed with melamine (molar ratio of CTO to melamine ranged from 1:1 to 1:10) and the mixture was ground in order to disperse the powders completely. After 1 – 36 h of calcination, the carbon nitride doped cesium titanate materials were obtained showing a yellow color.

OH-melem:

Typically, 0.17 g of starting material (melem, calcined melamine (16 h at 450 °C) or melon) and 4 ml water were put into a flask followed by various amounts of H_2SO_4 which were slowly added drop by drop while the solution was stirring. The flask was then heated in an oil bath at several temperatures (80 °C, 100 °C, or 120 °C) till the solution was totally transparent. After the

solution cooled down to room temperature, a base solution (NaOH or KOH 2 molL^{-1}) was slowly added to neutralize the solution to pH = 7 and a white precipitate was obtained. Then the precipitate was filtered and put in an oven overnight at 120 °C to obtain OH-melem.

Curriculum Vitae

Personal information

Name: Hongji Wang

Gender: Male

Date of Birth: November 10, 1982

Place of birth: Yantai, China

Citizenship: Chinese

Education

09/2001 – 07/2005:   Bachelor study in Department of Chemistry and Chemical Engineering, China University of Petroleum, Dongying, P. R. China

01.07.2005:   Bachelor of Applied Chemistry

09/2005 – 07/2008:   Master study in Department of Chemistry, Nanjing University, Nanjing, P. R. China

01.07.2008:   Master of Science, Chemistry. Mater thesis entitled

                       ''A Facile Way to Synthesize Mesoporous Materials and Functionalized Nanoporous Materials''

10/2008 – 10/2009:   Ph.D study in AK Bein at Department of Chemistry, LMU München

                       Research on mesoporous ZnO

10/2009 – Now: Ph.D study in AK Lotsch at Department of Chemistry, LMU München and MPI Stuttgart. Ph.D thesis entitled

                       ''Investigations into carbon nitrides and carbon nitride derivatives''